

การสังเคราะห์ตัวเร่งปฏิกิริยาคอมพอสิต ZSM-5/MCA-Pr-SO₃H สำหรับแอนิโซลแอลคิลเลชัน



บทคัดย่อและแฟ้มข้อมูลฉบับเต็มของวิทยานิพนธ์ตั้งแต่ปีการศึกษา 2554 ที่ให้บริการในคลังปัญญาจุฬาฯ (CUIR)
เป็นแฟ้มข้อมูลของนิสิตเจ้าของวิทยานิพนธ์ ที่ส่งผ่านทางบัณฑิตวิทยาลัย

The abstract and full text of theses from the academic year 2011 in Chulalongkorn University Intellectual Repository (CUIR)
are the thesis authors' files submitted through the University Graduate School.

วิทยานิพนธ์นี้เป็นส่วนหนึ่งของการศึกษาตามหลักสูตรปริญญาวิทยาศาสตรมหาบัณฑิต
สาขาวิชาเคมี ภาควิชาเคมี
คณะวิทยาศาสตร์ จุฬาลงกรณ์มหาวิทยาลัย
ปีการศึกษา 2558
ลิขสิทธิ์ของจุฬาลงกรณ์มหาวิทยาลัย

SYNTHESIS OF ZSM-5/MCA-Pr-SO₃H COMPOSITE CATALYST FOR ANISOLE ALKYLATION

Miss Siripan Samutsri



A Thesis Submitted in Partial Fulfillment of the Requirements
for the Degree of Master of Science Program in Chemistry

Department of Chemistry

Faculty of Science

Chulalongkorn University

Academic Year 2015

Copyright of Chulalongkorn University

ศิริพันธ์ สมุทรศรี : การสังเคราะห์ตัวเร่งปฏิกิริยาคอมพอสิต ZSM-5/MCA-Pr-SO₃H สำหรับแอนิโซลแอลคิเลชัน (SYNTHESIS OF ZSM-5/MCA-Pr-SO₃H COMPOSITE CATALYST FOR ANISOLE ALKYLATION) อ.ที่ปรึกษาวิทยานิพนธ์หลัก: ดร.ดวงกมล ตุงคะสมิต, 103 หน้า.

ตัวเร่งปฏิกิริยารูพรุนขนาดกลางโครงสร้างสี่เหลี่ยมลูกบาศก์ชนิด Ia-3d ที่มีหมู่ฟังก์ชันโพรพิลซัลโฟนิคติดอยู่ในโครงสร้างสามารถสังเคราะห์โดยตรงภายใต้ภาวะที่เป็นกรดโดยใช้ไตรบีสกโคพอลิเมอร์ชนิด P123 เป็นสารชั้นนำโครงสร้าง องค์ประกอบของเจลในสารสังเคราะห์รูพรุนขนาดกลางคือ 1 TEOS: 0.089 MPTMS: 0.018 P123: 2.0 HCl: 148 H₂O นอกจากนั้นผง ZSM-5 ถูกเติมเข้าไปในเจลของสารสังเคราะห์รูพรุนขนาดกลางเพื่อเปลี่ยนโครงสร้างให้เป็นวัสดุที่มีรูพรุนผสม ในขั้นตอนการสังเคราะห์ปริมาณของผง ZSM-5 เติมในช่วง 10-50% ของปริมาณแหล่งซิลิกาที่ทำให้เกิดการเปลี่ยนโครงสร้างเป็นวัสดุที่มีรูพรุนผสม โครงสร้างของวัสดุที่สังเคราะห์ได้ถูกตรวจสอบลักษณะเฉพาะด้วยเทคนิคการเลี้ยวเบนของรังสีเอกซ์ เทคนิคการดูดซับไนโตรเจน กล้องจุลทรรศน์อิเล็กตรอนแบบส่องกราด กล้องจุลทรรศน์อิเล็กตรอนแบบส่องผ่านและการหาค่าความเป็นกรดด้วยเทคนิคการดูดซับแอมโมเนีย จากผลการทดสอบเอกลักษณ์วัสดุที่มีรูพรุนผสมแสดงเอกลักษณ์ของทั้งวัสดุที่มีรูพรุนขนาดกลางและรูพรุนขนาดเล็ก ทดสอบประสิทธิภาพของตัวเร่งปฏิกิริยารูพรุนขนาดกลางที่มีหมู่โพรพิลซัลโฟนิคด้วยปฏิกิริยาแอนิโซลแอลคิเลชันและทำการเปรียบเทียบประสิทธิภาพในการเร่งปฏิกิริยากับ Amberlyst-15 และตัวเร่งปฏิกิริยาที่มีรูพรุนชนิดอื่น พบว่าตัวเร่งปฏิกิริยารูพรุนขนาดกลางที่มีหมู่โพรพิลซัลโฟนิคให้ประสิทธิภาพในการเร่งปฏิกิริยาในการให้ผลิตภัณฑ์อัลคิลมากที่สุด ตัวเร่งปฏิกิริยาที่มีรูพรุนผสมถูกทดสอบประสิทธิภาพด้วยภาวะที่ดีที่สุดของตัวเร่งปฏิกิริยารูพรุนขนาดกลางที่มีหมู่โพรพิลซัลโฟนิคในปฏิกิริยาแอนิโซลแอลคิเลชัน พบว่าตัวเร่งปฏิกิริยาที่มีรูพรุนผสมให้ผลิตภัณฑ์ชนิด *para*-alkylated anisole (4-TBA) มากที่สุด และให้ผลิตภัณฑ์อัลคิลรวมมากกว่าตัวเร่งปฏิกิริยา ZSM-5

ภาควิชา เคมี

สาขาวิชา เคมี

ปีการศึกษา 2558

ลายมือชื่อนิสิต

ลายมือชื่อ อ.ที่ปรึกษาหลัก

5672105023 : MAJOR CHEMISTRY

KEYWORDS: CUBIC IA-3D / COMPOSITE MATERIAL / ANISOLE ALKYLATION

SIRIPAN SAMUTSRI: SYNTHESIS OF ZSM-5/MCA-Pr-SO₃H COMPOSITE CATALYST FOR ANISOLE ALKYLATION. ADVISOR: DUANGAMOL TUNGASMITA, Ph.D.}, 103 pp.

Propylsulfonic acid functionalized cubic *la-3d* mesoporous (MCA) silica was synthesized by using co-condensation method in acidic condition and using triblock copolymer Pluronic P123 as structure directing agent. The gel composition of synthetic mesoporous material was 1 TEOS: 0.089 MPTMS: 0.018 P123: 2.0 HCl: 148 H₂O. In addition, ZSM-5 powder was added into *la-3d* mesopore silica gel with different amount of ZSM-5 powder in order to synthesize micro/mesoporous composite material. In the synthesis procedure, amount of ZSM-5 powder in the range of 10-50 wt% based on silica source exhibited the phase transition to composite material. The structure characterization, morphology and acidity of synthesized materials were characterized by XRD, N₂ adsorption desorption, SEM, TEM and NH₃-TPD. The results showed that composite materials exhibited both properties of mesoporous (MCA) and microporous ZSM-5 matters. Propylsulfonic acid functionalized MCA (MCA-Pr-SO₃H) was test catalytic activities in anisole alkylation and compared catalytic activities with Amberlyst-15 and other porous catalysts. MCA-Pr-SO₃H showed the highest efficient in alkylated product yield than other catalysts. The micro/mesoporous material was tested in anisole alkylation at optimum reaction parameter of MCA-Pr-SO₃H. The composite catalyst promoted selectivity of *para*-alkylated anisole (4-TBA) and increased the yield of *tert*-butyl anisole products when compared with ZSM-5 catalyst.

Department: Chemistry

Student's Signature

Field of Study: Chemistry

Advisor's Signature

Academic Year: 2015

ACKNOWLEDGEMENTS

The completion of this research can be credited to the all-embracing support and helpfulness from Dr. Duangamol Tungasmita, my thesis advisor. I would like to honest thanks to her for mean useful recommendation, direction and encouragement for all times in my research working as well as precious experiences in the whole time of work.

I would like to thanks the members of thesis committee consisting of Associate Professor Dr. Vudhichai Parasuk, Dr. Numpol Insin and Dr. Papapida Pornsuriyasak, the external examiner from PTT Phenol Company Limited, for all of their useful comment and advice for this research.

I would like to thanks Department of Chemistry, Faculty of Science, Chulalongkorn University for supporting a teacher assistant fund and valuable knowledge. In addition, I would like to thanks Thailand Japan Technology Transfer Project supported a loan by Japan Banks for International Cooperation (TJTTP-JBIC) for instrument support.

Finally, many thanks for the members of Materials Chemistry and Catalysis Research Unit and my friends in their sincere kindness and help. Lastly, I deeply wish to thank my family for their take care and moral support throughout my graduate study.

CONTENTS

	Page
THAI ABSTRACT.....	iv
ENGLISH ABSTRACT	v
ACKNOWLEDGEMENTS	vi
CONTENTS.....	vii
LIST OF TABLES.....	xiii
LIST OF FIGURES	xv
LIST OF SCHEMES.....	xviii
LIST OF ABBREVIATION	xix
CHAPTER I INTRODUCTIONS.....	1
1.1 Statement of problems	1
1.2 Literature reviews.....	3
1.2.1 Porous catalysts synthesis.....	3
1.2.2 Anisole alkylation	5
1.3 Objectives	6
1.4 Scopes of work	7
CHAPTER II THEORY	8
2.1 Catalysts	8
2.1.1 Type of catalyst.....	9
2.2 Porous molecular sieve	10
2.3 Microporous materials.....	10
2.3.1 Basic units of zeolites	12
2.3.2 Zeolite ZSM-5.....	15

2.3.4 Properties of zeolite ZSM-5.....	16
2.3.4.1 Acid site of ZSM-5	16
2.3.4.2 shape-selective of ZSM-5	17
2.4 Mesoporous materials	18
2.4.1 Classification of mesoporous materials.....	19
2.4.2 Formation mechanism of mesoporous materials	20
2.4.2.1 Liquid crystal templating mechanism	20
2.4.2.2 Folding sheet formation	21
2.4.2.3 Hydrogen bonding interaction.....	22
2.5 Cubic <i>la</i> -3d Mesoporous silica (MCA)	22
2.6 Modification of catalyst by organic functionalization	23
2.6.1 Co-condensation method	23
2.6.2 Post synthesis (Grafting).....	24
2.7 Composite materials	25
2.7.1 Synthesis of composite materials by recrystallization of mesoporous materials	27
2.7.2 Synthesis of composite materials by using zeolite seeds as framework-building units.....	28
2.7.3 Synthesis of composite materials by post-synthesis treatment of microporous materials.....	29
2.7.4 Synthesis of composite materials by substrate-template porous materials	29
2.8 Characterization of materials	30
2.8.1 X-ray powder diffraction (XRD)	30

	Page
2.8.2 N ₂ adsorption-desorption technique	31
2.8.3 Temperature-programmed desorption of ammonia (NH ₃ - TPD)	35
2.8.4 Scanning electron microscope (SEM)	35
2.8.5 Transmission electron microscope (TEM)	36
2.9 Anisole alkylation [41]	37
CHAPTER III EXPERIMENTS	39
3.1 Starting materials	39
3.1.1 Starting materials for MCA-Pr-SO ₃ H and ZSM-5/MCA-Pr-SO ₃ H composite catalysts preparation	39
3.1.2 Chemicals for butylation reaction	39
3.1.3 Chemicals for quantitative analysis	39
3.1.4 Chemicals for antioxidant test	40
3.2 Instruments and apparatus	40
3.2.1 X-ray power diffraction (XRD)	40
3.2.2 Surface area analyzer	40
3.2.3 Scanning electron microscopy (SEM)	40
3.2.4 Transmission electron microscope (TEM)	40
3.2.5 Temperature-programmed desorption of ammonia (NH ₃ - TPD)	41
3.2.6 Gas chromatograph (GC)	41
3.3 Synthesis of materials	42
3.3.1 Propylsulfonic acid functionalized cubic <i>la</i> -3d (MCA)	42
3.3.2 Composite ZSM-5/MCA-Pr-SO ₃ H materials	44
3.4 Acid-base titration	46

	Page
3.5 Parameter affecting catalytic preparation	46
3.5.1 Effect of ZSM amount	46
3.5.2 Effect of time	46
3.6 Procedure in alkylation of anisole	47
3.6.1 Effect of catalytic type	47
3.6.2 Effect of mole ratio	47
3.6.3 Effect of reaction temperature	47
3.6.4 Effect of reaction time	47
3.6.5 Effect of catalytic amount	47
3.6.6 Catalytic performance of ZSM-5/MCA-Pr-SO ₃ H.....	47
3.8 Recycle of catalysts	48
3.9 Antioxidant activity	48
3.9.1 Antioxidant test by UV-visible method	48
CHAPTER IV RESULTS AND DISCUSSION	49
4.1 Propylsulfonic acid functionalized cubic <i>l</i> α -3d (MCA)	49
4.1.1 The physical- chemical properties of Propyl sulfonic acid functionalized cubic <i>l</i> α -3d (MCA).....	49
4.1.1.1 XRD results	49
4.1.1.2 N ₂ sorption properties	50
4.1.1.3 SEM images	52
4.1.1.4 TEM images	53
4.2 Micro/mesoporous composite material	54
4.2.1 The physical-chemical properties of ZSM-5/MCA-Pr-SO ₃ H composite material	54

	Page
4.2.1.1 Effect of ZSM-5 amount	54
4.2.1.1.1 XRD results.....	54
4.2.1.1.2 N ₂ sorption properties.....	55
4.2.1.1.3 SEM images.....	57
4.2.1.1.4 TEM images.....	59
4.2.1. 2 Effect of time	60
4.2.1. 2. 1 XRD results.....	60
4.2.1. 2. 2 N ₂ sorption properties.....	62
4.2.2 Comparison of composite material with original material	64
4.2.2.1 XRD results.....	64
4.2.2.2 N ₂ sorption properties	65
4.2.2.3 SEM images	67
4.2.2.3 TEM images.....	68
4.3 Acidity of synthesized catalysts from NH ₃ -TPD	69
4.4 Anisole alkylation with <i>tert</i> -butanol over heterogeneous catalysts	71
4.5 Catalytic activity of propylsulfonic acid functionalized cubic Ia-3d mesoporous catalysts	74
4.5.1 Effect of mole ratio	74
4.5.2 Effect of reaction temperature	75
4.5.3 Effect of reaction time	76
4.5.4 Effect of catalytic amount	77
4.6 Catalytic performance of ZSM-5/MCA-Pr-SO ₃ H.....	78
4.7 Reusability of Catalysts.....	79

	Page
4.7.1 Reusability of MCA-Pr-SO ₃ H.....	79
4.7.1.1 Characterization of recyclable MCA-Pr-SO ₃ H.....	79
4.7.1.2 Activity of recyclable MCA-Pr-SO ₃ H.....	81
4.7.2 Reusability of ZM-30 composite catalyst	82
4.7.2.1 Characterization of recyclable ZM-30 composite catalyst	82
4.7.2.2 Activity of recyclable ZM-30 composite catalyst	84
4.8 Antioxidant activity	85
CHAPTER V CONCLUSIONS.....	87
REFERENCES	88
APPENDICES.....	94
VITA	103



LIST OF TABLES

Table	Page
Table 2.1 Comparison of homogeneous and heterogeneous catalysts	9
Table 2.2 IUPAC classification of porous materials [34]	10
Table 2.3 Various synthesis conditions of hexagonal mesoporous materials and the type of interaction between template and inorganic species	19
Table 2. 4 Properties of MCA and MCM-48[37].....	23
Table 2.5 Features of adsorption isotherms	33
Table 4.6 Textural properties of synthesized cubic mesoporous material.....	51
Table 4.7 Textural properties of composite materials	57
Table 4.8 Textural properties of extract-ZM-30 composite materials	63
Table 4.9 Physical properties of the composite material and original material	66
Table 4.10 The acidity of catalysts from NH ₃ -TPD	70
Table 4.11 Physicochemical and textural properties for catalysts	73
Table 4.12 Effect of catalytic type on product distribution and yield of products	73
Table 4.13 Effect of mole ratio on product yields and product distribution over MCA-Pr-SO ₃ H.....	74
Table 4.14 Effect of reaction temperature on product yields and product distribution over MCA-Pr-SO ₃ H.....	75
Table 4.15 Effect of time on product yields and product distribution over	76
Table 4.16 Effect of catalytic amount on product yields and product distribution over MCA-Pr-SO ₃ H.....	77
Table 4.17 Products distribution over on optimum condition of propylsulfonic acid functionalized mesoporous material.....	78

Table 4.18 Textural properties of fresh and reused MCA-Pr-SO ₃ H.....	81
Table 4.19 Activities of fresh and reused MCA-Pr-SO ₃ H.....	82
Table 4.20 Textural properties of fresh and reused ZM-30.....	84
Table 4.21 Activities of fresh and reused ZM-30.....	85



LIST OF FIGURES

Figure	Page
Figure 1.1 The DMC-DPC process that show side product from reaction [2].	1
Figure 2.1 The relationship between activation energy (E_a) and enthalpy (ΔH) of the reaction with and without a catalyst [32].	8
Figure 2.2 The structure of zeolites.	11
Figure 2.3 A primary building units of porous materials	12
Figure 2.4 Secondary building units found in zeolite structures.	13
Figure 2.5 Examples of the three types of pore openings in the zeolite molecular sieves, (a) small pore zeolite, (b) medium pore zeolite and, (c) large pore zeolite	14
Figure 2.6 (a) The pentasil unit and (b) three-dimensional structure of ZSM-5.	15
Figure 2.7 The generation of Brønsted and Lewis acid sites in zeolite	16
Figure 2.8 Three types of selectivity in zeolites	17
Figure 2.9 Types of silica surface Si-O species.	18
Figure 2.10 Structures of mesoporous M41S materials: a) MCM-41 (2D hexagonal, space group $p6mm$), b) MCM-48 (cubic, space group $Im\bar{3}m$), and c) MCM-50 (lamellar, space group $p2$).	20
Figure 2.11 Two possible ways for the LCT mechanism	21
Figure 2.12 Co-condensation methods (direct synthesis) for the organic modification of mesoporous pure silica phases. R=organic functional group.	24
Figure 2.13 Grafting (postsynthetic functionalization) for organic modification of mesoporous pure silica phases with terminal organosilanes of the type $(R'O)_3SiR$, R=organic functional group.	25

Figure 2.14 Schematic representation of possible reaction routes leading to the formation of micro/mesoporous composite.....	26
Figure 2.15 Mechanism of the Synthesis of composite materials by dual templating	27
Figure 2.16 Mechanism of self-organization of zeolite seeds onto mesoporous matrix	28
Figure 2.17 Polystyrene beads were used template in the preparation of hollow zeolite spheres.....	30
Figure 2.18 Diffraction of X-ray by regular planes of atoms.....	31
Figure 2.19 The IUPAC classification of adsorption isotherms.	32
Figure 2.20 Classification of adsorption isotherms with hysteresis loops.....	34
Figure 2.21 Diagram of SEM column and specimen chamber.....	35
Figure 2.22 Schematic diagram of transmission electron microscope	37
Figure 2.23 Dimethyl carbonate to Diphenyl carbonate (DMC-DPC) process.....	37
Figure 2.24 Alkylation of anisole with <i>tert</i> -butanol	38
Figure 3.1 GC heating condition for anisole alkylation.....	41
Figure 3.2 Curve of concentration versus % radical scavenging of inhibitor.....	48
Figure 4.1 XRD pattern of Propylsulfonic acid functionalized cubic <i>l</i> α -3d (MCA).....	50
Figure 4.2 Nitrogen sorption isotherm of a) MCAex, b) MCA-Pr-SO ₃ H.....	51
Figure 4.3 SEM images of synthesized MCAex ((a-1) \times 1,500 and (a-2)) \times 5,000, MCA-Pr-SO ₃ H ((b-1) \times 1,500 and (b-2) \times 5,000).....	52
Figure 4.4 TEM images of synthesized MCA-Pr-SO ₃ H.....	53
Figure 4.5 XRD patterns of synthesized ZM-x composite materials.....	55
Figure 4.6 Nitrogen sorption isotherms of ZM-x composite materials.....	56
Figure 4.7 SEM images of a) ZM-10, b) ZM-20, c) ZM-30, d) ZM-40 and e) ZM-50.....	58
Figure 4.8 TEM images of a) ZM-10, b) ZM-20, c) ZM-30, d) ZM-40, and e) ZM-50.....	59

Figure 4.9 XRD patterns of as-synthesis ZM-30 sample A) low angle and B) high angle	61
Figure 4.10 Nitrogen sorption isotherms of extract-ZM-30 composite materials	62
Figure 4.11 XRD patterns of composite materials	64
Figure 4.12 Nitrogen sorption isotherm of a) ZSM-5, b) MCA-Pr-SO ₃ H, c) ZM-30 composite material and d) P-ZM-30 composite material	66
Figure 4.13 SEM micrographs of samples; a) ZSM-5, b) MCA-Pr-SO ₃ H, c) ZM-30 composite material, and d) P-ZM-30 composite material	67
Figure 4.14 TEM images of a, b) MCA-Pr-SO ₃ H and c, d) ZM-30 composite material	68
Figure 4.15 The NH ₃ -TPD profiles of a) ZSM-5, b) MCA-Pr-SO ₃ H, c) ZM-30 composite material and d) P-ZM-30 sample	70
Figure 4.16 X-ray powder diffraction patterns of reused MCA-Pr-SO ₃ H.....	79
Figure 4.17 Nitrogen sorption isotherms of catalysts	80
Figure 4.18 X-ray powder diffraction patterns of reused ZM-30.....	83
Figure 4.19 Nitrogen sorption isotherms of catalysts	83
Figure 4.20 Comparison of radical scavenging of anisole, butylated anisole, BHT and reaction mixtures.....	86
Figure A- 1 Calibration curve of Anisole	97
Figure A- 2 Calibration curve of 2- <i>tert</i> -butyl anisole	98
Figure A- 3 Calibration curve of 4- <i>tert</i> -butyl anisole	99
Figure A- 4 GC chromatogram of products from anisole alkylation over on MCA-Pr-SO ₃ H catalyst	100
Figure A- 5 GC chromatogram of products from anisole alkylation over on ZM-30 catalyst	101
Figure A- 6 GC chromatogram of products from anisole alkylation over on ZSM-5 catalyst	102

LIST OF SCHEMES

Scheme	Page
Scheme 2.1 Schematic models representing “folding sheets” mechanism.....	21
Scheme 2.2 Schematic representation of the S° I° templating mechanism of formation of HMS.....	22
Scheme 3.1 Preparation diagram for propylsulfonic acid functionalized MCA	43
Scheme 3.2 Preparation diagram for ZSM-5/MCA-Pr-SO ₃ H.....	45
Scheme 3.3 Diagram for acid-base titration.....	46



LIST OF ABBREVIATION

Å	Angstrom
a.u.	Arbitrary unit
BET	Brunauer-Emmett-Teller
BJH	Barret, Joyner, and Halenda
°C	Degree Celsius
DPPH	α,α -Diphenyl- β -picrylhydroxyl
g	Gram (s)
hr	Hour (s)
MPTMS	(3-mercaptopropyl)trimethoxysilane
MS	Mass spectroscopy
μm	Micrometer (s)
ml	Milliliter (s)
min	Minute (s)
M	Molarity
nm	Nanometer (s)
%	Percentage
SEM	Scanning electron microscopy
TEM	Transmission electron microscopy
TEOS	Tetraethyl orthosilicate
XRD	X-ray diffraction

CHAPTER I

INTRODUCTIONS

1.1 Statement of problems

Anisole is a by-product from DMC-DPC (Dimethyl carbonate to Diphenyl carbonate) process, which shows in Figure 1.1. Diphenyl carbonate is used as a precursor in the production of polycarbonate through transesterification with Bisphenol A. Moreover, this process provided large amount of anisole. Therefore, anisole alkylation is a very useful process for increasing value on anisole. Amongst these, alkylation of anisole with tert-butanol [1] has been used to produce 4-tert-butyl anisole (4-TBA), 2-tert-butyl anisole (2-TBA) and 2, 4-di-tert-butyl anisole (2, 4-DTBA), which are intermediates for chemical industry. In addition, several mesoporous materials have been synthesized to improve catalytic activity for alkylation of anisole.

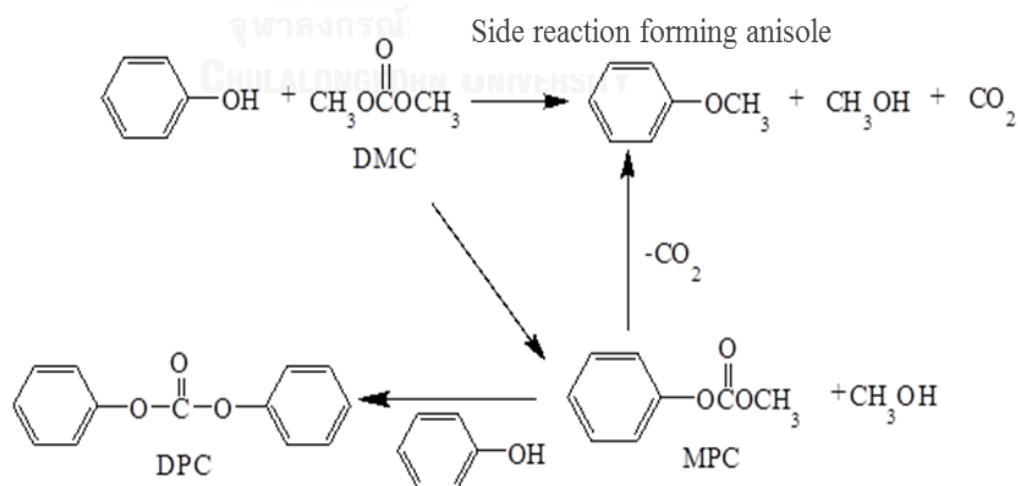


Figure 1.1 The DMC-DPC process that show side product from reaction [2].

Normally, Friedel-Crafts catalysts such as AlCl_3 , FeCl_3 , ZnCl_2 and H_2SO_4 [3] were used for alkylation of aromatics. However, the use of homogeneous catalysts provides rise to many problems concerning corrosive, toxic for environment, the presence of several side products and difficult in separation [4]. In order to avoid these disadvantages from conventional homogeneous catalysts, it is essential to find suitable heterogeneous solid acid catalysts for alkylation reaction that are more selective and environmental-friendly. The heterogeneous catalysts such as clays [5, 6], zeolites [7, 8] and ion exchange resins [9, 10] were used in alkylation of aromatics compound.

The ordered mesoporous MCM-41S family, which are very attractive materials because of their high specific surface area, narrow pore size distributions (from 2-10 nm) and high efficiency as a heterogeneous catalyst. They have been found in many applications as molecular sieves, catalysts, adsorbents, sensors and guest-host chemical supporters. The most well-known representatives of this class include the silica solids such as MCM-41, SBA-15 [11, 12] (with a hexagonal arrangement of the mesopores) and MCM-48 [13] (with a cubic arrangement of the mesopores). To develop application of these mesoporous materials has been modification of the surface by incorporating different the organic-inorganic functional groups widely explored. A wide range of functional groups, including thiol, amine, epoxide, imidazole, nitrile, alkyl, allyl and phenyl, have been incorporated into these silica materials [14-18]. However, the small pore size (>4nm) of these mesoporous materials would probably limit application in the catalytic field if the organic-inorganic functional groups were incorporated into the pore. The synthesis of cubic Ia-3d mesoporous silica with pores larger than 5 nm has attracted much recent attention for medium and large molecular applications. Large-pore mesoporous molecular sieve as a cubic Ia-3d [19, 20] has a three-dimensional (3D) structure which similar structure to MCM-48 structure, but cubic Ia-3d had larger pore diameter. The advantage of 3D structure and large pore can increase the diffusion speed of reactants in the pore and can work with large molecules is interesting to be utilized as catalyst in alkylation reaction [5].

Recently, the porous materials have been developed to the synthesis of various materials combining different porosity that formation of a new generation material which were combined between microporous and mesoporous materials. Zeolite such as ZSM-5, Beta and zeolite Y that are microporous materials (pore size < 2 nm) has been used in several applications [21, 22]. The large advantages of zeolite are good stability, selectivity and activity. In the contrast, the pore size of zeolite was small cannot be used as catalysts for reaction including large molecule. The mesoporous materials such as MCM-41, SBA-15 and MCM-48 (pore size in range of 2-50 nm) contain larger pore that would lead to higher diffusion of reactant when compared with zeolite. On the other hand, mesoporous material have disadvantage is low hydrothermal stability and acidity.

In this work, organic-functionalized cubic mesoporous material and composite material were prepared by using a modification of the method of Kubota et al. [18] In this method, microporous material as ZSM-5 was utilized, that incorporated into cubic Ia-3d (MCA) mesoporous material for synthesis of micro/mesoporous material. ZSM-5 was chosen as microporous material because of the last few decades have brought many reports concerning pore modification of ZSM-5 to enhance para-selectivity products [23]. Moreover, there is no report about the synthesis of ZSM-5/MCA-Pr-SO₃H bi-porous material with different amount of ZSM-5 powder. The prepared materials were test as acid catalysts on anisole alkylation with tert-butanol for produced tertiary butylated methoxy benzene.

1.2 Literature reviews

1.2.1 Porous catalysts synthesis

Phase transformation of the hexagonal mesostructure MCM-41 to the cubic mesostructure MCM-48 was studied by Landry et al [24]. Transformations were studied under conditions of high pH and temperatures between 100 °C and 190 °C. From the results, a model is proposed to explain the expected hexagonal to cubic transformation and illustrate the strong cooperatively between the organic and

inorganic regions in controlling the assembly of the mesostructure effects that control phase transformations in these systems.

The synthesis of cubic *la3d* mesoporous silica with pores larger than 5 nm has attracted much recent attention because this material has potential applications requiring easily accessible uniform large pores. Freddy Kleitz et al [25] reported a new synthesis route to high-quality large mesoporous cubic *la3d* silica, utilizing a commercially available triblock copolymer (EO₂₀PO₇₀EO₂₀)-butanol mixture for the structure direction in aqueous solution. The results show a high-quality, large mesoporous cubic *la3d* silica can be used as a template to fabricate new bicontinuous arrays of nanotube-type carbon (designated as CMK-9 mesoporous carbon), as well as rod-type (CMK-8).

The cubic *la-3d* mesoporous silica with ordered large pores was synthesized from tetraethoxysilane (TEOS) and 3-mercaptopropyltrimethoxysilane (MPTS) as the silica sources by using co-condensation method under the acidic conditions was reported by Kubota et al [18]. The triblock copolymer P123 (EO₂₀PO₇₀EO₂₀) was used as structure directing agent. The gel composition mole ratio was 1 TEOS: 0.089 MPTS: 0.018 P123: 2.0 HCl: 148 H₂O. In addition, the synthesized catalyst was test to synthesize bisphenol A using phenol and acetone as raw materials. From the results, the catalyst showed much higher selectivity of bisphenol A than commercial catalysts.

The synthesis of composites containing zeolite ZSM-5 as microporous phase and MCM-41 material as mesoporous matrix using dually template was reported by Karlsson et al[26]. The n-C₆H₁₃ (CH₃)₃NBr and n-C₁₄H₂₉ (CH₃)₃NBr templates are initially direct the formation of ZSM-5 and MCM-41, respectively. Composite materials were successfully synthesis. It was found that the relative of the two structures MFI and MCM-41 in the final products can be controlled by varying the ratio of the templates and tuning the synthesis temperature.

Composite materials Beta/MCM-48 [27] were synthesized via simultaneous HT treatment of mesoporous precursor solution and colloidal solution containing X-

ray amorphous zeolite seeds. The successfully synthesized micro/mesoporous composite effect to increase the total pore volume relative to zeolite Beta and shift of the pore condensation stepped to higher relative pressure. These materials are expected to provide a large active surface, improved mass transfer and relatively strong acidity, which will result in high catalytic qualities.

Composite micro/mesoporous ZSM-5/MCM-48[28] materials have been prepared using a simple two step crystallisation process. The synthesis process involved the assembly of precursor zeolite species, containing ZSM-5 units at various stages of crystallisation, into a mesostructured material. The varying of time allowed between 2 and 8 hours for the crystallisation of the precursor zeolite species, that able to modify the composition of the composite materials. From the result acidity, hydrothermal stability of the composite materials and textural properties of composite materials were dependent on the extent of zeolitisation.

A direct assembling of zeolite seeds into hexagonal, cubic, wormhole and foam-like framework structures under a variety of assembly conditions was used. Zeolite seeds can also be grafted onto the walls of pre-assembled frameworks to form more stable acidic derivatives. The acidity and hydrothermal stability of the composite materials was found to be dependent on the extent of zeolitization. For examples, zeolite-based composite materials were prepared by embedding Beta nanoparticles from aqueous colloidal solution into matrices of preformed MCM-41 mesoporous material [29].

1.2.2 Anisole alkylation

Kamala et al [1] used Al-MCM-41 molecular sieves as a catalyst for alkylation of anisole using *tert*-butylalcohol. Al-MCM-41 molecular sieves with Si/Al ratios 25, 50, 75 and 100 have been synthesized under hydrothermal condition. The results indicated that Al-MCM-41 (25) was found to be more active than its relatives. The major products are found to be 4-*tert*-butyl anisole (4-TBA), 2-*tert*-butyl anisole (2-TBA) and 2, 4 di-*tert*-butyl-anisole (2,4DTBA).

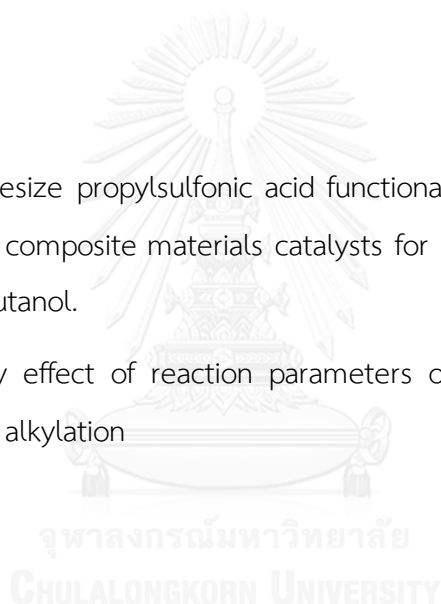
Hong-jun Dong and Li Shi [30] reported alkylation of toluene with *tert*-butylalcohol using three zeolite catalysts (HY, H, and HMCM-22). The main reaction products had been identified as 4-*tert*-butyltoluene and 3-*tert*-butyltoluene. The conversion of toluene over HMCM-22 was higher than other zeolites, because of its highest acidity.

Bao Shaohua et al [31] studied the effect of the alkylation of *p*-cresol with *tert*-butylalcohol catalyzed by the novel multiple-SO₃H ionic liquid (IL1). Under the optimum reaction conditions (*p*-cresol: TBA, 1:1; cyclohexane 3 ml; 343 K; 7 h.) the conversion of *p*-cresol and the selectivity to TBC were 85.3% and 95.2% respectively.

1.3 Objectives

1.3.1 To synthesize propylsulfonic acid functionalized cubic Ia-3d mesoporous silica and ZSN-5/MCA composite materials catalysts for using as catalysts in alkylation of anisole with *tert*-butanol.

1.3.2 To study effect of reaction parameters on product yield and product distribution in anisole alkylation



1.4 Scopes of work

1.4.1 Synthesize propylsulfonic acid functionalized cubic *Ia-3d* mesoporous silica by using co-condensation method.

1.4.2 Synthesize ZSM-5/MCA composite materials by using seeding method.

1.4.3 Characterize synthesized materials with XRD, N₂ adsorption-desorption, NH₃-TPD, SEM and TEM.

1.4.4 Determine the reaction parameter of anisole alkylation with *tert*-butanol

-Type of catalyst; ZSM-5, Amberlyst-15, SBA-15-Pr-SO₃H, MCA-Pr-SO₃H

-Mole ratio of anisole to *tert*-butanol; 1:1-1:9

-Reaction temperature; 120-175 °C.

-Reaction time; 1-10 h.

-Catalytic amount; 0-7.5 %wt base on total weigh

CHAPTER II

THEORY

2.1 Catalysts

A catalyst is a substance that speeds up the rate of a chemical reaction but is not consumed during the course of the reaction. A catalyst is substance that can make a reaction occur faster by reducing the activation energy (E_a), as shown in Figure 2.1 but the chemical unchange at the end of the reaction. The highest peak position referred the highest energy need to reach the transition state. In typically reaction, the input of energy to enter the transition state is high, whereas the catalytic reaction need lower amount of energy to start a reaction. In addition, a catalyst enable a chemical process to work more efficiently, more selective manner and often with less waste. Therefore, catalysts are essential in industrial chemistry.

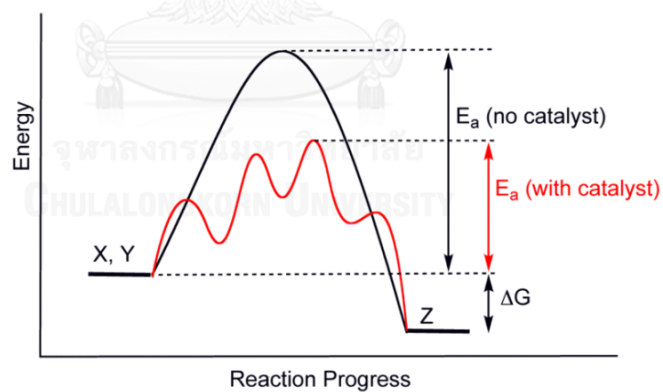


Figure 2.1 The relationship between activation energy (E_a) and enthalpy (ΔH) of the reaction with and without a catalyst [32].

2.1.1 Type of catalyst

Type of catalyst is classified into two main type by the boundary of the catalyst and the reactant [33]. Homogeneous catalysts are similar phase with the reagents, and heterogeneous catalysts, which are separated from the reactants by an interface (e.g. metals, metal oxides, etc.). The main characteristics of the catalysts are their activity and selectivity; in addition, they vary in heat resistance, mechanical strength (for heterogeneous systems), stability, resistance to catalyst poisons and other parameters. Summary of the advantage and disadvantage of two-type catalyst is presented in Table 2.1.

Table 2.1 Comparison of homogeneous and heterogeneous catalysts

Consideration	Homogeneous catalyst	Heterogeneous catalyst
1. Active centers	All metal atoms	Only surface atoms
2. Concentration	Low	High
3. Selectivity	High	Low
4. Diffusion problems	Practically absent	Present (mass-transfer-controlled reaction)
5. Reaction conditions	Mild (50-200°C)	Severe (often >250°C)
6. Applicability	Limited	Wide
7. Activity loss	Irreversible reaction with product (cluster formation), poisoning	Sintering of the metal crystallites, poisoning
8. Modification possibility	High	Low
9. Thermal stability	Low	High
10. Catalyst separation	Sometimes laborious (chemical decomposition, distillation, extraction)	Fixed-bed: unnecessary Suspension: filtration
11. Catalyst recycling	Possible	Unnecessary (fixed-bed) or easy (suspension)
12. Cost of catalyst	High	Low

2.2 Porous molecular sieve

Molecular sieves are porous materials that exhibit selective adsorption properties which can be classified on the IUPAC definitions into three main types depending on their pore sizes that are microporous materials, mesoporous materials, and macroporous materials. Properties and examples of these materials are shown in Table 2.2

Table 2.2 IUPAC classification of porous materials [34]

Type of porous molecular sieve	Pore size (Å)	Examples
Microporous materials	< 20	Zeolites, Activated carbon
Mesoporous materials	20 – 500	M41s, SBA-15, Pillared clays
Macroporous materials	> 500	Glasses

2.3 Microporous materials

Micropores are occasionally classified into smaller-size ultramicropores (less than 0.7 nm) and supermicropores that are larger than ultramicropores but smaller than mesopores. Microporous materials include carbon absorbents, silica gels, zeolites, certain clay types, etc. Due to the small distance between the pore walls, the absorption mechanism in micropores is drastically different from absorption of a flat surface or in large pores [35].

Zeolites are crystalline aluminosilicates with open 3D framework structures built of SiO_4 and AlO_4 tetrahedra linked to each other by sharing all the oxygen atoms to form regular intra-crystalline cavities and channels of molecular dimensions. The tetrahedral are cross-linked by the sharing of oxygen atoms as shown in Figure 2.2.

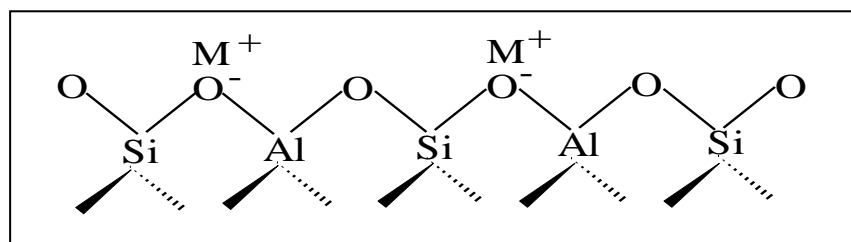


Figure 2.2 The structure of zeolites.

The Structure Commission of the International Zeolite Association (IZA) identified zeolite framework topology by a three capital letter code such as MER, MFI, MOR, MTT, RHO, TON and MWW. The different applications of these materials are related to their properties of ion exchange, acidity, high activity, thermal stability and shape selectivity [36].

The marvelous importance of zeolites and related materials in a variety of catalytic processes can be attributed to their superior properties in comparison with other types of materials. Some of their advantages are listed below:

1. Large surface area and adsorption capacity
2. The possibility of controlling the adsorption properties by tuning the hydrophobicity or hydrophilicity of the materials
3. The pore openings and cavities in the range of 5-12 Å
4. Insoluble materials and well defined pore structures
5. Different types, different properties
6. The presence of shape and size selectivity

2.3.1 Basic units of zeolites

A zeolite has a three dimensional network structure of tetrahedral primary building units (PBU) which made of four oxygen anions with either silicon $[\text{SiO}_4]$ or aluminum cation $[\text{AlO}_4]^-$ in the center as shown in Figure 2.3.

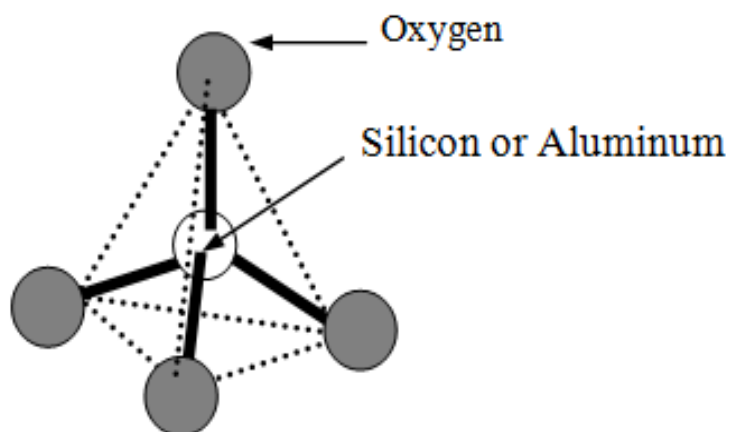


Figure 2.3 A primary building units of porous materials

Primary building units are linked together to form secondary building units. The secondary building units consist of n-ring structures which can contain as many as 20 tetrahedra. The secondary building units consist of 4, 6 and 8-member single ring, 4-4, 6-6 and 8-8 member double rings, and 4-1, 5-1 and 4-4-1 branched rings as illustrated in Figure 2.4

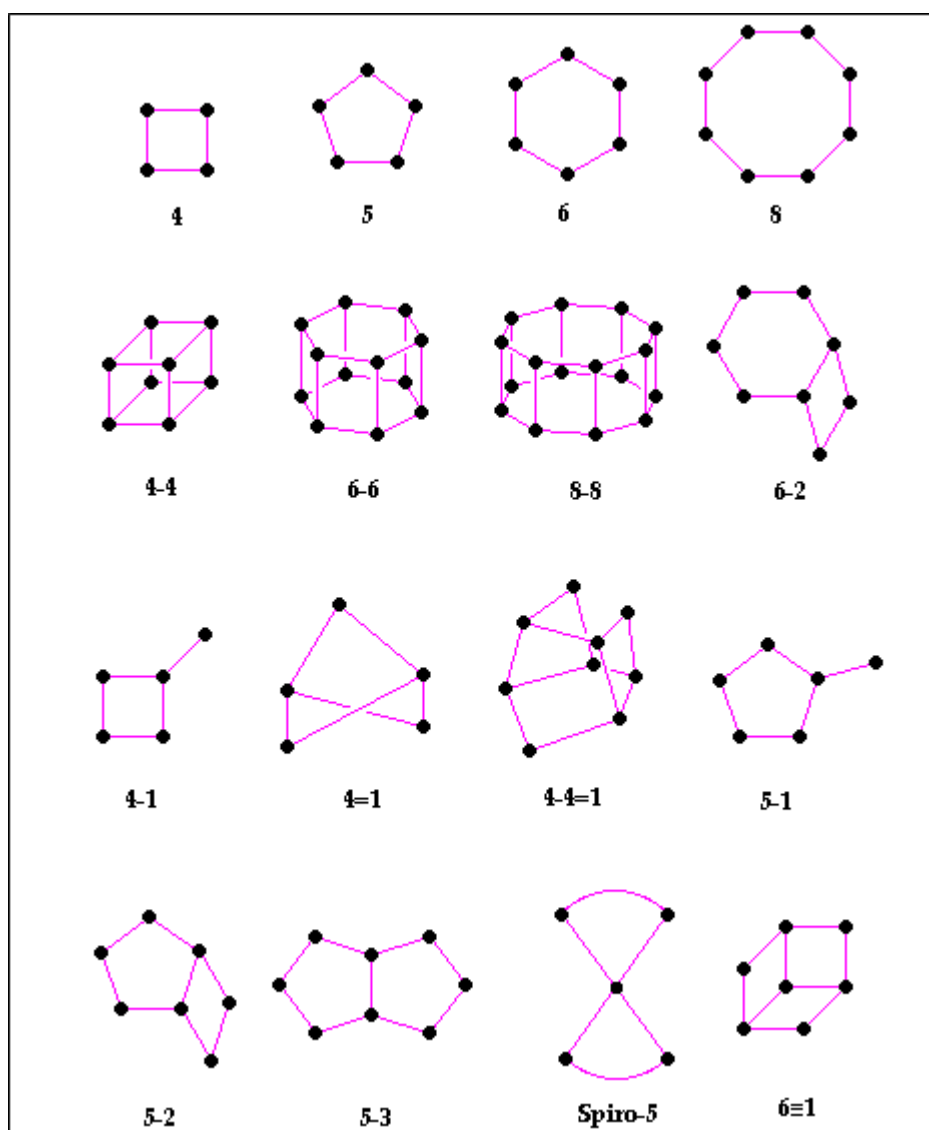


Figure 2.4 Secondary building units found in zeolite structures.

Most porous material frameworks can be generated from numerous different SBUs. For example, the sodalite framework can be built from either the single 6-member ring or the single 4-member ring. The different pore sizes found in zeolites were due to the different number of tetrahedral atoms defining the opening, as shown in Figure 2.5.

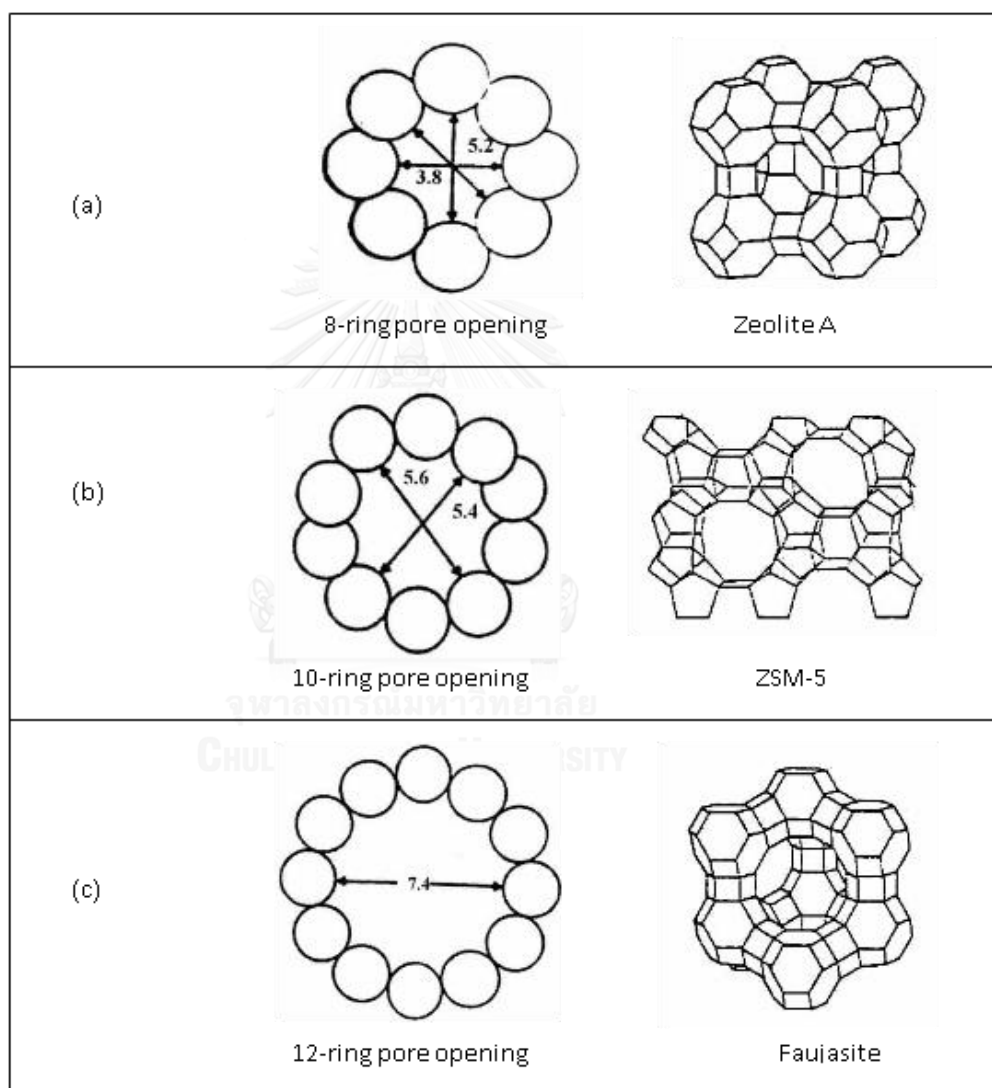


Figure 2.5 Examples of the three types of pore openings in the zeolite molecular sieves, (a) small pore zeolite, (b) medium pore zeolite and, (c) large pore zeolite

2.3.2 Zeolite ZSM-5

ZSM-5, Zeolite Socony Mobil-5, (framework type, MFI) is an aluminosilicate zeolite belonging to the pentasil family of zeolites. Structurally zeolites ZSM-5 are the crystalline aluminosilicates with a framework based on an extensive three-dimensional network of oxygen ions. ZSM-5 is composed of several pentasil units linked together by oxygen bridges to form pentasil chains. A pentasil unit consists of eight five-membered rings. From Figure 2.6 show pentasil unit and three-dimensional structure of ZSM-5. ZSM-5 is a medium pore zeolite with channels defined by ten-membered rings.

ZSM-5 has high silicon to aluminum ratio. Whenever an Al^{3+} cation replaces a Si^{4+} cation, an additional positive charge is required to keep the material charge-neutral. With proton (H^+) as the cation, the material becomes very acidic. Thus the acidity is proportional to the Al content. The very regular 3-D structure and the acidity of ZSM-5 can be utilized for acid-catalyzed reactions such as hydrocarbon isomerization and the alkylation of hydrocarbons.

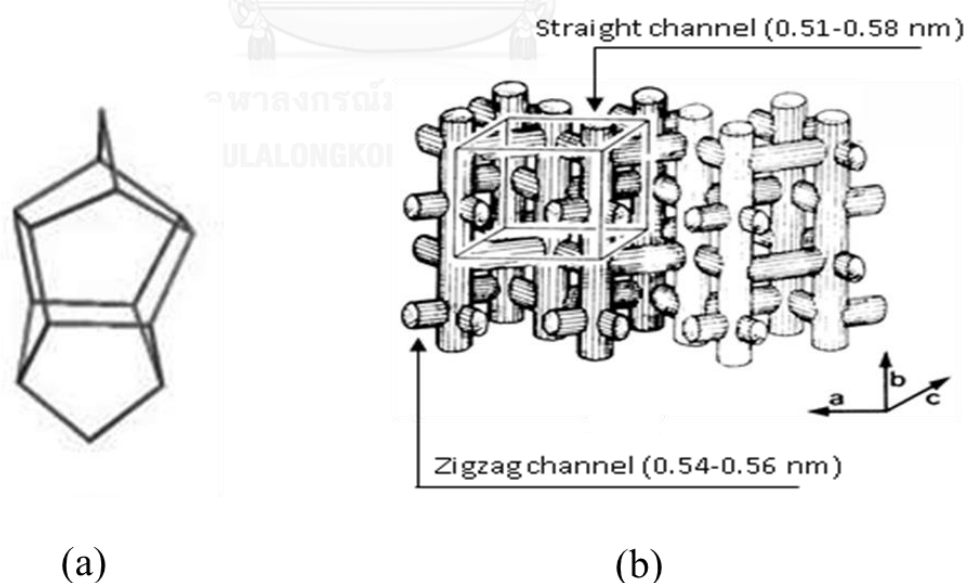


Figure 2.6 (a) The pentasil unit and (b) three-dimensional structure of ZSM-5.

2.3.4 Properties of zeolite ZSM-5

Zeolite ZSM-5 was used in many industrially catalytic processes and had been the subject of extensive research. The accessibility to the catalytic sites in ZSM-5 is best viewed by considering its channel system as three-dimensional structure. And also, the shape-selective and acidity of ZSM-5 were used industrially catalytic processes.

2.3.4.1 Acid site of ZSM-5

Zeolite acts as the acid catalyst due to the present of acid site. Brønsted acidity is at the proton donor site, and electron deficient atom that can accept an electron pair behaves a Lewis acid site. Both types of acid site of zeolite were shown in Figure 2.7.

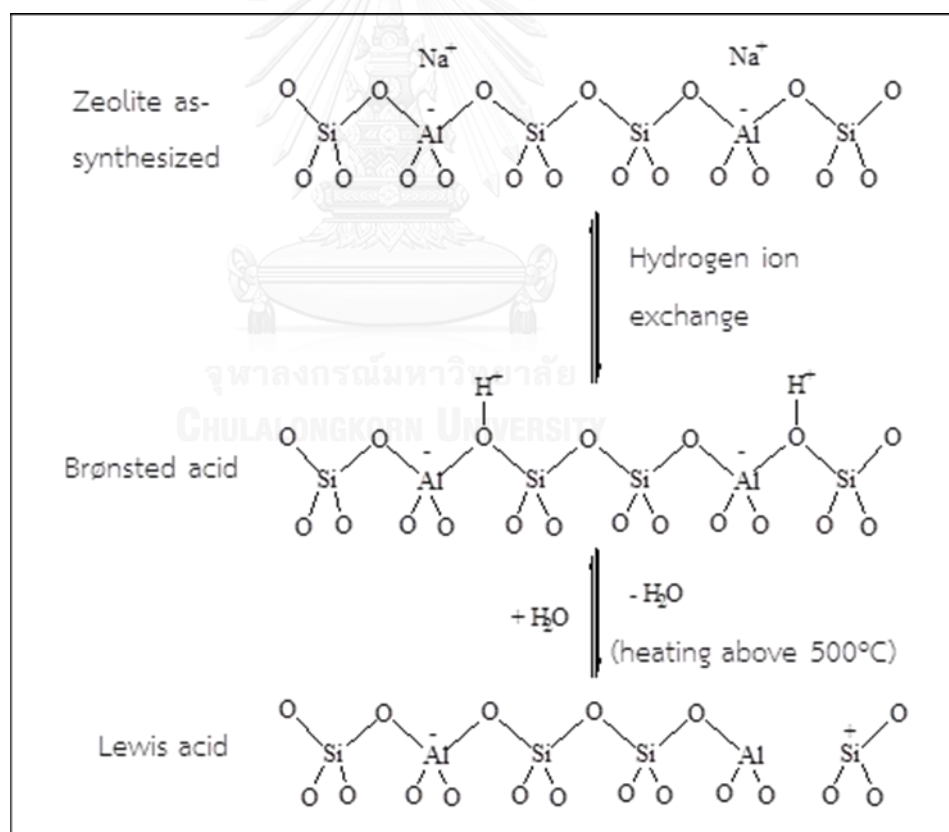


Figure 2.7 The generation of Brønsted and Lewis acid sites in zeolite

2.3.4.2 shape-selective of ZSM-5

There are three types of shape selective characteristics of zeolites as reactants shape selectivity, products shape selectivity and transition states shape selectivity. These types of selectivity are showed in Figure 2.8

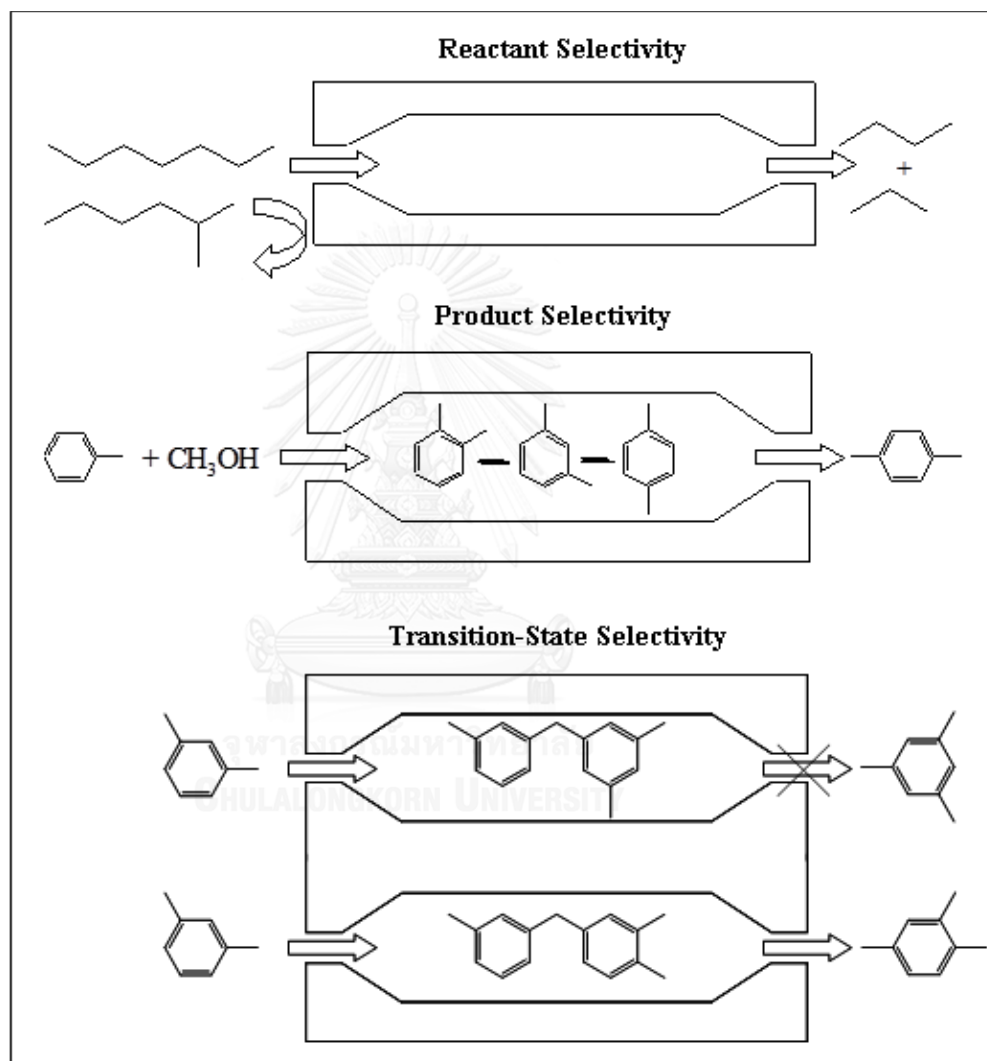


Figure 2.8 Three types of selectivity in zeolites.

2.4 Mesoporous materials

Mesoporous materials are a class of molecules with a large and uniform pore size, highly regular nanopores, and a large surface area. Mesoporous silica has uniform pore sizes from 20 to 500 Å and has found great utility as catalysts and sorption media because of the regular arrays of uniform channels. Larger surface area is desired for enhancing of the efficient in the reactions.

The silica surface catalyst contains reactive silanol (Si-OH) groups which easily react with organic functionalities for allowing to organic/inorganic hybrid material creation. The silica surface comprises a combination of isolated silanols (Figure 2.9(a)), germinal silanols (Figure 2.9 (b)), vicinal silanols (Figure 2.9 (c)) and siloxane bridges (Figure 2.9(d)). All of silanol species can be alter to prepare organic/inorganic hybrid material [30].

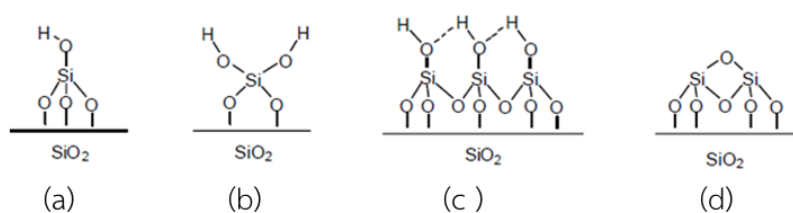


Figure 2.9 Types of silica surface Si-O species.

2.4.1 Classification of mesoporous materials

Mesoporous materials can be classified by different synthetic methods. By varying different types of templates used and pH of gel for synthesizing hexagonal mesoporous materials new hexagonal materials can be obtained. The interaction of various types of template with inorganic species for assembling these materials are different as summarized in Table 2.3, together with the condition typically employed for a synthesis.

Table 2.3 Various synthesis conditions of hexagonal mesoporous materials and the type of interaction between template and inorganic species

Surfactant type	Inorganic type	Interaction type	example materials
Cationic (S^+)	I^-	S^+I^-	MCM-41, MCM-48
	I^+X^-	$S^+X^-I^+$	SBA-1, SBA-2, zinc phosphate
	I^0F^-	$S^+F^-I^0$	silica
Anionic (S^-)	I^+	S^-I^+	Al, Mg, Mn, Ga
	I^-M^+	$S^-M^+I^-$	alumina, zinc oxide,
Neutral S^0 or N^0	I^0	S^0I^0 or N^0I^0	HMS, MSU-X, aluminum oxide
	I^+X^-	$S^0X^-I^+$	SBA-15

Where S^x or N^x : surfactant with charge of X

I^x : inorganic species with charge of X

X^- : halogenide anions

F^- : fluoride anion

M^{n+} : with charge of X

There are three different mesophases in M41S family have been identified i.e., lamellar, hexagonal and cubic phase. MCM41 has a hexagonally packed array of cylindrical pores. The structure of MCM48 has a three-dimensional, cubic-ordered pore structure and MCM-50 contains a lamellar structure as illustrated in Figure 2.10.

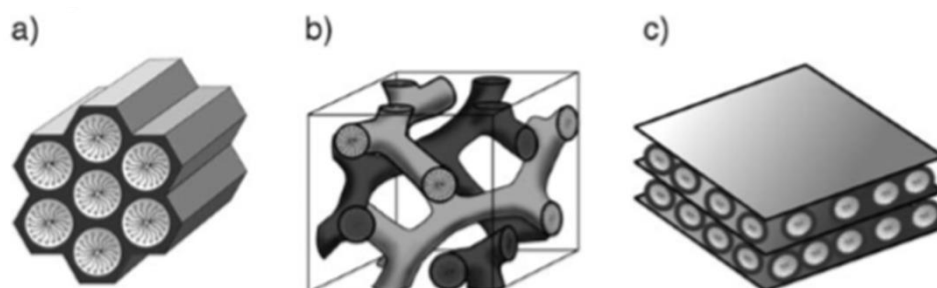


Figure 2.10 Structures of mesoporous M41S materials: a) MCM-41 (2D hexagonal, space group $p6mm$), b) MCM-48 (cubic, space group $la3-d$), and c) MCM-50 (lamellar, space group $p2$).

2.4.2 Formation mechanism of mesoporous materials

2.4.2.1 Liquid crystal templating mechanism

In true liquid-crystal templating (TLCT), the concentration of the surfactant is so high that under the prevailing conditions (temperature, pH) a lyotropic liquid-crystalline phase is formed without requiring the presence of the precursor inorganic framework materials (normally tetraethyl- (TEOS) or tetramethylorthosilica (TMOS)). On the other hand, it is also possible that this phase forms even at lower concentrations of surfactant molecules, for example, when there is cooperative self-assembly of the SDA and the already added inorganic species, in which case a liquid-crystal phase with hexagonal, cubic, or laminar arrangement can develop

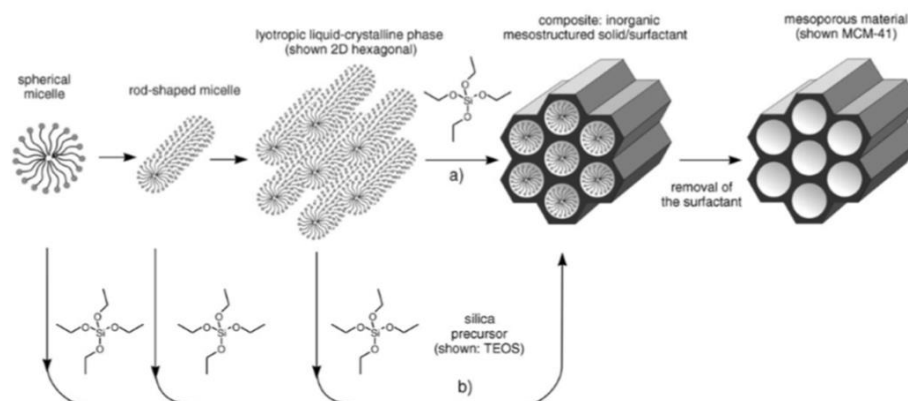


Figure 2.11 Two possible ways for the LCT mechanism

2.4.2.2 Folding sheet formation

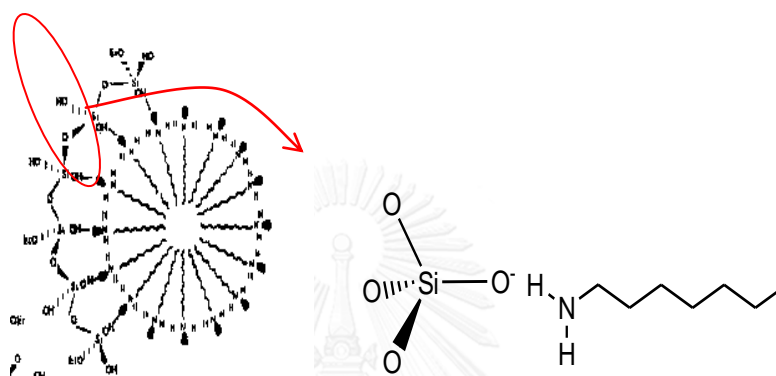
The intercalation of ammonium surfactant into hydrated sodium silicate, which is composed of single-layered silica sheets called kanemite, produces the lamellar-to-hexagonal phase in FSM-16. After surfactants were ion-exchanged into the layered structure, the silicate sheets were folded around the surfactants and condensed into hexagonal mesostructure.



Scheme 2.1 Schematic models representing "folding sheets" mechanism

2.4.2.3 Hydrogen bonding interaction

This neutral templating synthesis route produced mesoporous silicates with thicker walls and higher thermal stability compared to the LCT-derived silicates. The silicate framework in the resulting mesophase was neutrally charged. From this reason, the surfactant can be easily removed by solvent extraction.



Scheme 2.2 Schematic representation of the $S^0 I^0$ templating mechanism of formation of HMS

2.5 Cubic $Ia-3d$ Mesoporous silica (MCA)

The cubic $Ia-3d$ mesoporous silica (MCA) was synthesized by using Pluronic P123 as the structure directing agent [20]. This mesoporous silica with pores larger than 5 nm has attracted much recent attention for potential applications requiring easily accessible uniform large pores. The cubic $Ia-3d$ mesoporous has similarly mesostructure with MCM-48, which was synthesized by using cetyltrimethylammonium bromide (CTAB) as the structure directing agent. Moreover, the pore size of MCA is larger than MCM-48 so it can react with larger molecules. Comparison of MCA and MCM-48 properties were shown in Table 2. 4

Table 2. 4 Properties of MCA and MCM-48[37]

Properties	MCA	MCM-48
Pore size (nm)	5.3-7.5	3.3-3.1
Pore volume (cm ³ /g)	1.03-1.30	0.53-0.80
Surface area (m ² /g)	1,022-1,152	660-1,010

2.6 Modification of catalyst by organic functionalization

Nowadays, the attachment of organic functionalities such as sulfonic acid groups to the surface of siliceous mesoporous material is an interesting research area in heterogeneous catalysis and green chemistry. Alkyl sulfonic acid functionalized mesoporous silica can be usually prepared by two methods; Co-condensation method and Grafting method.

2.6.1 Co-condensation method

This method is one-step process in which hydrolysis and condensation of tetraethoxysilane (TEOS) and 3-mercaptopropyltrimethoxysilane (MPTMS) in the presence of the corresponding structure-directing agent as show in Figure 2.12. Calcination the synthetic material will destroy the incorporated organic functional groups. Extraction technique can be most effectively accomplished by ethanol solution. Although this process provides a better control of the distribution of organic functional group in the surface of mesoporous material.

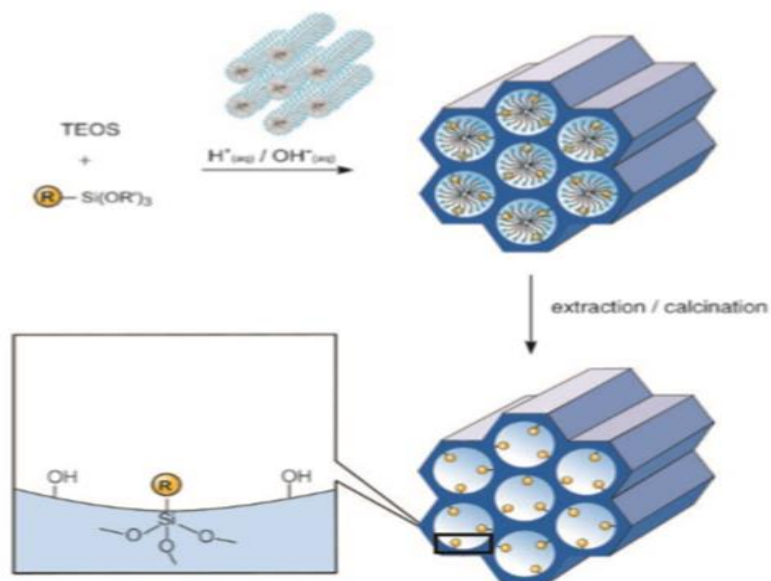


Figure 2.12 Co-condensation methods (direct synthesis) for the organic modification of mesoporous pure silica phases. R=organic functional group.

2.6.2 Post synthesis (Grafting)

Grafting procedure based on modification of the silica surface with organic groups through silylation reaction occurring on isolated ($\equiv Si-OH$). Synthesis of sulfonic functionalized mesoporous materials by post synthesis is shown Figure 2.13. In typical procedure, calcined material is treated with a silylating agent like 3-mercaptopropyltrimethoxysilane (MPTMS) in nonpolar solvent (commonly toluene) to immobilize thiol groups on the surface. These thiol functionalities are then oxidized, normally using hydrogen peroxide (H_2O_2). The most apparent advantage of this procedure is good preservation of the mesostructure after post-modification.

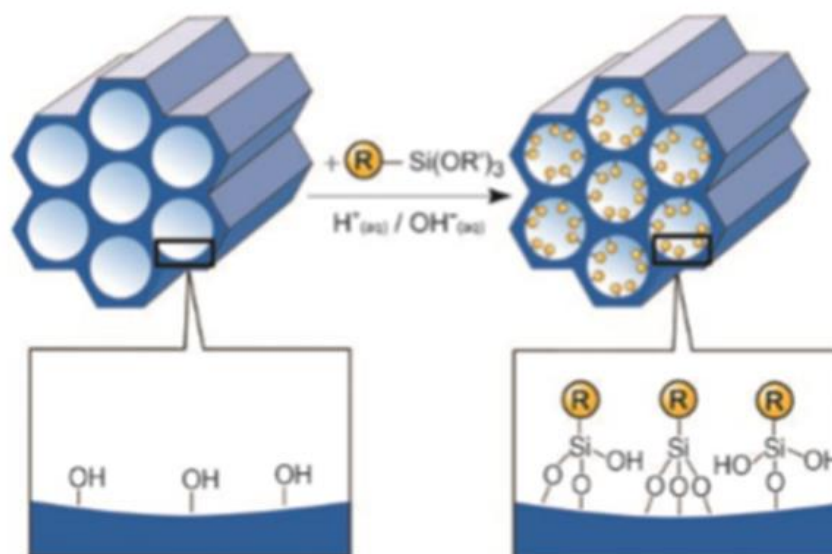


Figure 2.13 Grafting (postsynthetic functionalization) for organic modification of mesoporous pure silica phases with terminal organosilanes of the type $(\text{R}'\text{O})_3\text{SiR}$, R=organic functional group.

2.7 Composite materials

Porous materials are widely applied for various applications in industry. During the last several years, these materials have been developed to the synthesis of various materials combining different porosity that formation of a new generation material which were combined between microporous material and mesoporous material. Zeolite such as ZSM-5, Beta and zeolite Y that are microporous material (pore size < 2 nm) has been used several applications. The large advantages of zeolite are good stability, selectivity and activity. In the contrast, the pore size of zeolite was small cannot be used as catalysts for reaction including large molecule. The mesoporous materials such as MCM-41, SBA-15 and MCM-48 (pore size in range of 2-50 nm) contain large pore that would lead to higher diffusion of reactant when compared with zeolite. On the other hand, mesoporous material have disadvantage is low hydrothermal stability and acidity. Therefore, have several report effort to

combine advantages of both micro and mesoporous material is to prepare catalysts in order to overcome disadvantage of these material.

Synthesis of composite materials

There are numerous approaches for preparation of micro/mesoporous materials were foreseen, a significant progress in the preparation of composite compounds with improved properties is attained via :(i) a partial crystallization of amorphous pore walls; (ii) the use of zeolite seeds as framework building units; (iii) preparation of mesoporous zeolites and post-synthesis treatment of microporous materials, and (iv) substrate-templated approach [38]. Schematic representation of possible reaction routes leading to the formation of micro/mesoporous composite was shown in Figure 2.14.

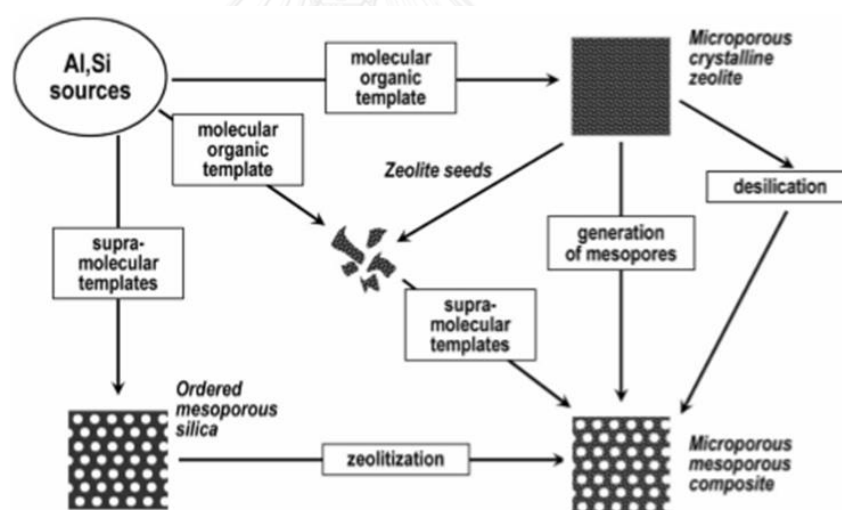


Figure 2.14 Schematic representation of possible reaction routes leading to the formation of micro/mesoporous composite.

2.7.1 Synthesis of composite materials by recrystallization of mesoporous materials

There are two templates were used in synthesis of composite materials. This approach comprises the synthesis of amorphous mesoporous precursor followed by an additional hydrothermal treatment resulting in the formation of partially microporous crystalline walls of the mesoporous matrix. This method is called “dual templating”, and show in Figure 2.15.

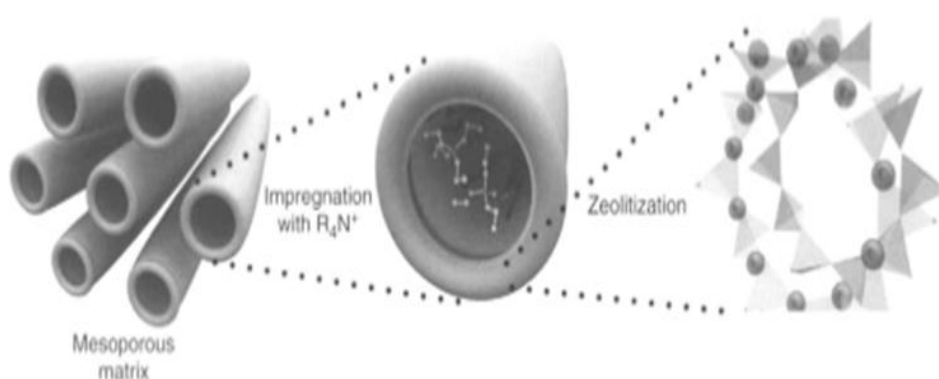


Figure 2.15 Mechanism of the Synthesis of composite materials by dual templating

For example, the synthesis of ZSM-5/MCM-41 [26] composites material, The zeolite ZSM-5 as microporous phase and MCM-41 material as mesoporous matrix using dual templated gels. There are two templates as $n\text{-C}_6\text{H}_{13}(\text{CH}_3)_3\text{NBr}$ and $n\text{-C}_{14}\text{H}_{29}(\text{CH}_3)_3\text{NBr}$ are initially direct the formation of ZSM-5 and NCM-41. Moreover, the amount of templates, $n\text{-C}_6\text{H}_{13}(\text{CH}_3)_3\text{NBr}$ are the most important factors controlling the preparation of micro/mesoporous structures.

2.7.2 Synthesis of composite materials by using zeolite seeds as framework-building units

Zeolite seeds are used to promote the formation of micro/mesoporous composites and also are used as building blocks for self-organization in the mesoporous matrices (Figure 2.16). A direct assembling of zeolite seeds into hexagonal, cubic, wormhole and foam-like framework structure under a variety of assembly conditions was used. The main advantage of composite materials by using zeolite seeds is the substantial increase of their hydrothermal stability and increase in the acidity related to the properties of zeolite [39].

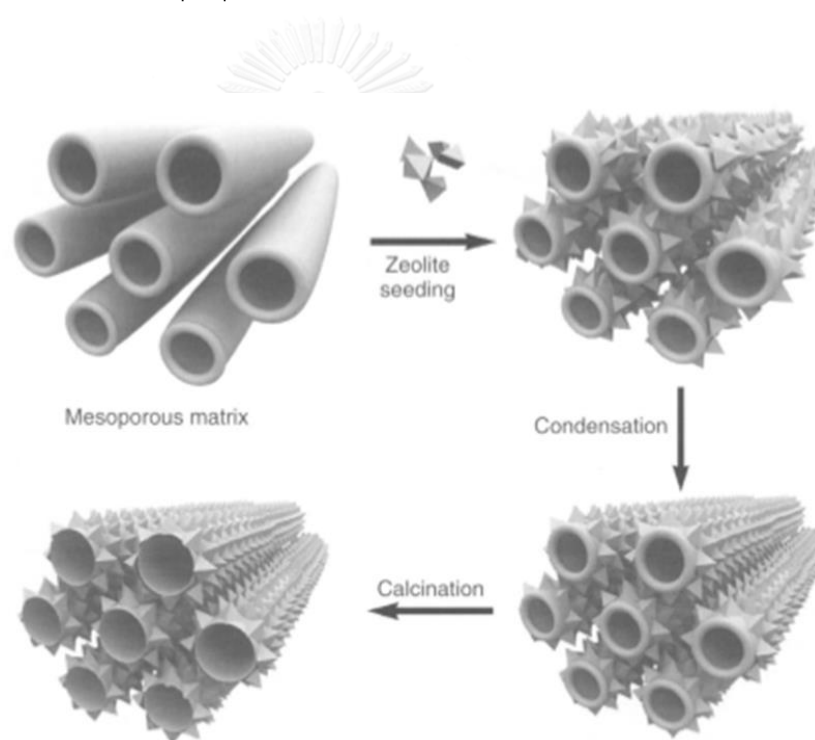


Figure 2.16 Mechanism of self-organization of zeolite seeds onto mesoporous matrix

2.7.3 Synthesis of composite materials by post-synthesis treatment of microporous materials

Post-synthesis treatments of parent zeolites used to alter the Si/Al ratio and the corresponding acidic properties, also create certain extra-porosity due to the presence of defect sites in the zeolite framework upon post-treatment. The alkaline treatment is more novel and leads to a significant mesopore formation, a lower Si/Al ratio, and small changes in framework acidity. The removal of silicon atom occurs upon treatment of the zeolite in alkaline solution and was initially applied to ZSM-5 structures in the treated zeolites, like the preferential dissolution of Si and Al. The mesopores provide improved access to the micropores and shorten the diffusion path length, thereby enhancing the rate of diffusion and thus the catalytic performance. Synthesis of composite materials can be prepared by treatment of natural zeolites, which results to high stability of materials led to application for removal of contaminants from water, pathogens from sewage and organic compounds from oilfield water.

2.7.4 Synthesis of composite materials by substrate-template porous materials

The composite materials from this method can be prepared by the extension of the template strategy originally employed in the synthesis of zeolites. In addition, the utilization of templates with specific macromorphological features is controlling both the shape and the size of the solids. Silica-containing plants, polystyrene beads and anion exchange resins are the most frequently used templates resulting in self-bonded macrostructures with different appearance, porosity and mechanical strength upon template removal. For example, the polystyrene beads were employed in the preparation of hollow zeolite spheres, which show in Figure 2.17.

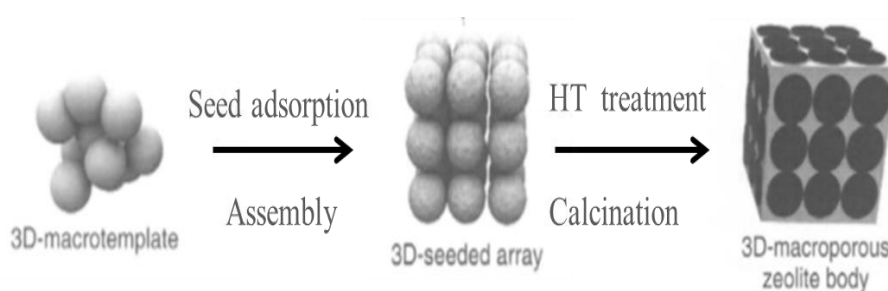


Figure 2.17 Polystyrene beads were used template in the preparation of hollow zeolite spheres.

2.8 Characterization of materials

A variety of experimental techniques of materials including X-ray powder diffraction (XRD), N_2 adsorption-desorption technique, temperature-programmed desorption of ammonia (NH_3 -TPD), acid-base titration, scanning electron microscope (SEM), and transmission electron microscope (TEM).

2.8.1 X-ray powder diffraction (XRD)

X-ray powder diffraction (XRD) is an instrumental technique used to identify minerals, as well as other crystalline materials. XRD can provide additional information beyond basic identification. In general, crystal diffracts the X-ray beam differently, depending on its structure and orientation. The diffracted X-ray is collected by an area detector. The diffraction pattern consists of reflections of different intensity which can be used to determine the structure of the crystal. The XRD peaks appear at low angle (2θ angle between 0.5 and 3 degree) identify cubic mesoporous structure and high angle (2θ angle between 5 and 50 degree) identify ZSM-5 microporous structure. For the composite materials, XRD patterns in both 2θ regions are commonly collected and compared with pure materials. The resolution of an X-ray diffraction detector is determined by the Bragg equation.

Braggs' law is able to determine the interplanar spacing of the samples, from diffraction peak according to Bragg angle.

$$n\lambda = 2d \sin\theta$$

Where the integer n is the order of the diffracted beam, λ is the wavelength; d is the distance between adjacent planes of atoms (the d -spacings) and θ is the angle of between the incident beam and these planes.

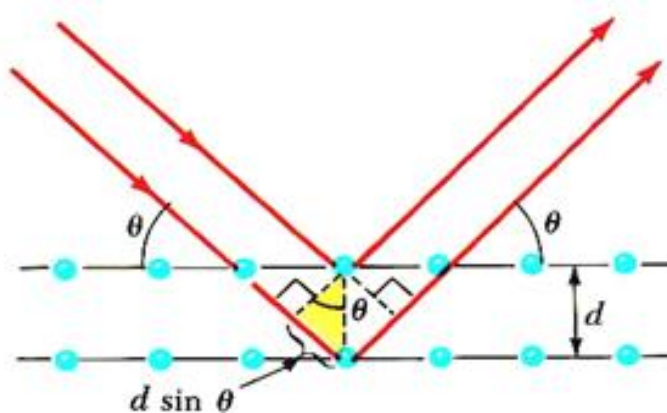


Figure 2.18 Diffraction of X-ray by regular planes of atoms

จุฬาลงกรณ์มหาวิทยาลัย
CHULALONGKORN UNIVERSITY

2.8.2 N₂ adsorption-desorption technique

The N₂ adsorption technique is used to determine the physical properties of porous materials, such as the surface area, pore volume, and pore-size distribution of solid catalysts. Adsorption of gas by a porous material is described by an adsorption isotherm, the amount of adsorbed gas by the material at a fixed temperature as a function of pressure. The porosity of the samples is determined in physisorption experiments and expressed as isotherm. The type of the porosity of materials is discussed further based on IUPAC classification of adsorption isotherms is illustrated in Figure 2.19. There are microporous (type I), nonporous or macroporous (types II, III, and VI) or mesoporous (types IV and V). The specific surface area was calculated from adsorption data in the relative pressure (P/P_0) range = 0.1-0.25 using the

Burnauer-Emmett-Teller (BET) whereas the distribution of the pores and total pore volume were evaluated by use of *Barrett-Joyner -Halenda* (BJH) method, and the micropore volume and external surface area were evaluated by *t*-plot method.

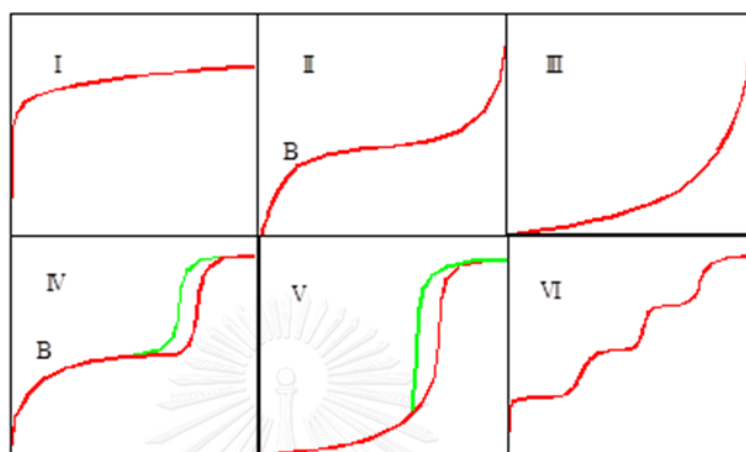


Figure 2.19 The IUPAC classification of adsorption isotherms.

Adsorption isotherms are described as shown in Table 2.5 based on the strength of the interaction between the sample surface and gas adsorbate, and the existence or absence of pores.

Table 2.5 Features of adsorption isotherms

Type	Features	
	Interaction between sample surface and gas adsorbate	Porosity
I	Relatively strong	Micropores
II	Relatively strong	Nonporous
III	Weak	Nonporous
IV	Relatively strong	Mesopore
V	Weak	Micropores or Mesopore
VI	Relatively strong sample surface has an even distribution of energy	Nonporous

The hysteresis loops can be divided into four categories based on the IUPAC guideline, as shown in Figure 2.20. The shapes of hysteresis loops are associated with specific pore structures[40].

H1 type loops tend to have relatively narrow distributions of pore size such as SBA-15 and MCM-41. The adsorption and desorption branches of H1 are almost vertical and nearly parallel over an appreciable range of gas uptake.

H2 type loops, the hysteresis loop is wide, and the desorption curve is more precipitous than the adsorption curve. This situation usually occurs when the distributions of pore size radii are wide.

H3 type loops, the hysteresis loop associated with slit-shaped pores and panel-shaped particles.

H4 type loops, the adsorption and desorption branches of H4 are almost horizontal and nearly parallel over a wide range of relative pressure. However, the exhibition of H4 loops indicates the existence of the micro porous materials.

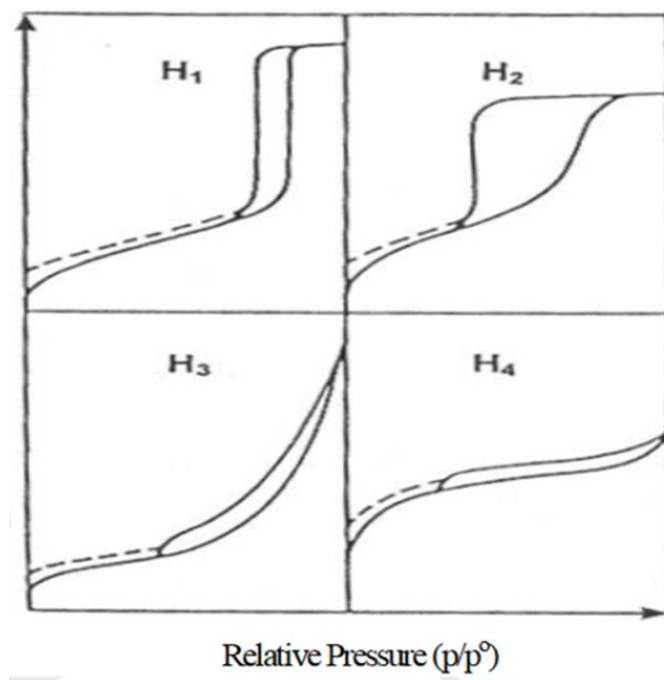


Figure 2.20 Classification of adsorption isotherms with hysteresis loops

2.8.3 Temperature-programmed desorption of ammonia (NH₃- TPD)

The acidity of catalysts was analyzed by temperature programmed desorption of NH₃ (NH₃-TPD), which is one of the most widely used and flexible techniques for characterizing the acid sites on oxide surfaces. Normally, zeolites provide desorption two peaks of TPD spectra, these are lower temperature peak (L-peak) and higher temperature peak (H-peak), respectively. The H-peak is the desorption peak of ammonia adsorbed on the strong acid site, whereas the L-peak was assigned to ammonia weakly held or physically adsorbed on sites like silanol groups. Only the H-peak region was found to correlate with the A1 content, acidity, and catalytic activity of zeolite.

2.8.4 Scanning electron microscope (SEM)

The scanning electron microscope (SEM) has unique capabilities for analyzing surfaces and morphology of materials. The diagram in Figure 2.21 showed the major components of an SEM. These components are part of seven primary operational systems: vacuum, beam generation, beam manipulation, beam interaction, detection, signal processing, and display and record. These systems function together to determine the results and qualities of a micrograph such as magnification, resolution, depth of field, contrast, and brightness.

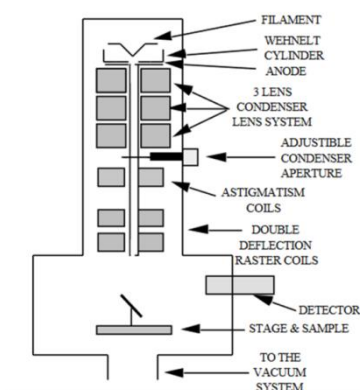


Figure 2.21 Diagram of SEM column and specimen chamber

The scanning electron microscope (SEM) is one of the most versatile instruments available for the examination and analysis of the microstructure morphology and chemical composition characterizations. It is necessary to know the basic principles of light optics in order to understand the fundamentals of electron microscopy. The unaided eye can discriminate objects subtending about $1/60^\circ$ visual angle, corresponding to a resolution of ~ 0.1 mm (at the optimum viewing distance of 25 cm). Optical microscopy has the limit of resolution of $\sim 2,000$ Å by enlarging the visual angle through optical lens. The electron microscopy has been developed by replacing the light source with high energy electron beam. In this section, we will, for a split second, go over the theoretical basics of scanning electron microscopy including the resolution limitation, electron beam interactions with specimens, and signal generation.

2.8.5 Transmission electron microscope (TEM)

The transmission electron microscope is a very powerful tool for material science. This technique is used for measuring the size, size distribution and morphology of particles. TEM involves a beam of accelerated electron, 50-200 keV, emitted by a tungsten filament cathode in vacuum. A high energy beam of electrons is shone through a very thin sample, and the interactions between the electrons and the atoms can be used to observe features such as the crystal structure. A schematic diagram of transmission electron microscope is shown in Figure 2.22. The images from electron microscopes indicate the shape of a sample crystallite which can be used to determine size and morphology of solid nanoparticles.

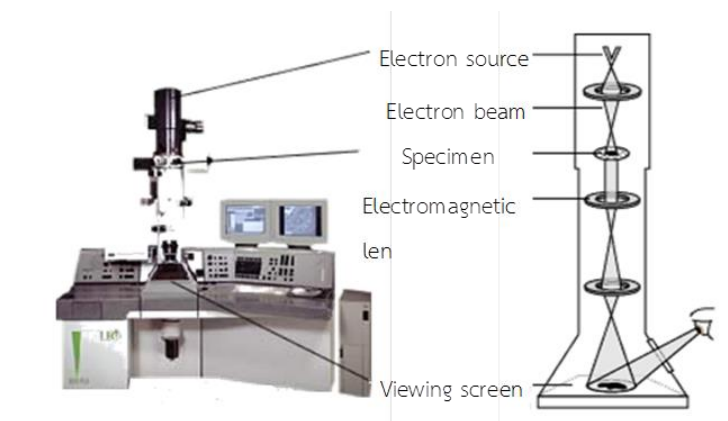


Figure 2.22 Schematic diagram of transmission electron microscope

2.9 Anisole alkylation [41]

Tertiary butylatedmethoxy benzene was produced from alkylation of methoxybenzene which are used for variety of benefits in chemical industry. Anisole alkylation is very important process for increase valuable of anisole because anisole is a by-product from DMC-DPC [2] (Dimethyl carbonate to Diphenyl carbonate) process. Diphenyl carbonate is used as a precursor in produce of polycarbonate through transesterification with Bisphenol A.

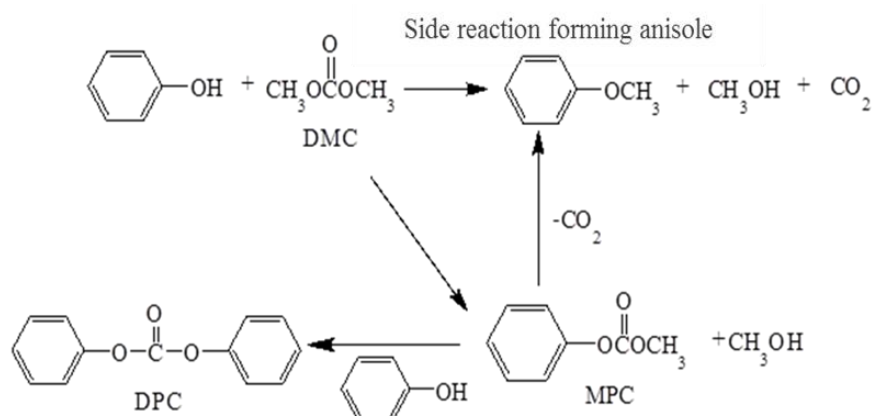


Figure 2.23 Dimethyl carbonate to Diphenyl carbonate (DMC-DPC) process

Alkylation of anisole with *tert*-butanol (Figure 2.24) has been used for produced 4-*tert*-butyl anisole (4-TBA), 2-*tert*-butyl anisole (2-TBA) and 2, 4-di-*tert*-butyl anisole (2, 4-DTBA), which are an intermediate for chemistry industrial such as such as antioxidants, dye developers and stabilizers for fats, oils, plastic, rubber, etc [42].

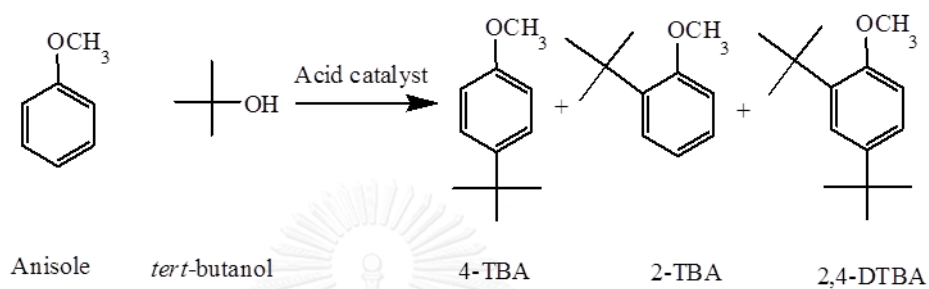


Figure 2.24 Alkylation of anisole with *tert*-butanol

CHAPTER III

EXPERIMENTS

3.1 Starting materials

3.1.1 Starting materials for MCA-Pr-SO₃H and ZSM-5/MCA-Pr-SO₃H composite catalysts preparation

1) Triblock copolymer pluronic P123, PEO₂₀-PPO₇₀-PEO₂₀, average molecular weight = 5800 (Aldrich)

2) Tetraethyl orthosilicate, TEOS (Fluka, 98 %)

3) Commercial ZSM-5 (Si/Al=28)

4) Hydrochloric acid, HCl (Fluka, 37 %)

5) (3-Mercaptopropyl)trimethoxysilane, MPTMS (Aldrich, 95 %)

6) Hydrogen peroxide, H₂O₂ (Merck, 30 %)

7) Sulfuric acid, H₂SO₄ (Merck, 95-97%)

8) Deionized water

3.1.2 Chemicals for butylation reaction

1) *tert*-Butanol, C₄H₁₀O (Fluka, ≥99%)

2) Anisole, C₇H₈O

3.1.3 Chemicals for quantitative analysis

1) *tert*-butyl anisole, C₁₁H₁₆O

2) 4-*tert*-butyl anisole, C₁₁H₁₆O

4) n-octane, C₈H₁₈

5) Tetrahydrofuran (THF), C₄H₈O

3.1.4 Chemicals for antioxidant test

- 1) Butylated hydroxyanisole, $C_{11}H_{16}O_2$ (Aldrich, 99%)
- 2) α,α -Diphenyl- β -picrylhydrazyl, $C_{18}H_{12}N_5O_6$ (Aldrich)

3.2 Instruments and apparatus

3.2.1 X-ray power diffraction (XRD)

The XRD patterns of resulting materials were characterized using a Rigaku D/MAX-2200 Ultima⁺ X-ray diffractometer equipped with Cu target X-ray tube (40 kV, 30mA). The 2-theta angle was ranged from 0.5 to 3.00 degree and from 3 to 50 degree. The scan speed was used at 1.00 degree/min and sampling width of 0.02 degree. The scattering slit, divergent slit and receiving slit were fixed at 0.5 degree, 0.5 degree, and 0.15 mm, respectively. The measured diffractograms were analyzed using MDI software (Jade 6.5).

3.2.2 Surface area analyzer

Nitrogen sorption measurements were performed on a BEL Japan BELSORP-mini28SP adsorptometer. Before measurement, the samples were pretreated at 120 °C for 2 h. The specific surface area was calculated from adsorption data in the relative pressure (P/P₀) range = 0.1-0.25 using the Burnauer-Emmett-Teller (BET) whereas the distribution of the pores and total pore volume were evaluated by use of Barrett-Joyner -Halenda (BJH).

3.2.3 Scanning electron microscopy (SEM)

Morphology and size of composite material particles were observed with a JEOL JSM-6480 LV scanning electron microscope. All materials were coated with spluttering gold under vacuum.

3.2.4 Transmission electron microscope (TEM)

The microstructure and pore size of composite materials were investigated by JEOL; JEM-2100 transmission electron microscopy.

3.2.5 Temperature-programmed desorption of ammonia (NH₃-TPD)

Acid strength of catalyst was determined using the BET-CAT Japan instrument. For analyzing, 0.08 g of the functionalized materials were pretreated in pure helium at 150 °C for 1 h and then cooled at 50 °C prior to adsorption ammonia. The profile of NH₃-TPD was recorded from 50 to 600 °C under heating rate of 10 °C /min.

3.2.6 Gas chromatograph (GC)

Reaction mixture from alkylation of anisole with *tert*-butanol analyzer using a Varian CP-3800 gas chromatograph equipped with a 30-m long and 0.25-mm inner diameter CP-sil 5 (0.25 μm film thickness) column. GC detectors are flame ionization detectors (FID). The reaction mixture weights were 0.10xx g. The tetrahydrofuran (THF) was used as solvent and n-octane was used internal standard. The column oven-heating program was illustrated in Figure 3.1 for butylated products analysis.

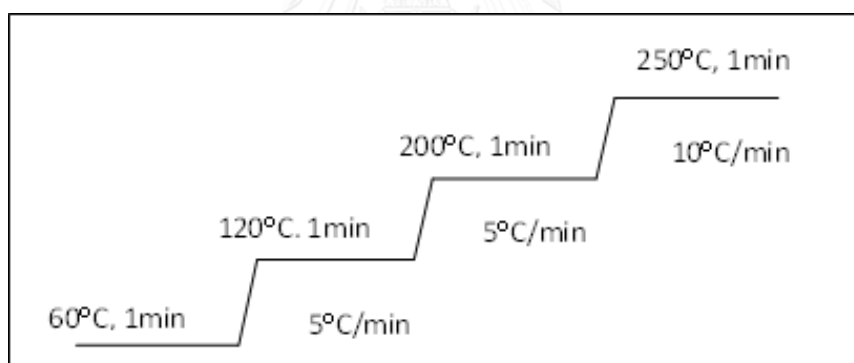
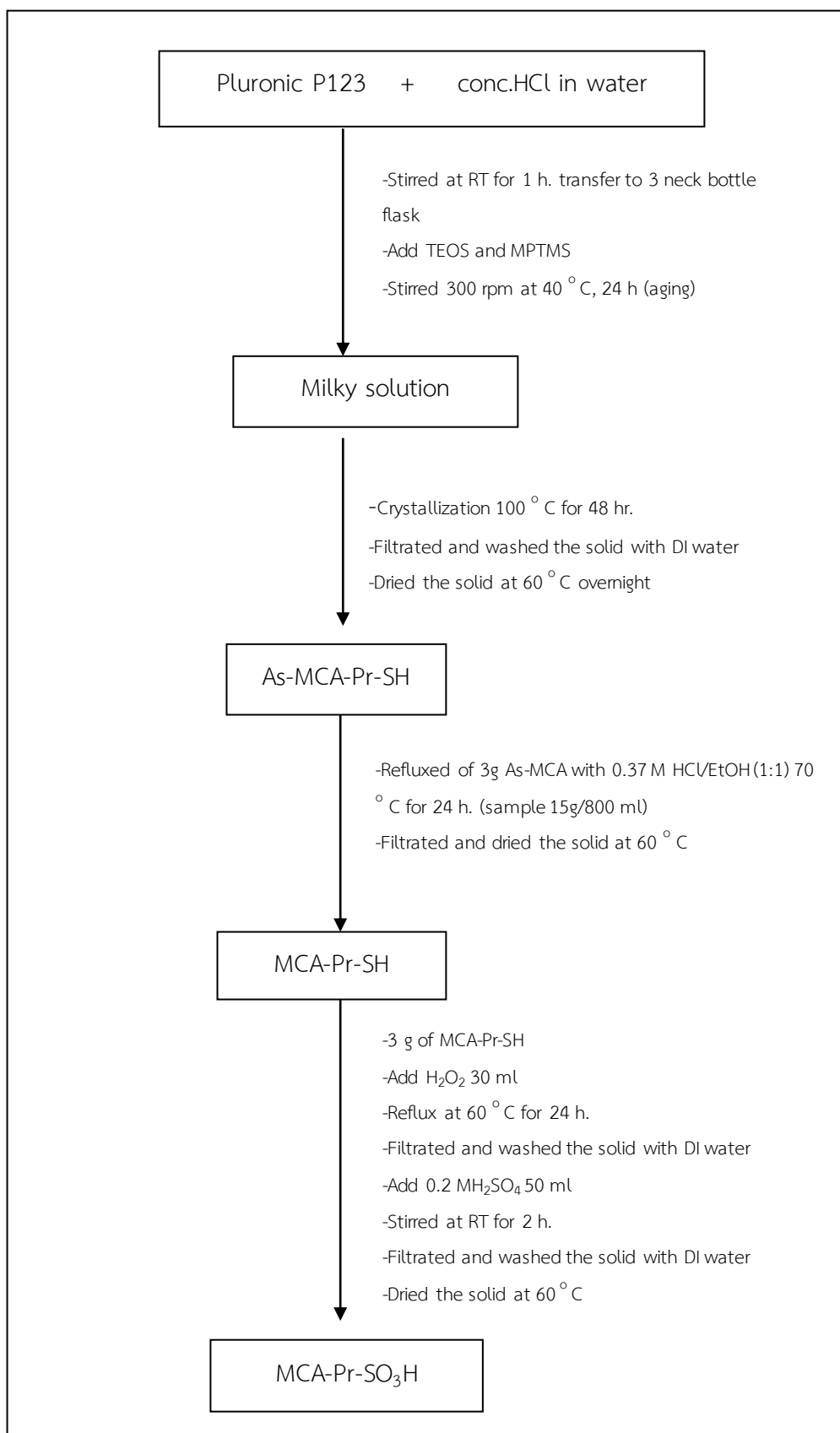


Figure 3.1 GC heating condition for anisole alkylation

3.3 Synthesis of materials

3.3.1 Propylsulfonic acid functionalized cubic Ia-3d (MCA)

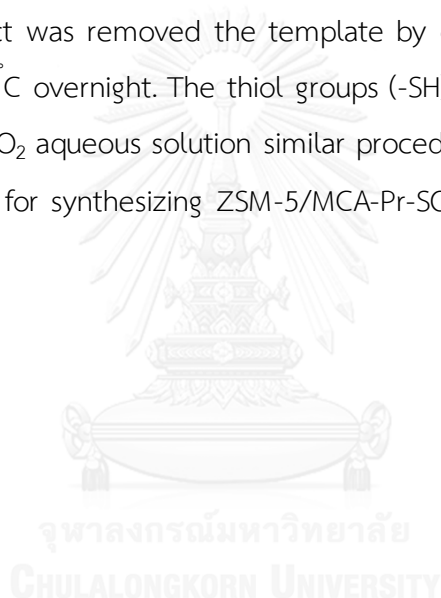
The propylsulfonic acid functionalized cubic Ia-3d mesoporous material, defined hereafter as MCA-Pr-SO₃H (MCA; mesoporous cubic amorphous), was prepared by using the direct synthesis method [18], which involved the co-condensation of TEOS (8.19 g.) and MPTMS (0.69 g.) in the presence of P123 (4.0 g), conc. HCl (7.8 g) and deionized water (100 mL), and then aged at 40 °C for 24 h with stirring. Thus, the gel composition (mol ratio) was 1 TEOS: 0.089 MPTMS: 0.018 P123: 2.0 HCl: 148 H₂O. After aging, the milky reaction mixture was transferred into a Teflon-lined stainless steel autoclave and crystallized in an oven at 100 °C for 48 h. The white product was filtered, washed and dried at 60 °C overnight, and is denoted as as-syn MCA. The P123 surfactant was then removed from the as-syn MCA by extracting with 0.37 M HCl in EtOH and dried at 70 °C for 24 h. The extracted sample is denoted as MCA_{ex}. The thiol groups (-SH) in the MCA_{ex} sample were converted to sulfonic groups (-SO₃H) [43] by oxidation with 30 wt% H₂O₂ aqueous solution (10 g of solution per 3.0 g of MCA_{ex} was used) at 60 °C for 24 h. The white sample was then further stirred with 50 mL of 0.2 M H₂SO₄ at room temperature for 2 h, filtered and dried overnight, and is denoted as MCA-Pr-SO₃H. The procedure for synthesizing MCA-Pr-SO₃H was illustrated in scheme 3.1.

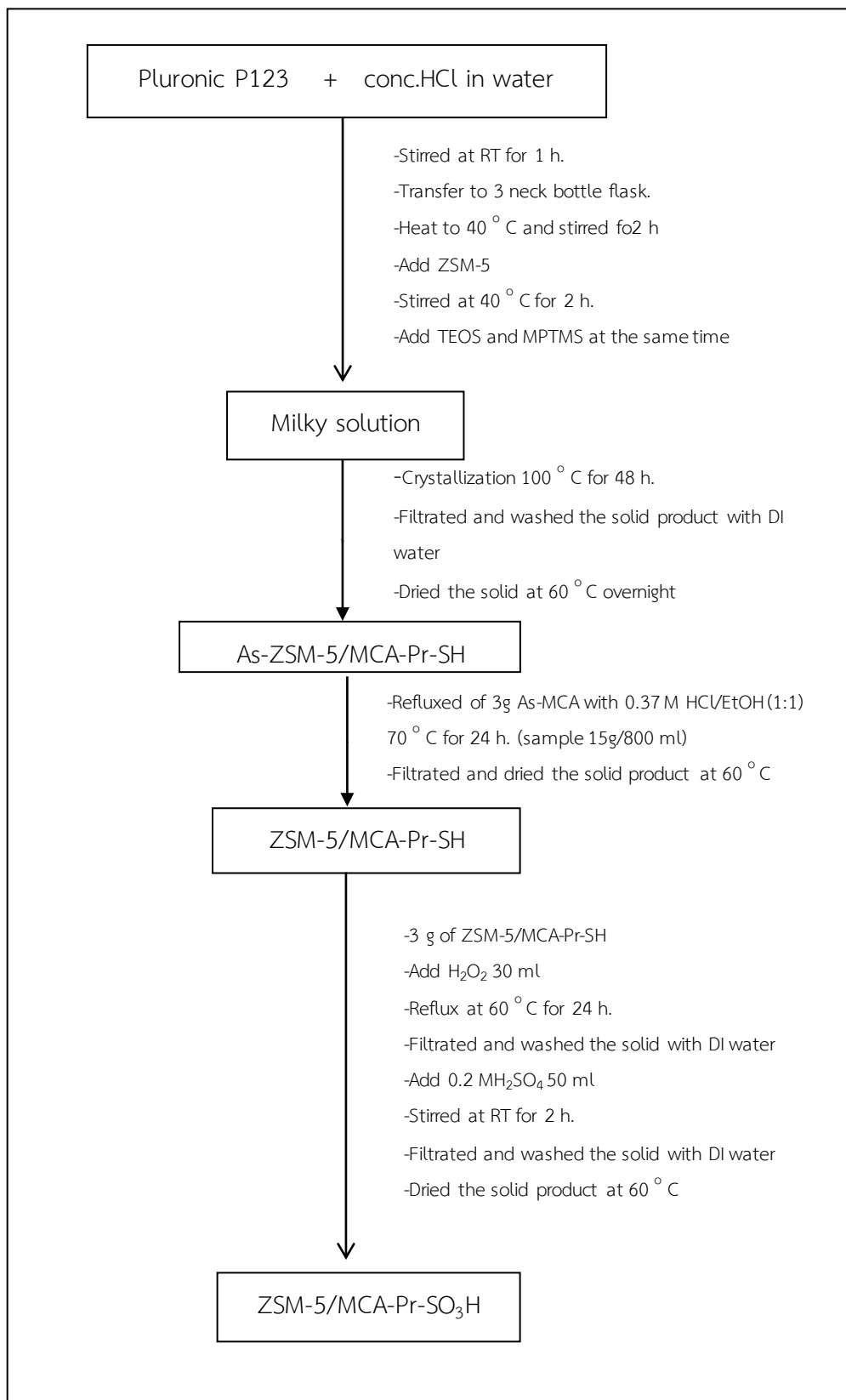


Scheme 3.1 Preparation diagram for propylsulfonic acid functionalized MCA

3.3.2 Composite ZSM-5/MCA-Pr-SO₃H materials

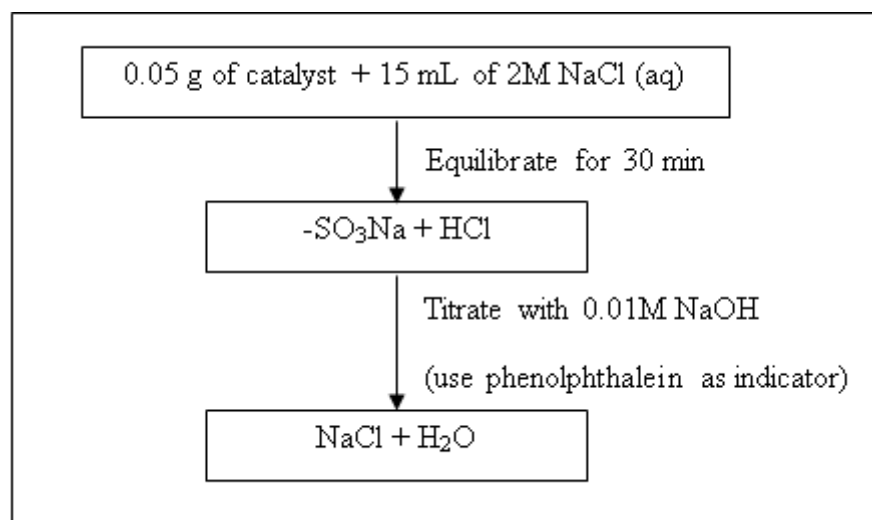
The synthetic method of propylsulfonic functionalized ZSM-5(x)/MCA composite materials were modified to described by Y. Kubota et al [18]. The modification was adding different amounts of commercial ZSM-5 (Si/Al=28) by seeding method [44]. The ZSM-5 powder was added in to homogeneous P123 surfactant solution at 40 °C. The mixture was stirred for 2 h and then, TEOS and MPTMS were added in to the mixture. The solution mixture was continuous stirred for 24 h. After that, this solution was transferred into autoclave and crystallized in an oven at 100 °C for 48 h. The white product was filtered, washed and dried at 60 °C overnight. The product was removed the template by extracting with 0.37 M HCl in EtOH and dried at 70 °C overnight. The thiol groups (-SH) in composite materials were oxidized with 30% H₂O₂ aqueous solution similar procedure with synthesis of MCA-Pr-SO₃H. The procedure for synthesizing ZSM-5/MCA-Pr-SO₃H was illustrated in scheme 3.3.



Scheme 3.2 Preparation diagram for ZSM-5/MCA-Pr-SO₃H

3.4 Acid-base titration

The acid capacities of sulfonic acid groups in the composite catalysts were quantified using 2.0 M NaCl solution as the ion-exchange agent (Scheme 3.3). Approximately 0.05x g of the catalysts was exchanged with 15 ml of NaCl solution for 30 min under constant agitation at room temperature and titration with 0.01 M NaOH by using phenolphthalein as indicator [45].



Scheme 3.3 Diagram for acid-base titration

3.5 Parameter affecting catalytic preparation

3.5.1 Effect of ZSM amount

The composite materials were signified as ZM-x, where x is ZSM-5 contents. The ZSM-5 content was varied in the range of 10- 50 wt % based on volume of TEOS.

3.5.2 Effect of time

The time of ZSM-5 adding before TEOS was varied in the range of 0-2 h.

3.6 Procedure in alkylation of anisole

The catalytic efficiency was investigated in anisole alkylation with *tert*-butanol. Before the reaction, the catalysts were heated overnight at 70 °C. Anisole alkylation was carried out in PARR autoclave reactor, model 4565 mini. After completion, the reaction mixture was cooled down and then the catalyst was separated by centrifugation. The liquid product was analyzed by gas chromatography (Varian CP 3800) equipped with a Flame Ionization detector (FID) using Varian CP-sil5 capillary column (30 m x .25 mm). And also, the products were confirmed by gas chromatography equipped with a mass selective detector (MSD) using Agilent Technologies 5973N.

3.6.1 Effect of catalytic type

Catalytic activities of MCA-Pr-SO₃H were compared with SBA-15-Pr-SO₃H and commercial catalysts such as ZSM-5 and Amberlyst-15.

3.6.2 Effect of mole ratio

The mole ratio of anisole to *tert*-butanol was varied in the range 1:1, 1:3; 1:6 and 1:9.

3.6.3 Effect of reaction temperature

The reaction temperature was varied in the range of 120°C - 175°C.

3.6.4 Effect of reaction time

The reaction time was varied in the range of 1-10 h.

3.6.5 Effect of catalytic amount

The catalytic loading was varied from 0 to 7.5 wt% based on total weight of reaction mixture.

3.6.6 Catalytic performance of ZSM-5/MCA-Pr-SO₃H

ZSM-5/MCA-Pr-SO₃H composite catalyst was tested in alkylation of anisole over on optimum condition of functionalized mesoporous catalyst.

3.8 Recycle of catalysts

After the first reaction, the used catalyst was filtered and washed several times with ethanol. The catalyst was dried at 80°C overnight, and then this catalyst was denoted as reused catalyst. This reused catalyst was test in anisole alkylation.

3.9 Antioxidant activity

Anisole, 2-*tert*-butyl anisole, 4-*tert*-butyl anisole and reaction mixture from butylation reaction were examined for antioxidant activity by using V-visible method. This method was used to estimate half maximal inhibitory concentration (IC₅₀) value of them.

3.9.1 Antioxidant test by UV-visible method

The radical scavenging activity of the butylated phenol derivatives against α , α -Diphenyl- β -picrylhydrazyl radical was determined by measuring UV absorbance at 517 nm by Sunrise™ microplate reader. Butylated hydroxyanisole (BHA) was used as standard for comparison. All evaporated samples and standard were prepared with methanol in the following concentrations, 1 ppm, 0.5 ppm, 0.25 ppm, 0.125 ppm and 0.0625 ppm. The 50 μ l of each prepared concentrations and blank were placed into microplate. Then 250 μ l of DPPH solution (11.8 mg in 100 ml of methanol) was added to all of them and incubated for 30 min and the absorbance was read [46].

The calculated % radical scavenging relative with concentration was plotted to compute concentration at 50% radical scavenging or half maximal inhibitory concentration (IC₅₀ value) as seen in Figure 3.2

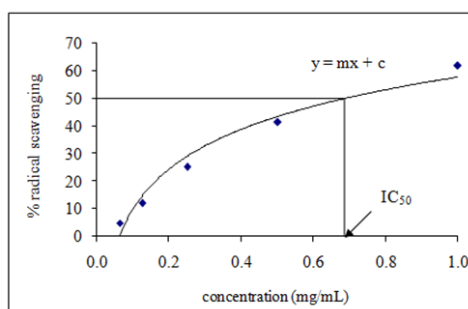


Figure 3.2 Curve of concentration versus % radical scavenging of inhibitor

CHAPTER IV

RESULTS AND DISCUSSION

4.1 Propylsulfonic acid functionalized cubic *Ia-3d* (MCA)

4.1.1 The physical- chemical properties of Propyl sulfonic acid functionalized cubic *Ia-3d* (MCA)

4.1.1.1 XRD results

The XRD patterns of as-syn MCA, extracted MCA (MCAex) and propylsulfonic acid functionalized MCA (MCA-Pr-SO₃H) were shown in Figure 4.1. The pattern of all materials was similar to the typical pattern of cubic *Ia-3d* mesoporous material. The results showed 2 diffraction peaks as (211) and (200) plane in the range of $2\Theta = 0.7-3.0^\circ$ with high periodic orderliness of mesoporosity and excellent textural uniformity [20]. In comparison MCA (ex) and MCA-Pr-SO₃H, peak position of MCA-Pr-SO₃H slightly shifted to higher angle when compared with MCAex. It's indicated that the pore size of MCAex was decreased by bulky sulfonic group grafting on the surface. Furthermore, the crystallinity of MCA-Pr-SO₃H showed lower intensity than MCAex because the organic group incorporated into mesoporous material.

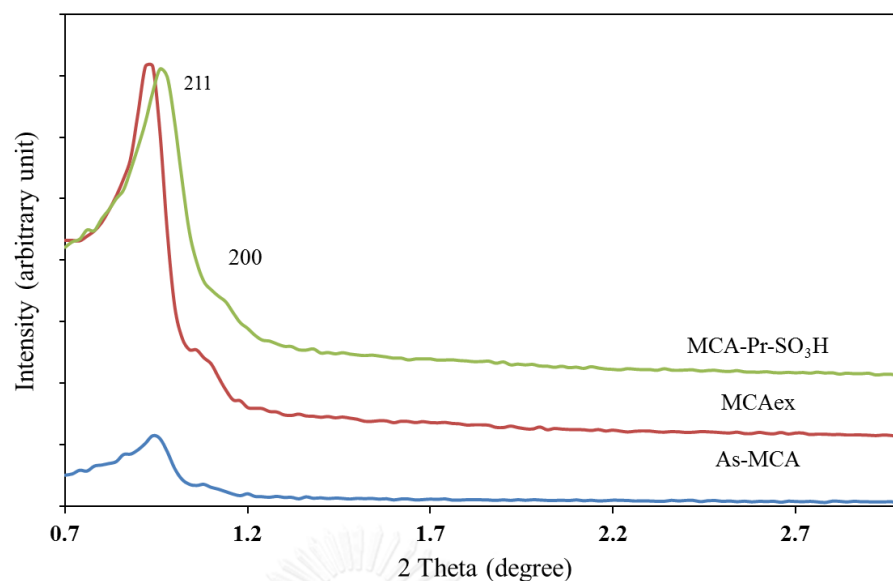


Figure 4.1 XRD pattern of Propylsulfonic acid functionalized cubic *la*-3d (MCA)

4.1.1.2 N_2 sorption properties

The N_2 sorption isotherms of cubic mesoporous materials (MCA) were shown in Figure 4.2. The isotherm of MCA (ex) and MCA-Pr-SO₃H presented in type IV isotherm with a well-defined H2 hysteresis loop according to the IUPAC classification relative to the mesoporous materials [47]. A H2 hysteresis loop type was indicated not well-defined distribution of pore size shape because mesoporous materials were functionalized organic groups into the surface. Moreover, when the organic functional groups were increased in the pore, this hysteresis loop occurs at a wide range of relative pressure as show in Figure 4.2b. In addition, the appearance properties of surface and pore were exhibited in Table 4.6. The total specific surface area of MCAex and MCA-Pr-SO₃H increased in the range of $466 \text{ m}^2 \text{ g}^{-1}$ to $762 \text{ m}^2 \text{ g}^{-1}$, when the structure directing agents were removed from the synthesized materials. Furthermore, the wall thickness and mesopore diameter of MCAex give value close to MCA-Pr-SO₃H. Nevertheless, the pore volume of MCA-Pr-SO₃H decreased because the thiol groups (-SH) in the MCAex were converted to sulfonic groups. This result corresponded with XRD pattern peak of MCA-Pr-SO₃H broader than MCAex.

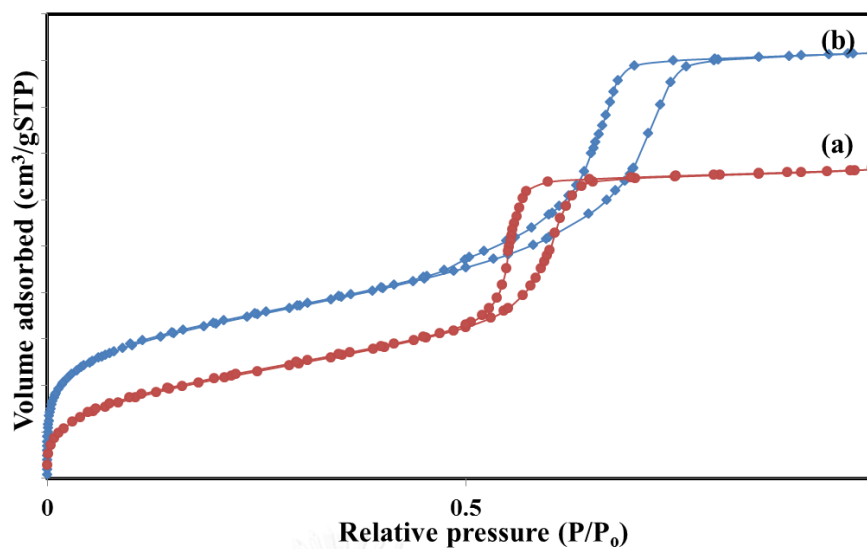


Figure 4.2 Nitrogen sorption isotherm of a) MCAex, b) MCA-Pr-SO₃H

Table 4.6 Textural properties of synthesized cubic mesoporous material.

Catalysts	a_0^c	BET surface area (m ² g ⁻¹) ^a	Total pore volume (cm ³ g ⁻¹) ^a	Pore diameter (nm) ^b	Wall thickness (nm) ^d
MCAex	21.5	465.6	0.82	5.52	9.4
MCA-Pr-SO ₃ H	21.2	762.1	0.79	5.52	9.5

^a Calculated using the BET plot method

^b Calculated using the BJH and MP method

^c Calculated as: $a_0 = \sqrt{6 \times d}$ where d is d -spacing of the (211) reflection plane from XRD method

^d Wall thickness $T_{wall} = a_0 \times \sqrt{(2/2 - d_{pore})}$, where d_{pore} and a_0 are pore distribution and cubic unit cell parameter, respectively [48].

4.1.1.3 SEM images

The SEM images showed the morphology of MCAex and MCA-Pr-SO₃H in Figure 4.3. From the images, morphology of MCAex and MCA-Pr-SO₃H were different in particle shape with similar to stone. Moreover, the morphology of MCA-Pr-SO₃H slightly changed from morphology of MCAex after oxidation with H₂O₂ as the thiol (-SH) functional group converted to sulfonic acid group (-SO₃H).

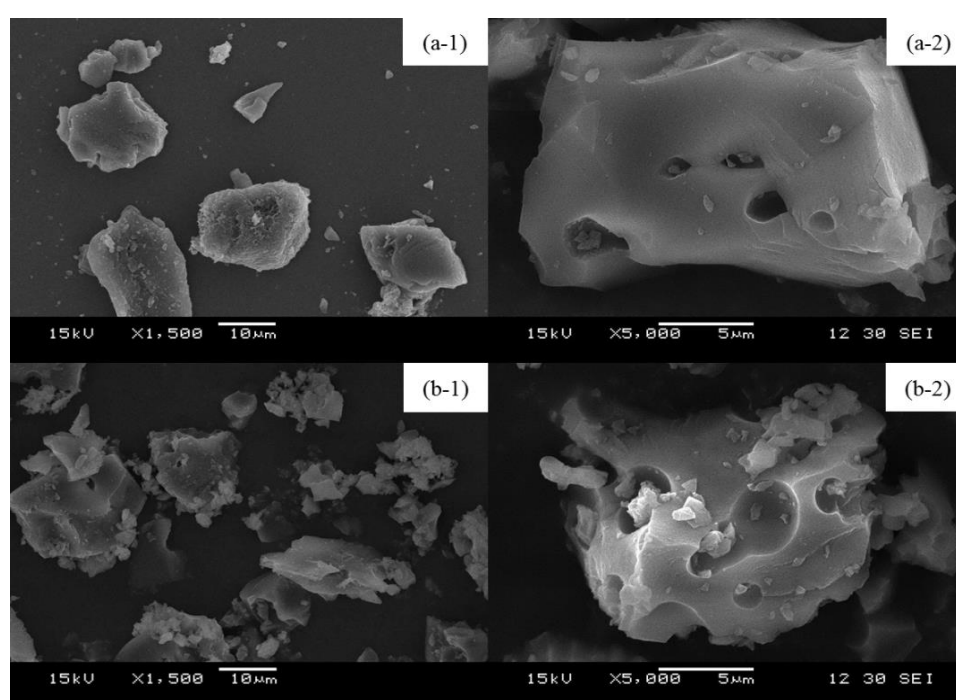


Figure 4.3 SEM images of synthesized MCAex ((a-1) × 1,500 and (a-2) × 5,000), MCA-Pr-SO₃H ((b-1) × 1,500 and (b-2) × 5,000)

4.1.1.4 TEM images

The TEM images of mesoporous MCA-Pr-SO₃H were shown in Figure 4.4. These indicated the well-ordered cubic mesostructure with three dimensional channels [20] which was confirmed by the longitudinal section view image and the cross-sectional images were used to measure the pore size of materials. The cross section images were used to measure the pore size of catalyst at lattice plane (200) and it is about 5.6 nm.

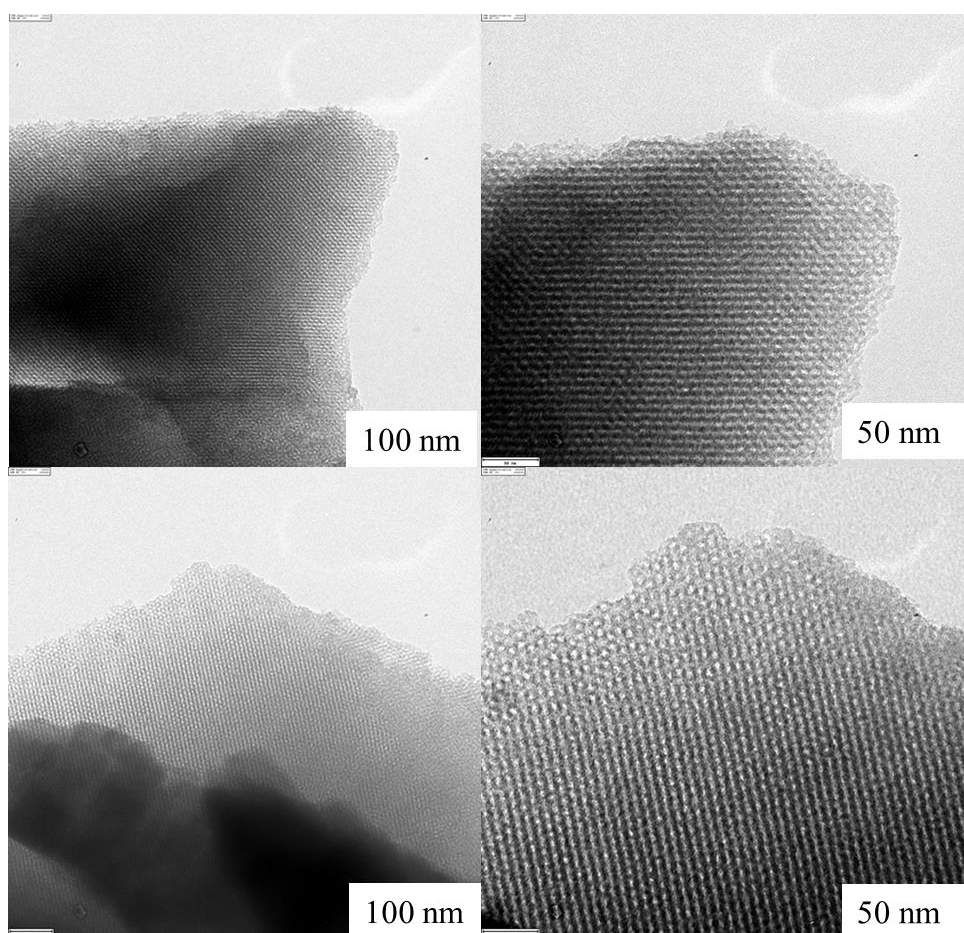


Figure 4.4 TEM images of synthesized MCA-Pr-SO₃H

4.2 Micro/mesoporous composite material

4.2.1 The physical-chemical properties of ZSM-5/MCA-Pr-SO₃H composite material

4.2.1.1 *Effect of ZSM-5 amount*

4.2.1.1.1 XRD results

The Figure 4.5 showed XRD patterns of pure ZSM-5, MCA-Pr-SO₃H and synthesized composite material (ZM-x) with different amount of ZSM-5. The typical of cubic *la-3d* mesoporous (MCA) and ZSM-5 were characterized by low-angle XRD pattern and wide-angle XRD pattern, respectively. From the result, the amount of ZSM-5 influenced the formation of MCA. When the percent of ZSM-5 was increased up to 30% (ZM-30), showed higher intensity pattern of MCA phase and ZSM-5 phase. Moreover, the percent of ZSM-5 addition increased up to 50%, the intensity pattern of MCA phase decreased but intensity pattern of ZSM-5 phase increased. Therefore, the composite material, ZM-30 showed both good structured of MCA mesoporous and ZSM-5 microporous because it represented better MCA structure than others. In addition, the broaden (211) diffraction peak of low-angle XRD pattern indicated that the crystallinity of cubic structure was decreased when compared with pattern of MCA-Pr-SO₃H

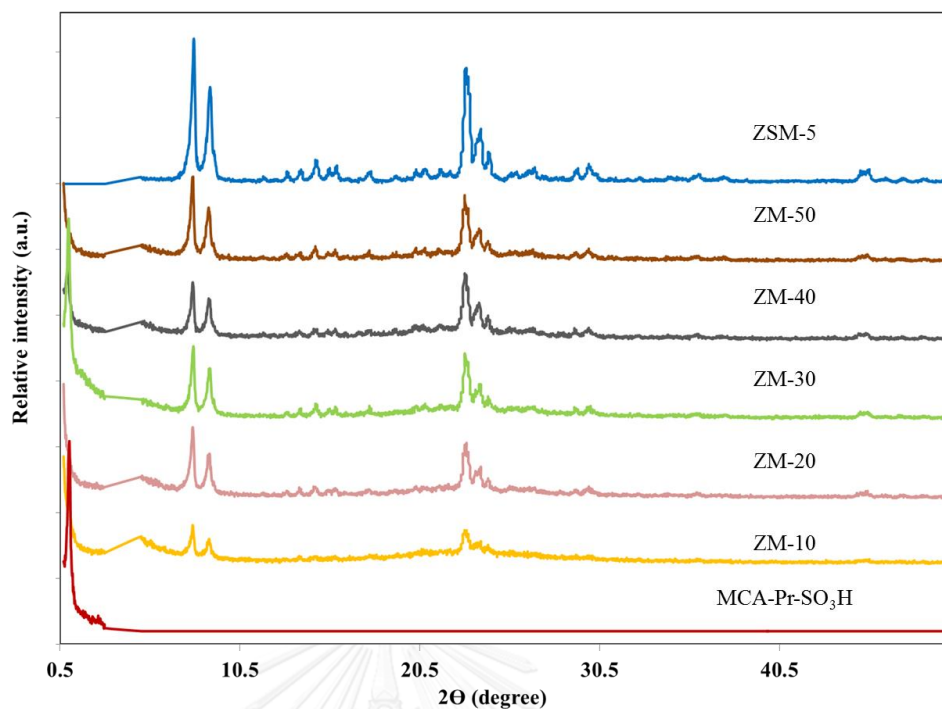


Figure 4.5 XRD patterns of synthesized ZM-x composite materials

4.2.1.1.2 N_2 sorption properties

The adsorption isotherm of ZM-x composite materials were showed in Figure 4.6 The nitrogen adsorption isotherm of all samples exhibited type IV in accord with the IUPAC classification, which confirmed mesoporous material [47]. In addition, the adsorption isotherm of ZM-x samples showed a hysteresis loop at a P/P_0 ranging from 0.4-0.7. And also, these samples presented the smaller hysteresis loop observed at a high relative pressure ($P/P_0 > 0.7$) could be due to N_2 condensation inside the interparticle voids, generated from their particle agglomerate.

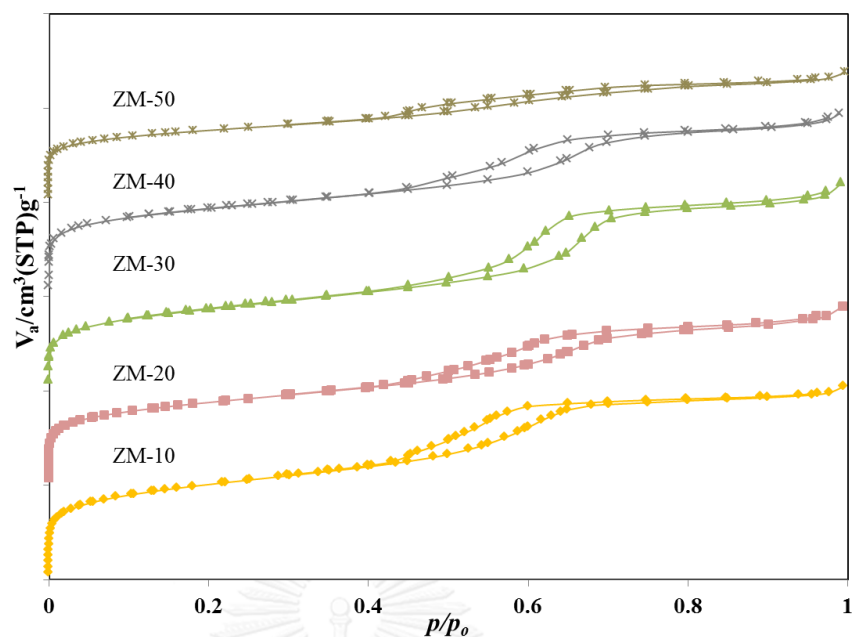


Figure 4.6 Nitrogen sorption isotherms of ZM-x composite materials

The textural properties of ZM-x composite materials were summarized in Table 4.7. The surface area, mesopore volume and mesopore diameter were decreased when increasing the amount of ZSM-5 into the mesostructure. In the contrast, the pore wall thicknesses of ZM-x samples were increased when increasing the ZSM-5 powder in the mesophase

Table 4.7 Textural properties of composite materials

Sample	a_0^c	BET surface area ($m^2 g^{-1}$) ^a	Total pore volume ($cm^3 g^{-1}$) ^a	Pore diameter (nm) ^b	Wall thickness (nm) ^d	Mesopore area ($m^2 g^{-1}$) ^b	Mesopore volume ($cm^3 g^{-1}$) ^b
ZM-10	22.3	727	0.63	4.87	10.9	434	0.48
ZM-20	22.4	635	0.58	4.75	11.1	350	0.44
ZM-30	22.7	577	0.43	4.69	11.4	262	0.38
ZM-40	23.3	546	0.42	4.47	12.0	236	0.27
ZM-50	24.1	540	0.41	4.25	12.8	227	0.26

^a Calculated using the BET plot method

^b Calculated using the BJH and MP method

^c Calculated as: $a_0 = \sqrt{6 \times d}$ where d is d-spacing of the (211) reflection plane from XRD method

^d Wall thickness $T_{wall} = a_0 \times \sqrt{(2/2 - d_{pore})}$, where d_{pore} and a_0 are pore distribution and cubic unit cell parameter, respectively

4.2.1.1.3 SEM images

The particle shape, surface morphology of ZM-x composite samples were investigated by scanning electron microscopy (SEM). The SEM images of all samples were presented in Figure 4.7. The particle of micro/mesoporous ZM-x gave different morphological appearance from MCA-Pr-SO₃H which appeared particle of ZSM-5 at the particle surface of MCA because ZSM-5 seeds coated in composite material.

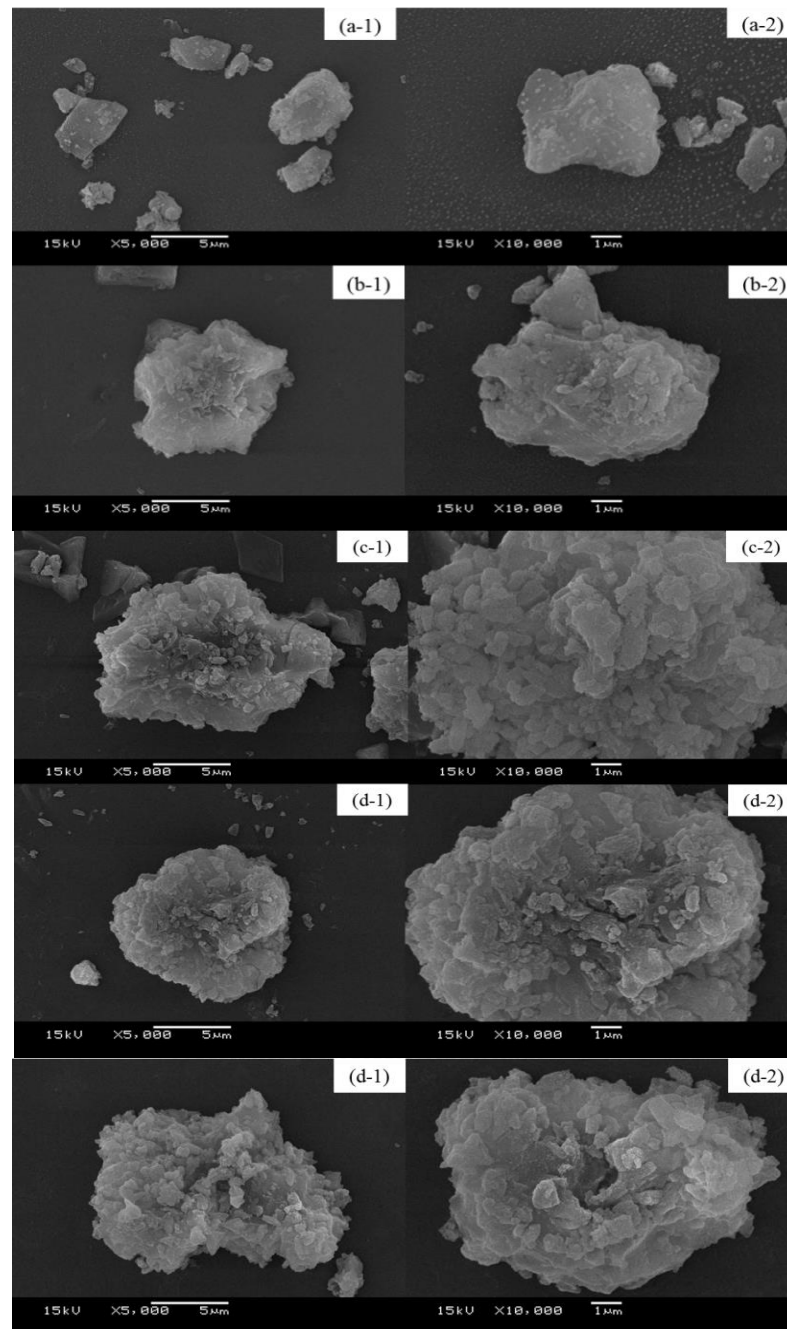


Figure 4.7 SEM images of a) ZM-10, b) ZM-20, c) ZM-30, d) ZM-40 and e) ZM-50

4.2.1.1.4 TEM images

The structural pore ordering of materials were investigated by using transmission electron microscopy (TEM). The TEM images of all composite samples were presented Figure 4.8. From the results, the TEM images indicated the zeolite ZSM-5 deposited in cubic $Ia-3d$ mesoporous wall, these caused to disordered pore channel.

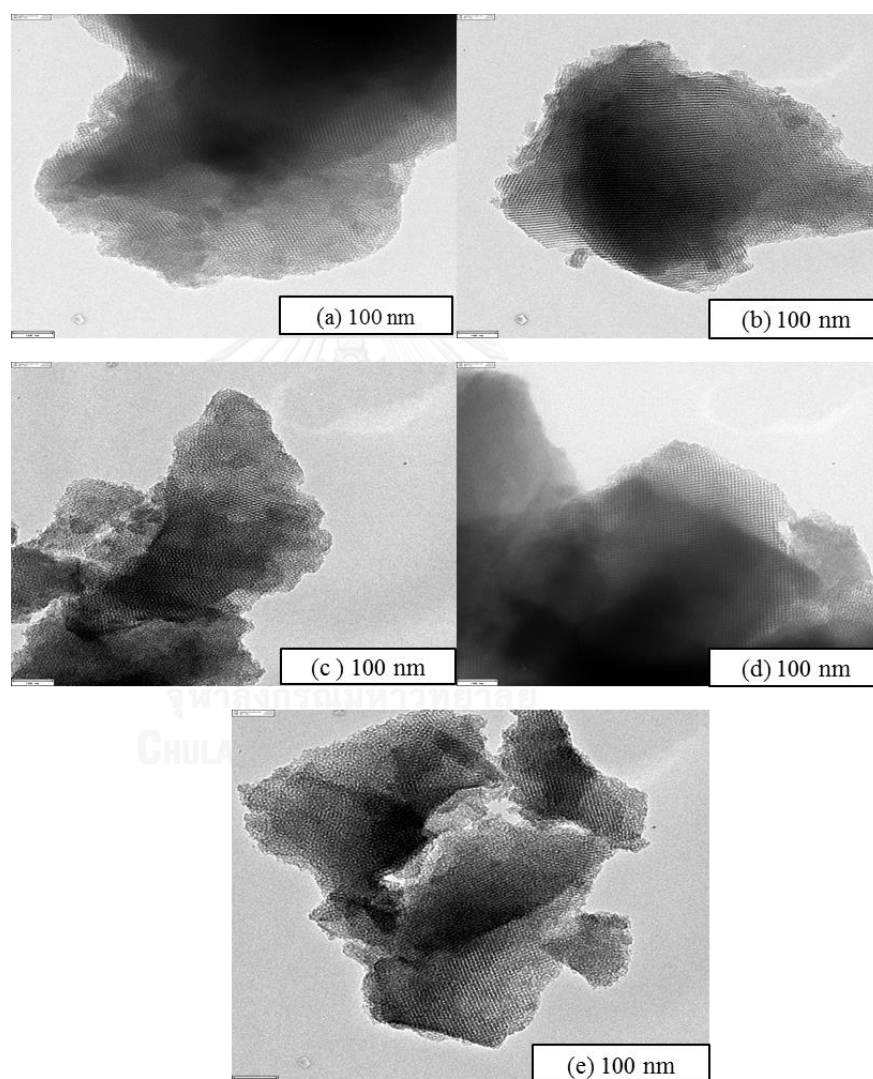


Figure 4.8 TEM images of a) ZM-10, b) ZM-20, c) ZM-30, d) ZM-40, and e) ZM-50

4.2.1. 2 Effect of time

4.2.1. 2. 1 XRD results

The study effects of ZSM-5 adding time before TEOS and MPTMS were performed at 0, 0.5, 1, 2 or 2.5 hr. The XRD patterns of as-synthesized ZM-X composite materials were shown in Figure 4.9. Figure 4.9A showed the XRD patterns of low angle and Figure 4.9B showed the XRD patterns of high angle when the adding time of ZSM-5 powder was increased from 0 - 0.5 h, the XRD patterns of low angle do not showed the diffraction peaks (211) and (200), which are characteristic peaks of cubic $la-3d$ mesostructure. When the time was increased up to 2.5 h, the XRD patterns of low angle showed diffraction peaks (211) and (200). And also, the XRD patterns of high angle showed ZSM-5 characteristic peaks [49]. The (211) diffraction peak of low-angle XRD pattern broadens indicated that the crystallinity of cubic structure was decreased because ZSM-5 was embedded into the pore wall of MCA. When increasing the ZSM-5 adding time leads to higher crystallinity of material. From these results, the time of ZSM-5 addition showed a significant influence in the formation of MCA.

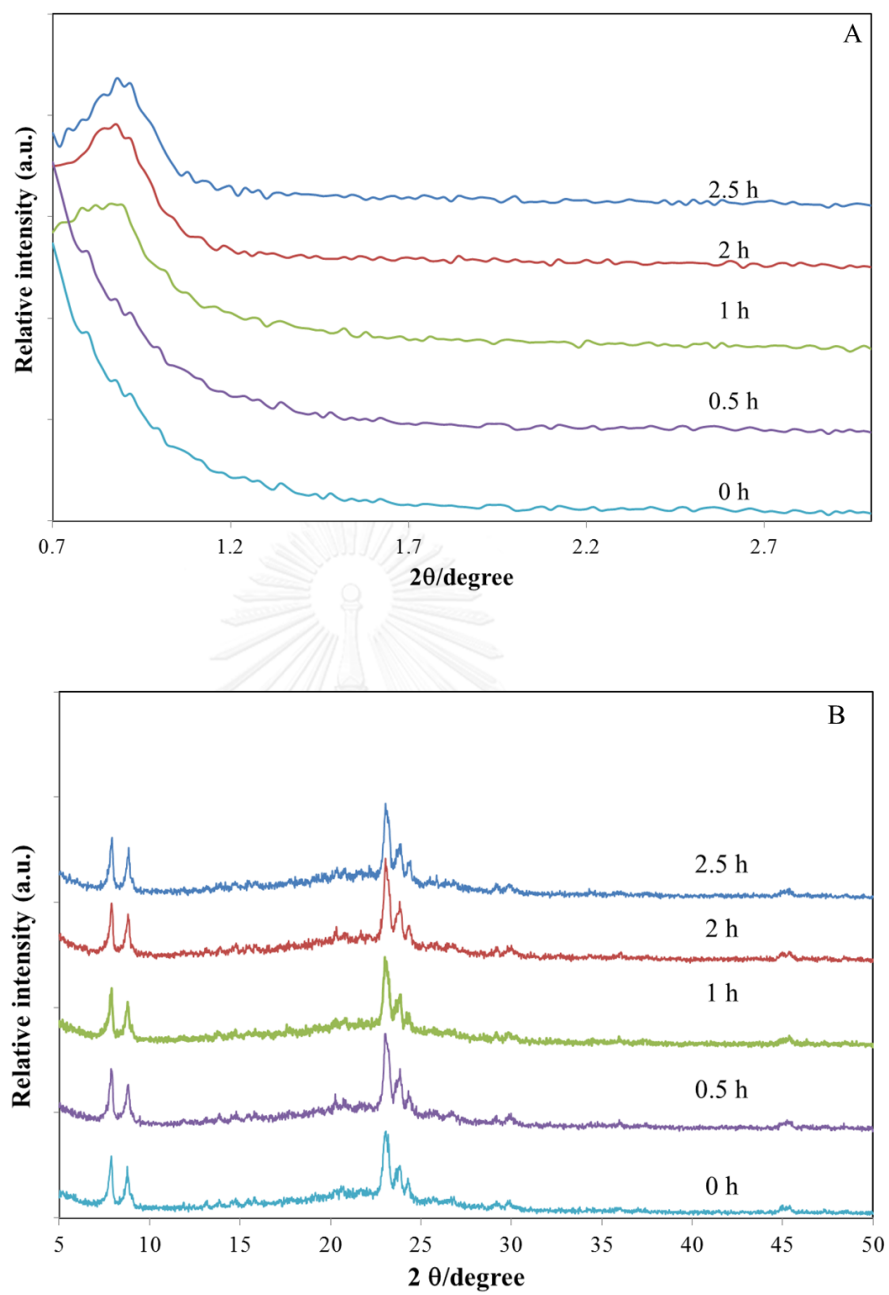


Figure 4.9 XRD patterns of as-synthesis ZM-30 sample A) low angle and B) high angle

4.2.1. 2. 2 N₂ sorption properties

Figure 4.10 shows the adsorption isotherm of extract-ZM-30 composite material samples that varied ZSM-5 adding time before TEOS and MPTMS adding at 0, 0.5, 1, 2, 2.5 hr. The adsorption isotherm of all samples performed a typical type IV with a well-defined H2 hysteresis loop in accord with the IUPAC classification for mesoporous materials. Furthermore, the hysteresis loops of sample 0-0.5h exhibited almost horizontal and nearly parallel over a wide range of relative pressure that showed slimly exhibition of H4 loops indicates the existence of the micropore. This result coincided with

Figure 4.9, the XRD patterns exhibited only XRD pattern of ZSM-5. In addition, the properties of extract-ZM-30 composite materials were exhibited in Table 4.8. From the results, the total surface area, the pore volume and wall thickness were increased with increasing of ZSM-5 adding time. Comparison of the results when study the effects of ZSM-5 adding time before TEOS and MPTMS, found that time of ZSM-5 addition at 2 hr. gave the best structure, which provided well-ordered cubic Ia-3d mesostucture when added ZSM-5 unite co-condensation with mesopore structure forming.

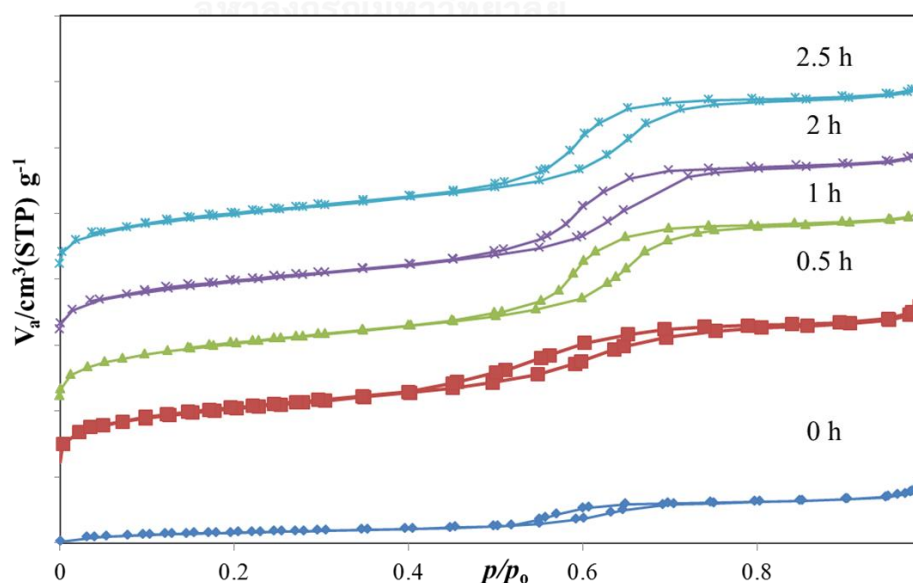


Figure 4.10 Nitrogen sorption isotherms of extract-ZM-30 composite materials

Table 4.8 Textural properties of extract-ZM-30 composite materials

Samples	BET surface area (m ² g ⁻¹) ^a	Total pore volume (cm ³ g ⁻¹) ^a	Pore diameter (nm) ^b	Wall thickness (nm) ^d
0 h	299	0.42	5.52	9.4
0.5 h	303	0.40	5.52	9.4
1 h	352	0.43	5.52	10.5
2 h	370	0.45	5.52	11.2
2.5 h	367	0.45	5.52	11.4

^aCalculated using the BET plot method

^bCalculated using the BJH and MP method

^cCalculated as: $a_0 = \sqrt{6 \times d}$ where d is d-spacing of the (211) reflection plane from XRD method

^dWall thickness $T_{\text{wall}} = a_0 \times \sqrt{(2/2 - d_{\text{pore}})}$, where d_{pore} and a_0 are pore distribution and cubic unit cell parameter, respectively [48].

4.2.2 Comparison of composite material with original material

Comparison of the results for composite materials (ZM-30), which are chemical mixing sample (ZM-30) and physical mixing sample of ZSM-5 (30%) and MCA-Pr-SO₃H (100%) as (P-ZM-30).

4.2.2.1 XRD results

The XRD pattern of chemical mixing sample (ZM-30) and physical mixing sample (P-ZM-30) showed in Figure 4.11. The patterns of both materials were similar to the typical pattern of cubic *la-3d* mesoporous material, which showed 2 diffraction peaks of (211) and (200) planes at low angle XRD pattern. And also, these samples showed similar to the typical pattern of ZSM-5 material at high angle XRD pattern.

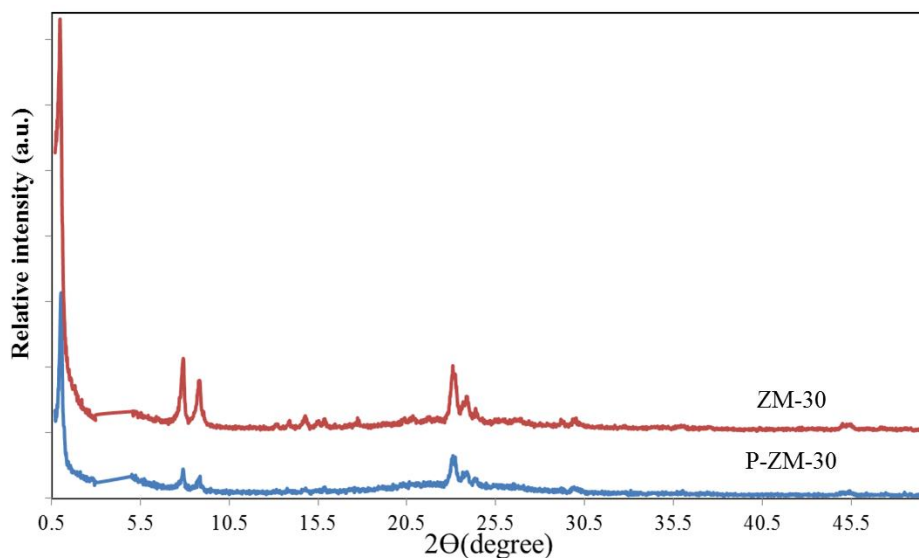


Figure 4.11 XRD patterns of composite materials

4.2.2.2 N_2 sorption properties

The textural properties of ZSM-5, MCA-Pr-SO₃H, ZM-30 composite material and P-ZM-30 samples were compared by using N₂ adsorption-desorption measurement, the nitrogen adsorption isotherms were shown in Figure 4.12 and the physical properties of the composite material and original material were shown in Table 4.9. The nitrogen adsorption isotherm of MCA-Pr-SO₃H and composite materials exhibited type IV in according with the IUPAC classification, which confirmed mesoporous material. The isotherm of ZM-30 composite material showed a hysteresis loop at P/P_o of 0.5-0.7 and > 0.7 . Moreover, this hysteresis loop exhibited almost horizontal over a wide range of relative pressure, which was consistent with the presence of microporous zeolite[50]. The surface area, mesopore volume and mesopore diameter were decreased when compared to MCA-Pr-SO₃H. Compared to P-ZM-30 composite material, the isotherm of this sample was quite similar with that MCA-Pr-SO₃H. Furthermore, the wall thickness and mesopore diameter of P-ZM-30 sample showed value close to MCA-Pr-SO₃H.

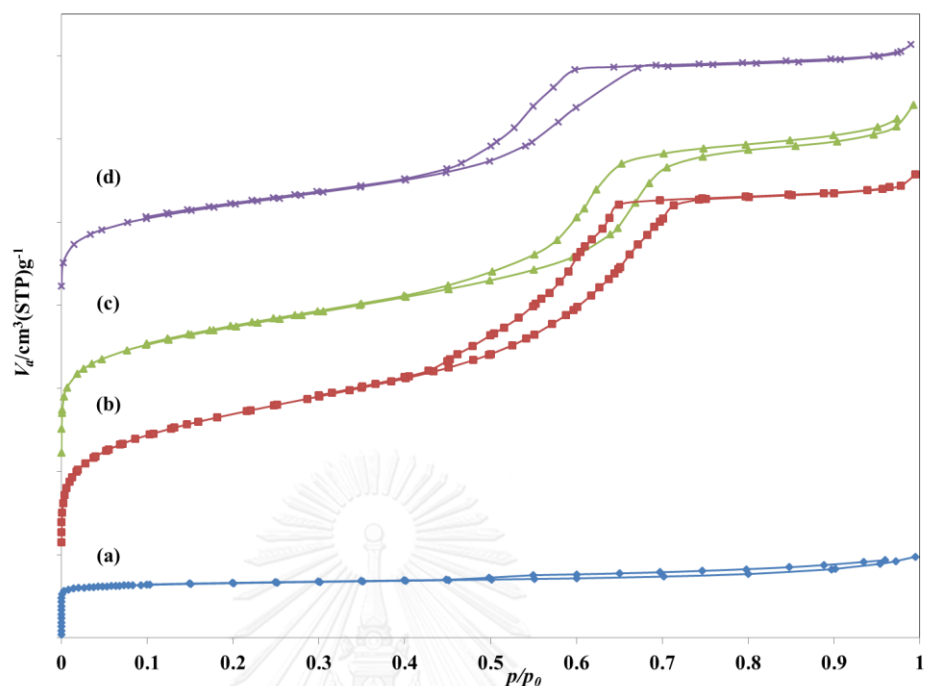


Figure 4.12 Nitrogen sorption isotherm of a) ZSM-5, b) MCA-Pr-SO₃H, c) ZM-30 composite material and d) P-ZM-30 composite material

Table 4.9 Physical properties of the composite material and original material

Sample	a_o^c	BET surface area ($m^2 g^{-1}$) ^a	Total pore volume ($cm^3 g^{-1}$) ^a	Pore diameter (nm) ^b	Wall thickness (nm) ^d
MCA-Pr-SO ₃ H	21.2	762	0.79	5.52	9.5
ZM-30	22.7	577	0.43	4.69	11.4
P-ZM-30	20.8	436	0.49	4.85	9.9
ZSM-5	-	315	0.19	0.60	-

^aCalculated using the BET plot method

^bCalculated using the BJH and MP method

^cCalculated as: $a_o = \sqrt{6 \times d}$ where d is d-spacing of the (211) reflection plane from XRD method

^dWall thickness $T_{wall} = a_o \times \sqrt{(2/2 - d_{pore})}$, where d_{pore} and a_o are pore distribution and cubic unit cell parameter, respectively [48].

4.2.2.3 SEM images

The particle shape, surface morphology of synthesis materials were investigated by scanning electron microscopy (SEM). The SEM images of composite materials were shown in Figure 4.13. The particle of ZM-30 sample (Figure 4.13C) had different morphological appearance from MCA-Pr-SO₃H (Figure 4.13b) which appeared particle of ZSM-5 at the particle surface because ZSM-5 seeds were fixed into composite material. However, ZM-30 composite material exhibited a difference of ZSM-5 dispersion on MCA-Pr-SO₃H surface when compared P-ZM-30 was shown in Figure 4.13d, which clearly separated particles for both types.

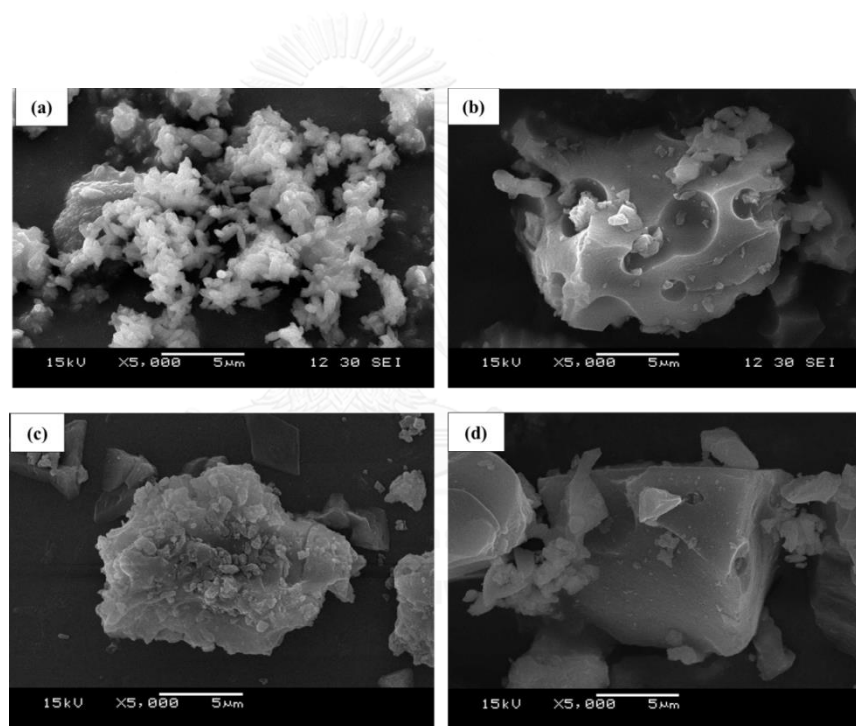


Figure 4.13 SEM micrographs of samples; a) ZSM-5, b) MCA-Pr-SO₃H, c) ZM-30 composite material, and d) P-ZM-30 composite material

4.2.2.3 TEM images

The TEM images of all composite samples were presented in Figure 4.14. From the Figure 4.14 (a, b) were the TEM images of MCA-Pr-SO₃H, which confirmed the well-defined *Ia*-3d cubic structure. The TEM images of ZM-30 composite material were shown in figure 38(c, d), which indicated the zeolite ZSM-5 deposited in cubic *Ia*-3d mesoporous wall, causing disordered pores channel.

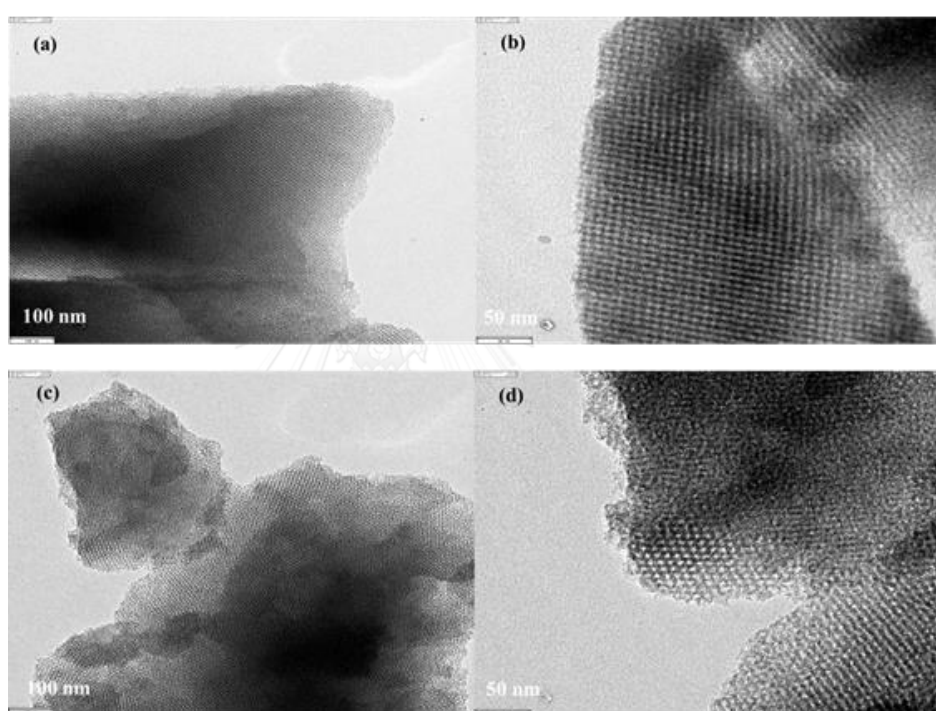


Figure 4.14 TEM images of a, b) MCA-Pr-SO₃H and c, d) ZM-30 composite material

4.3 Acidity of synthesized catalysts from NH₃-TPD

The NH₃-TPD profiles of ZSM-5, MCA-Pr-SO₃H, ZM-30 composite material and P-ZM-30 composite material were shown in Figure 4.15. Normally, zeolites provide desorption two peaks of TPD spectra, these are lower temperature peak (L-peak) and higher temperature peak (H-peak), respectively [51]. The H-peak is the desorption peak of ammonia adsorbed on the strong acid site, whereas the L-peak is assigned to ammonia weakly held or physically adsorbed on sites like silanol groups. Only the H-peak region was found to correlate with the Al content, acidity, and catalytic activity of zeolite. In the case of ZSM-5, strongly adsorbed NH₃ associated with strong acidic sites occurred at 340-520 °C. The NH₃-TPD profile of MCA-Pr-SO₃H showed broad peak at 370-600 °C, which corresponding to desorption of ammonia on the strong acidic sites. This peak was probably due to the decomposition of ammonia that reacted with SO₃H groups. The composite ZM-30 catalyst showed three peaks of TPD profiles. The TPD profile of ZM-30 showed small broad peak at 300-420°C associated with strong acidic sites of Al content in ZSM-5. And maximum peak at 480-600°C was assigned to strong acidic sites from SO₃H groups. In addition, the P-ZM-30 sample showed three peaks of TPD profiles. This sample showed broad peak at 370-600 °C, which corresponding to desorption of ammonia on the strong acidic sites from SO₃H groups and Al content in ZSM-5. The acidity of catalysts was shown in Table 4.10. When compare acidity of all catalysts, it was found that acidity ranked in the following order P-ZM-30 >ZM-30>MCA-Pr-SO₃H>ZSM-5. The P-ZM-30 catalyst has more acidity than ZM-30 catalyst because the ZSM-5 powder was embedded into the pore wall of MCA material less than 30%.

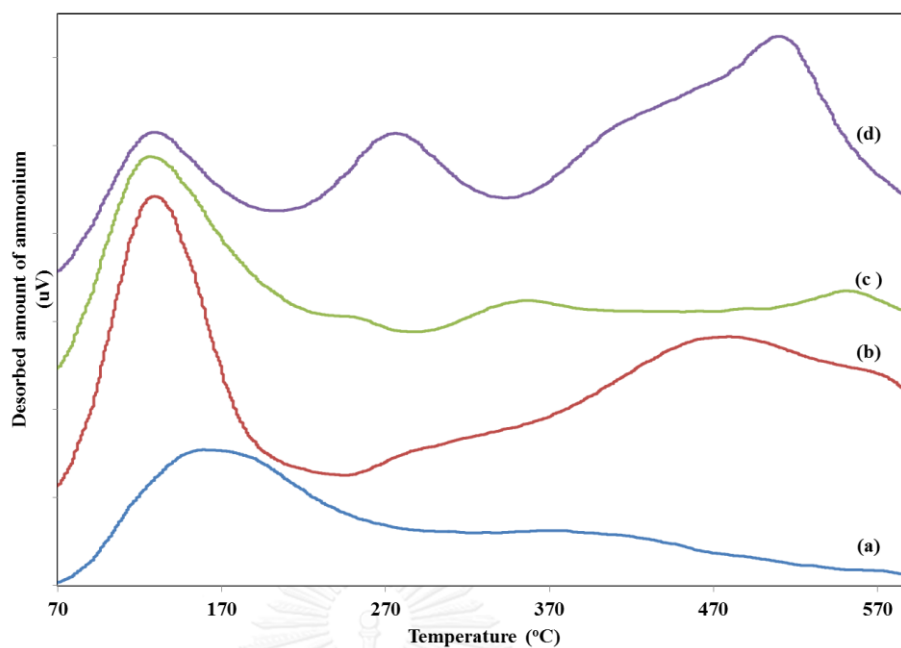


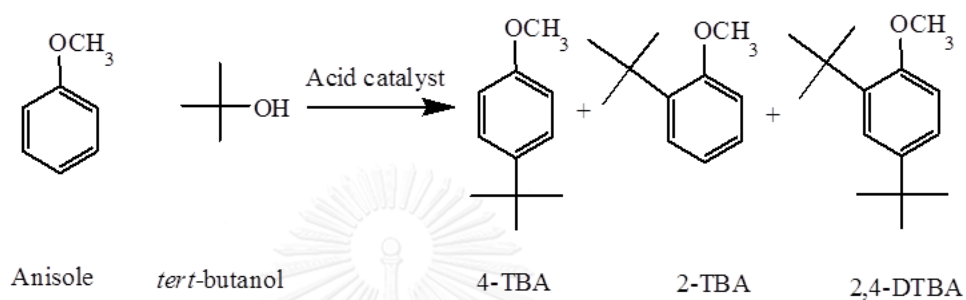
Figure 4.15 The NH_3 -TPD profiles of a) ZSM-5, b) MCA-Pr- SO_3H , c) ZM-30 composite material and d) P-ZM-30 sample

Table 4.10 The acidity of catalysts from NH_3 -TPD

Catalyst	Acidity(mmol/g)
ZSM-5	0.97
MCA-Pr- SO_3H	1.94
ZM-30	2.07
P-ZM-30	2.47

4.4 Anisole alkylation with *tert*-butanol over heterogeneous catalysts

The various catalysts including commercial Amberlyst-15, ZSM-5, MCA-Pr-SO₃H and SBA-15-Pr-SO₃H were investigated in anisole alkylation with *tert*-butanol at mole ratio of anisole to *tert*-butanol as 1:3 for 5 hours at 150 °C. The major products were shown in scheme 4.1 as 2-TBA, 4-TBA and 2, 4-DTBA.



Scheme 4.1 Alkylation of anisole with *tert*-butanol

The results are presented in Table 4.12, which showed the efficacy of various catalysts in order of their activity and selectivity of 2-TBA, 4-TBA and 2, 4-DTBA. From the result, it was found that MCA-Pr-SO₃H gave higher anisole conversion and total yield of *tert*-butylated product than other catalysts. This is because MCA-Pr-SO₃H had much higher specific surface area and acidity. Usually, the efficiency of catalysts does not depend on higher specific surface area but also depend on pore volume, pore size and acidity of catalysts. MCA-Pr-SO₃H gave relatively high pore volume at 0.796 cm³/g. When consider acid amount of catalyst, it was found that in order Amberlyst-15>MCA-Pr-SO₃H>SBA-15-Pr-SO₃H>ZSM-5. Furthermore, MCA-Pr-SO₃H had a cubic structure with a three-dimensional cavity that had an advantage to increase the diffusion speed of reactants into the pore [18]. On the other hand, the hexagonal structured SBA-15-Pr-SO₃H had structure of one-dimensional cavity [14]. SBA-15-Pr-SO₃H performed less conversion of anisole and total yield of product due to lower specific surface area and acidity than MCA-Pr-SO₃H. Furthermore, Amberlyst-15 contained higher acidity than other catalysts. The Amberlyst-15 gave relatively high conversion but the total yield of products was not high as expected due to by-product induction. In case of zeolite, the pore size is small (micro pore < 20 Å), which gave lower total yield of products. The pore size of ZSM-5 formed by 10-membered oxygen rings opening exhibited the lowest catalytic activity that provided lower conversion and total yield of products but interestingly its pore shape of MFI is selective to *para*-alkylated product. Then in the next experiment, MCA-Pr-SO₃H structure was selected to optimize the anisole alkylation test.

Table 4.11 Physicochemical and textural properties for catalysts

Catalyst	Dimension of oxygen membered ring (MR) [49, 52]	Pore volume ^a (cm ³ g ⁻¹)	Pore size (nm) ^b	Total specific surface area (m ² g ⁻¹) ^a	Acidity (mmol/g) ^c
ZSM-5 (SiO ₂ /Al ₂ O ₃ = 28)	5.1×5.5 Å [10 MR], 5.3×5.6 Å [10 MR]	0.19	0.70	315	0.49
Amberlyst-15[53]	-	0.40	3.00	53	2.19
ZSM-5-Pr-SO ₃ H	-	0.19	0.70	249	0.78
MCA-Pr-SO ₃ H	-	0.79	5.52	762	0.79
SBA-15-Pr-SO ₃ H	-	0.75	8.06	429	0.60

^aCalculated using the BET plot method

^bCalculated using the BJH and MP method

^cCalculated using acid-bases titration method

Table 4.12 Effect of catalytic type on product distribution and yield of products

Catalysts	Conversion%	Selectivity%			Total yield of products %
		2-TBA	4-TBA	2,4-DTBA	
MCA-Pr-SO ₃ H	94	34	55	7	90
SBA-15-Pr-SO ₃ H	84	36	53	6	80
ZSM-5	41	0.7	98	0	19
Amberlyst-15	84	24	44	6	64

Reaction Condition; 150°C, anisole: *t*-BuOH = 1:3 by mole, 5 wt% of catalyst based on total weight, 5h

4.5 Catalytic activity of propylsulfonic acid functionalized cubic Ia-3d mesoporous catalysts

4.5.1 Effect of mole ratio

The effect of anisole to *tert*-butanol mole ratio was investigated in the range of 1:1 to 1:9 and shown in Table 4.13. When amount of *tert*-butanol was increased from 1:1 to 1:3, the anisole conversion was enhanced and attained to 94% as like the total yield of product attained to a maximum value 90% and gave the highest selectivity of 4-TBA. On the other hand, when the mole ratio was further increase to 1:9, there was a significant change in the rate of reaction, while the anisole conversion was as high as 96% at 1:6 mole ratio but the total yield of product was lower (56%) than that of 1:3 mole ratio. This effect may be caused by the consumption of butylating agent by side reaction of excess *tert*-butanol. That induced high volume of isobutylene and subsequent oligomerization to produce *di*-isobutylene and *tri*-isobutylene [54], respectively. Furthermore, the optimum mole ratio was deduced to 1:3 and will be used in the next study.

Table 4.13 Effect of mole ratio on product yields and product distribution over MCA-Pr-SO₃H

Anisole : <i>t</i> -BuOH mole ratio	Conversion (%)	Selectivity %			Total yield of product %
		2-TBA	4-TBA	2,4- DTBA	
1:1	53	21	48	5	46
1:2	87	15	55	7	66
1:3	94	34	55	7	90
1:6	96	22	34	6	56
1:9	89	18	18	5	36

Reaction Condition: reaction temperature 150 °C; catalytic amount 5wt% base on total weight; reaction time 5 h.

4.5.2 Effect of reaction temperature

The impact of the reaction temperature on yield and selectivity of the butylated anisole product was investigated at various temperature from 120-175°C. From Table 4.14, when the temperature was increased from 120°C up to 150°C the conversion of anisole and total yield of product increased and reached the maximum to 94% and 90%, respectively. At the same time, selectivity of 4-TBA gave the highest of butylated products. However, from 150°C to 175°C, the conversion of anisole and total yield of product decreased because at these relatively high temperature, TBA itself could react with excess carbocation to produce 2,4-di-tert-butyl anisole (2,4-DTBA) and by-products, such as *di*-isobutylene and *tri*-isobutylene, could be produced from the reaction of excess isobutylene molecule [55]. Then the reaction temperature 150°C was selected to study in the next parameter effect.

Table 4.14 Effect of reaction temperature on product yields and product distribution over MCA-Pr-SO₃H

Temperature (°C)	Conversion (%)	Selectivity %			Total yield of product %
		2-TBA	4-TBA	2,4-DTBA	
120	12	38	53	7	12
150	94	34	55	7	90
175	92	27	27	7	72

Reaction condition; mole ratio 1:3; catalytic amount 5 wt% base on total weight; reaction time 5 h.

4.5.3 Effect of reaction time

The influence of reaction time on butylation was shown in Table 4.15. The conversion and butylated products yield were enhanced with increasing reaction time from 1 h to 5 h. On the other hand, when the reaction was continued to 10 h., the conversion of anisole and total yield of product were gradually decreased. It could be explained by de-alkylation or elimination of butyl group. Therefore, the suitable reaction time was concluded at 5 h.

Table 4.15 Effect of time on product yields and product distribution over

MCA-Pr-SO₃H

Time (h.)	Conversion (%)	Selectivity %			Total yield of product %
		2-TBA	4-TBA	2,4-DTBA	
1	74	32	42	6	65
2.5	91	34	45	6	78
5	94	34	55	7	90
7	92	23	55	6	78
10	91	20	58	6	76

Reaction Condition: mole ratio 1:3; reaction temperature 150°C, catalytic amount 5 wt% base on total weight.

4.5.4 Effect of catalytic amount

The effect of catalyst amount on the reaction was studied by varying from 0 to 7.5 wt% of the reactant as shown in Table4.16. With an increase in catalytic amount up to 2.5wt%, the conversion and yield of product increased. The greatest yield of product (92%) was obtained at the catalytic loading of 2.5wt%. At 5 to 7.5 wt%, the conversion of anisole was constant and yield of product decreased. The acid catalyst was important to induce the *tert*-butyl carbocation intermediate of butylation. However, the catalyst overloading might be impeded the phase mixing of anisole and *tert*-butanol.

Table4.16 Effect of catalytic amount on product yields and product distribution over MCA-Pr-SO₃H

Catalytic amount wt%	Conversion (%)	Selectivity %			Yield of products %
		2-TBA	4-TBA	2,4-DTBA	
0	0	0	0	0	0
0.5	66	32	46	9	57
1	90	33	53	7	84
2.5	93	34	57	7	92
5	94	34	55	7	90
7.5	92	17	50	6	67

Reaction Condition: mole ratio 1:3; reaction temperature 150°C; reaction time 5 h.

4.6 Catalytic performance of ZSM-5/MCA-Pr-SO₃H

Comparison of the anisole conversion and *para*-selectivity butylated anisole product over MCA-Pr-SO₃H, ZSM-5, ZSM-5-Pr-SO₃H, ZM-30 and physical mixing (P-ZM-30) catalysts were shown in Table 4.17. From the result, the composite ZM-30 catalyst gave the selectivity of 4-TBA as 96.8% which was higher than MCA-Pr-SO₃H, ZSM-5-Pr-SO₃H, and P-ZM-30 catalysts. In contrast, the anisole conversion of ZM-30 catalyst was lower than MCA-Pr-SO₃H and P-ZM-30 catalysts because of incorporated ZSM-5 in the mesoporous material. Moreover, P-ZM-30 catalyst gave the result close to MCA-Pr-SO₃H catalyst because ZSM-5 powder cannot incorporate into the pore wall of MCA-Pr-SO₃H structure, indicated from nitrogen sorption isotherm in Figure 4.12. ZSM-5 zeolite showed superior catalytic performance selectively to *para*-selectivity product [23]. In addition, ZM-30 catalyst gave the selectivity of 4-TBA close to commercial ZSM-5 but showed higher anisole conversion because ZM-30 exhibited higher total specific surface area, pore volume and also acidity than ZSM-5. Although, ZSM-5 was modified with propylsulfonic group in order to improve the acidic property. The anisole conversion and 4-TBA selectivity of ZSM-5-Pr-SO₃H was lower than ZM-30 material.

Table 4.17 Products distribution over on optimum condition of propylsulfonic acid functionalized mesoporous material.

Catalysts	%Conversion	%Selectivity		
		2-TBA	4-TBA	2,4-DTBA
MCA-Pr-SO ₃ H	93.1	34.2	57.3	6.8
ZSM-5	25.6	2.5	97.5	0
ZSM-5-Pr-SO ₃ H	36.1	3.3	82.9	0
ZM-30	51.4	3.2	96.8	0
P-ZM-30	90.4	34.9	59.7	5.4

Reaction condition; 150°C, *anisole*: *t*-BuOH = 1:3 by mole, 2.5 wt% of catalyst based on total weight, 5h

4.7 Reusability of Catalysts

The reusability of catalysts was tested in optimum condition of anisole alkylation. The catalysts were recovered from the reaction mixture by filtration and washing with acetone. After that, the sample was dried at 70°C overnight. The catalysts could be repeatedly used in anisole alkylation.

4.7.1 Reusability of MCA-Pr-SO₃H

4.7.1.1 Characterization of recyclable MCA-Pr-SO₃H

From the XRD recyclable MCA-Pr-SO₃H was shown in Figure 4.16. The reused of MCA-Pr-SO₃H still exhibited cubic *1a-3d* mesostructure, which was analogous to fresh MCA-Pr-SO₃H catalyst configuration. However, the crystallinity of recyclable catalyst was partly damaged, by stirring reaction condition and remaining of coke in pore system, that indicated by decreasing of characteristic peaks intensity.

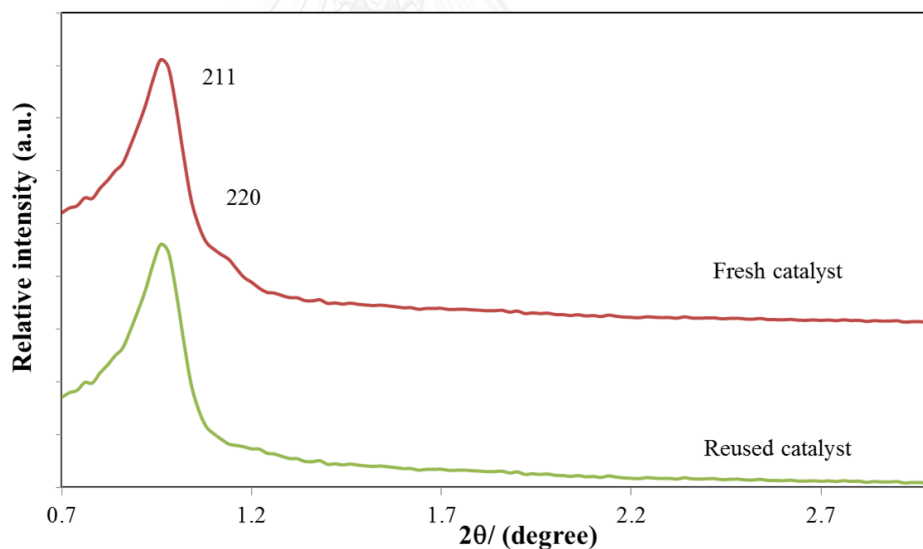


Figure 4.16 X-ray powder diffraction patterns of reused MCA-Pr-SO₃H

The isotherms of fresh and reused MCA-Pr-SO₃H were shown in Figure 4.17. The results performed the characteristic isotherm of mesoporous material. The properties of fresh and reused MCA-Pr-SO₃H catalysts were presented in Table 4.18. Comparing with fresh catalyst, the total specific surface area and pore volume of reused MCA-Pr-SO₃H were decreased because some residues remaining in the pore of catalyst that effected to lower acid site. Moreover, acidity of reused catalyst was decreased because breakdown of sulfonic acid group on the catalytic surface.

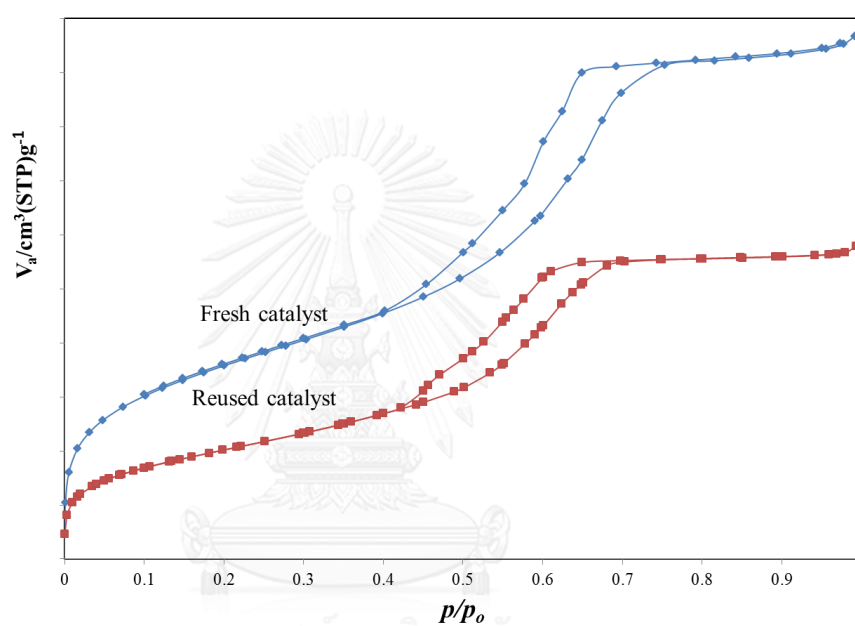


Figure 4.17 Nitrogen sorption isotherms of catalysts

Table 4.18 Textural properties of fresh and reused MCA-Pr-SO₃H

Sample	a_0^c	BET surface area (m ² g ⁻¹) ^a	Total pore volume (cm ³ g ⁻¹) ^a	Pore diameter (nm) ^b	Wall thickness (nm) ^d	Acidity (mmol/g) ^e
Fresh catalyst	21.2	762	0.7964	5.52	9.5	0.79
Reused catalyst	21.2	407	0.4458	5.52	9.5	0.57

^aCalculated using the BET plot method

^bCalculated using the BJH and MP method

^cCalculated as: $a_0 = \sqrt{6 \times d}$ where d is d-spacing of the (211) reflection plane from XRD method

^dWall thickness $T_{\text{wall}} = a_0 \times \sqrt{(2/2 - d_{\text{pore}})}$, where d_{pore} and a_0 are pore distribution and cubic unit cell parameter, respectively [48].

4.7.1.2 Activity of recyclable MCA-Pr-SO₃H

The reused MCA-Pr-SO₃H catalyst was tested in optimum condition that carried out with anisole:tert-butanol mole ratio as 1: 3, catalytic amount 2.5 wt% base on total weigh of reactant at 150°C for 8 hr. In addition, the comparison of catalytic activity between reused and fresh MCA-Pr-SO₃H were shown in Table 4.18. The activity of MCA-Pr-SO₃H was decreased in reused run, the anisole conversion declined from 94.3% to 66.1% and the total yield of product was maintained at 45.7%.

Table 4.19 Activities of fresh and reused MCA-Pr-SO₃H

MCA-Pr-SO ₃ H	Conversion	Selectivity			Yield of products
		2TBA	4TBA	24-DTBA	
Fresh catalyst	94.3	34.2	55.1	6.6	90.5
Reused catalyst	66.1	37.9	57.3	4.9	45.7

Reaction condition; 150 °C, *anisole*: *t*-BuOH = 1:3 by mole, 2.5 wt% of catalyst based on total weight, 5h

4.7.2 Reusability of ZM-30 composite catalyst

4.7.2.1 Characterization of recyclable ZM-30 composite catalyst

From the XRD recyclable ZM-30 was shown in Figure 4.18. The reused of ZM-30 still exhibited cubic *la-3d* mesostructure, which was analogous to fresh MCA-Pr-SO₃H catalyst configuration. And also, this catalyst still presented zeolite MFI structure. However, the intensity of peaks of both patterns were decreased because recyclable of ZM-30 sample was damaged from stirring reaction and coke remaining in pore system. Figure 4.19 and Table 4.20 showed the characterization results of reused catalyst with fresh ZM-30 catalyst. The isotherms of both catalysts performed the hysteresis loop type IV that remained almost horizontal over a wide range of relative pressure, which was consistent with the presence of microporous zeolite. The comparison of both materials revealed that the reused ZM-30 catalyst was decreased in the total specific surface area and pore volume. The possible reason may be due to the coke formation and encapsulation of remained reactants and products within pore of catalyst.

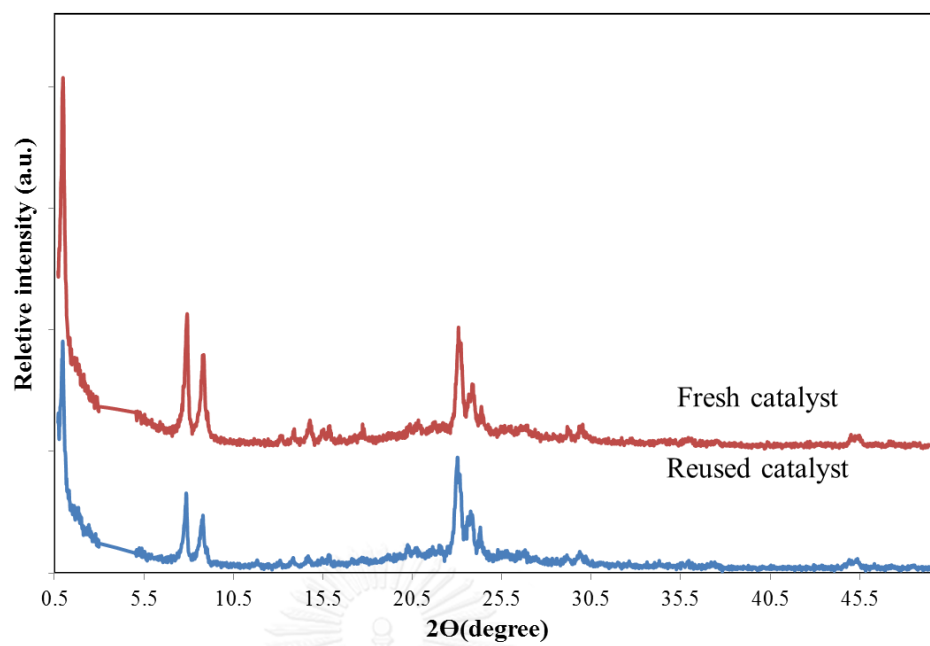


Figure 4.18 X-ray powder diffraction patterns of reused ZM-30

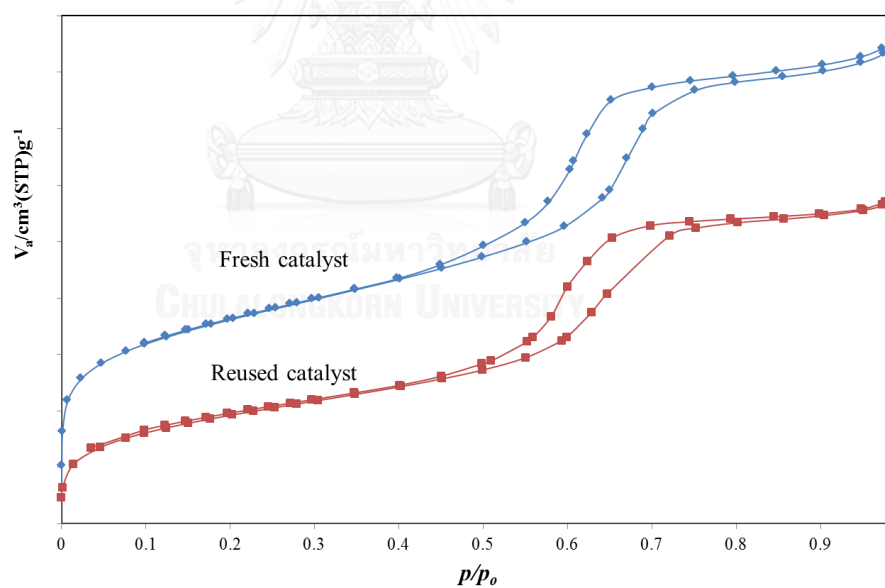


Figure 4.19 Nitrogen sorption isotherms of catalysts

Table 4.20 Textural properties of fresh and reused ZM-30

ZM-30	a_0^c	BET surface area ($m^2 g^{-1}$) ^a	Total pore volume ($cm^3 g^{-1}$) ^a	Pore diameter (nm) ^b	Wall thickness (nm) ^d	Acidity (mmol/g) ^e
Fresh catalyst	22.7	577.2	0.4287	4.69	11.4	1.28
Reused catalyst	22.7	270.6	0.3744	4.60	11.3	1.20

^a Calculated using the BET plot method

^b Calculated using the BJH and MP method

^c Calculated as: $a_0 = \sqrt{6 \times d}$ where d is d-spacing of the (211) reflection plane from XRD method

^d Wall thickness $T_{wall} = a_0 \times \sqrt{2/2 - d_{pore}}$, where d_{pore} and a_0 are pore distribution and cubic unit cell parameter, respectively [48].

4.7.2.2 Activity of recyclable ZM-30 composite catalyst

The reused ZM-30 composite catalyst was tested in an optimum condition that carried out with anisole: *tert*-butanol mole ratio as 1: 3, catalytic amount 2.5 wt% based on total weight of reactant at 150°C for 8 hr. The reused ZM-30 gave the conversion of anisole decreased in 50% but this reused catalyst remained in high selectivity of 4-TBA as 96%.

Table 4.21 Activities of fresh and reused ZM-30

ZM-30	Conversion	Selectivity			Yield of 4-TBA
		2TBA	4TBA	24-DTBA	
Fresh catalyst	51.1	3.2	96.8	0.0	27.1
Reused catalyst	24.0	4.8	95.9	0.0	21.2

Reaction condition; 150 °C, *anisole*: *t*-BuOH = 1:3 by mole, 2.5 wt% of catalyst based on total weight, 5h.

4.8 Antioxidant activity

Antioxidant abilities of standard chemical (BHT), anisole, purified products and reaction mixtures were shown in Figure 4.20. Low of IC₅₀ value demonstrated high ability of radical termination. In the case of butylated products, radical scavenging capacities were increased as following order; 2-*tert*-butyl anisole < 4-*tert*-butyl anisole < anisole. Butylated anisoles showed higher performance of radical scavenger than anisole, which was substrate. Also, antioxidant ability of reaction mixture was considered to eliminate the separation process. Reaction mixture (MCA-Pr-SO₃H) showed larger efficiency than reaction mixture (ZM-30) due to more quantity of 2-*tert*-butyl anisole and 2, 4-di-*tert*-butyl anisole that exhibited high ability of radical elimination.

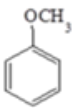
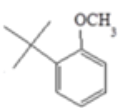
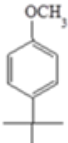
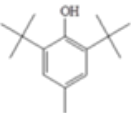
 Anisole	 2-TBA	 4-TBA
$IC_{50} = 10.63 \text{ mg/ml}$	$IC_{50} = 0.11 \text{ mg/ml}$	$IC_{50} = 2.78 \text{ mg/ml}$
 BHT	Reaction mixture (MCA-Pr-SO ₃ H) Conversion =94.3%, % Yield of TBAs=90.5%	Reaction mixture (ZM-30) Conversion =51.4%, % Yield of TBAs=25.74%
$IC_{50} = 0.04 \text{ mg/ml}$	$IC_{50} = 0.71 \text{ mg/ml}$	$IC_{50} = 1.18 \text{ mg/ml}$

Figure 4.20 Comparison of radical scavenging of anisole, butylated anisole, BHT and reaction mixtures



CHAPTER V

CONCLUSIONS

Propylsulfonic acid functionalized cubic *1a-3d* mesoporous (MCA) silica was successfully synthesized by co-condensation of TEOS and MPTMS under acidic condition with the P123 surfactant as the structure directing agent. Moreover micro/mesoporous material, ZSM-5-MCA, was successfully prepared by using zeolite seeds method. The zeolite, ZSM-5 seeds were incorporated into the wall of mesoporous material. The united ZSM-5 structure had stronger rigidity than amorphous silicate, so ZSM-5 could be easily formed in the wall of mesostructure. In addition, the containing of zeolite in micro/mesoporous composite material influenced to increase acidity. The MCA-Pr-SO₃H catalyst is a highly active acid catalyst, which provided the highest conversion of anisole and total yield of product due to its cubic 3D mesostructure with sulfonic functional groups. Large cubic 3D mesostructure can increase the diffusion speed of reactants and alkylated products in the pore. And also, sulfonic functional group was added to improve their acidities for anisole alkylation. Comparing with ZSM5-MCA (ZM-30) composite catalyst that could promote the selectivity of 4-TBA because the ZSM-5 in composite catalyst predominated the *para*-aromatic structure.

The suggestion for future work

1. To modify porous material with other alkyl sulfonic porous materials
2. To study the efficiency of regeneration catalysts in anisole alkylation

REFERENCES

- [1] Kamala, P. and Pandurangan, A. Mesoporous molecular sieves: alkylation of anisole using tert-butyl alcohol. Catalysis Letters 110(1): 39-45.
- [2] Haubrock, J., et al. Reaction from Dimethyl Carbonate (DMC) to Diphenyl Carbonate (DPC). 2. Kinetics of the Reactions from DMC via Methyl Phenyl Carbonate to DPC. Industrial & Engineering Chemistry Research 47(24) (2008): 9862-9870.
- [3] Feng, Y.-F., Yang, X.-Y., Di, Y., Du, Y.-C., Zhang, Y.-L., and Xiao, F.-S. Mesoporous Silica Materials with an Extremely High Content of Organic Sulfonic Groups and Their Comparable Activities with that of Concentrated Sulfuric Acid in Catalytic Esterification. The Journal of Physical Chemistry B 110(29) (2006): 14142-14147.
- [4] Di, Z., Yang, C., Jiao, X., Li, J., Wu, J., and Zhang, D. A ZSM-5/MCM-48 Based Catalyst for Methanol to Gasoline Conversion. Fuel 104 (2013): 878-881.
- [5] Yadav, G.D. and More, S.R. Green alkylation of anisole with cyclohexene over 20% cesium modified heteropoly acid on K-10 acidic montmorillonite clay. Applied Clay Science 53(2) (2011): 254-262.
- [6] Cativiela, C., et al. Clay-catalyzed Friedel-Crafts alkylation of anisole with dienes. Applied Catalysis A: General 123(2) (1995): 273-287.
- [7] Krishnan, V., Ojha, K., and Pradhan, N.C. Alkylation of Phenol with Tertiary Butyl Alcohol over Zeolites. Organic Process Research & Development 6(2) (2002): 132-137.
- [8] Song, K., Guan, J., Wu, S., Yang, Y., Liu, B., and Kan, Q. Alkylation of Phenol with tert-Butanol Catalyzed by Mesoporous Material with Enhanced Acidity Synthesized from Zeolite MCM-22. Catalysis Letters 126(3) (2008): 333-340.
- [9] Tateiwa, J.-i., Horiuchi, H., Hashimoto, K., Yamauchi, T., and Uemura, S. Cation-Exchanged Montmorillonite-Catalyzed Facile Friedel-Crafts Alkylation of Hydroxy and Methoxy Aromatics with 4-Hydroxybutan-2-one To Produce

- Raspberry Ketone and Some Pharmaceutically Active Compounds. The Journal of Organic Chemistry 59(20) (1994): 5901-5904.
- [10] Harmer, M.A. and Sun, Q. Solid acid catalysis using ion-exchange resins. Applied Catalysis A: General 221(1-2) (2001): 45-62.
- [11] Beck, J.S., et al. A new family of mesoporous molecular sieves prepared with liquid crystal templates. Journal of the American Chemical Society 114(27) (1992): 10834-10843.
- [12] Zhao, D., et al. Triblock Copolymer Syntheses of Mesoporous Silica with Periodic 50 to 300 Angstrom Pores. Science 279(5350) (1998): 548-552.
- [13] Alfredsson, V. and Anderson, M.W. Structure of MCM-48 Revealed by Transmission Electron Microscopy. Chemistry of Materials 8(5) (1996): 1141-1146.
- [14] Margolese, D., Melero, J.A., Christiansen, S.C., Chmelka, B.F., and Stucky, G.D. Direct Syntheses of Ordered SBA-15 Mesoporous Silica Containing Sulfonic Acid Groups. Chemistry of Materials 12(8) (2000): 2448-2459.
- [15] Wight, A.P. and Davis, M.E. Design and Preparation of Organic-Inorganic Hybrid Catalysts. Chemical Reviews 102(10) (2002): 3589-3614.
- [16] Zhang, X., Zhao, N., Wei, W., and Sun, Y. Chemical fixation of carbon dioxide to propylene carbonate over amine-functionalized silica catalysts. Catalysis Today 115(1-4) (2006): 102-106.
- [17] Liang, J., Owens, J.R., Huang, T.S., and Worley, S.D. Biocidal hydantoinylsiloxane polymers. IV. N-halamine siloxane-functionalized silica gel. Journal of Applied Polymer Science 101(5) (2006): 3448-3454.
- [18] Kubota, Y., Jin, C., and Tatsumi, T. Performance of organic-inorganic hybrid catalysts based on Ia-3d mesoporous silica. Catalysis Today 132(1-4) (2008): 75-80.
- [19] El-Safty, S.A., Hanaoka, T., and Mizukami, F. Large-Scale Design of Cubic Ia3d Mesoporous Silica Monoliths with High Order, Controlled Pores, and Hydrothermal Stability. Advanced Materials 17(1) (2005): 47-53.

- [20] Huang, J., Tian, G., Wang, H., Xu, L., and Kan, Q. Large-pore cubic Ia-3d mesoporous silicas: Synthesis, modification and catalytic applications. Journal of Molecular Catalysis A: Chemical 271(1-2) (2007): 200-208.
- [21] Naber, J.E., de Jong, K.P., Stork, W.H.J., Kuipers, H.P.C.E., and Post, M.F.M. Industrial applications of zeolite catalysis. in J. Weitkamp, H.G.K.H.P. and Hölderich, W. (eds.), Studies in Surface Science and Catalysis, pp. 2197-2219: Elsevier, 1994.
- [22] Restuccia, D., et al. New EU regulation aspects and global market of active and intelligent packaging for food industry applications. Food Control 21(11) (2010): 1425-1435.
- [23] Van Vu, D., Miyamoto, M., Nishiyama, N., Egashira, Y., and Ueyama, K. Selective formation of para-xylene over H-ZSM-5 coated with polycrystalline silicalite crystals. Journal of Catalysis 243(2) (2006): 389-394.
- [24] Landry, C.C., et al. Phase Transformations in Mesostructured Silica/Surfactant Composites. Mechanisms for Change and Applications to Materials Synthesis. Chemistry of Materials 13(5) (2001): 1600-1608.
- [25] Kleitz, F., Choi, S.H., and Ryoo, R. Cubic Ia3d large mesoporous silica: synthesis and replication to platinum nanowires, carbon nanorods and carbon nanotubes. Chemical Communications (2003): 2136-2137.
- [26] Karlsson, A., Stöcker, M., and Schmidt, R. Composites of micro- and mesoporous materials: simultaneous syntheses of MFI/MCM-41 like phases by a mixed template approach. Microporous and Mesoporous Materials 27(2-3) (1999): 181-192.
- [27] Prokešová, P., Mintova, S., Čejka, J., and Bein, T. Preparation of nanosized micro/mesoporous composites via simultaneous synthesis of Beta/MCM-48 phases. Microporous and Mesoporous Materials 64(1-3) (2003): 165-174.
- [28] Xia, Y. and Mokaya, R. On the synthesis and characterization of ZSM-5/MCM-48 aluminosilicate composite materials. Journal of Materials Chemistry 14(5) (2004): 863.

- [29] Ooi, Y.-S., Zakaria, R., Mohamed, A.R., and Bhatia, S. Synthesis of composite material MCM-41/Beta and its catalytic performance in waste used palm oil cracking. Applied Catalysis A: General 274(1-2) (2004): 15-23.
- [30] Dong, H.-j. and Shi, L. Alkylation of Toluene with t-Butyl Alcohol over Zeolite Catalysts. Industrial & Engineering Chemistry Research 49(5)(2010): 2091-2095.
- [31] Bao, S., Quan, N., Zhang, J., and Yang, J. Alkylation of p-Cresol with tert-Butanol Catalyzed by Novel Multiple-SO₃H Functioned Ionic Liquid. Chinese Journal of Chemical Engineering 19(1) (2011): 64-69.
- [32] catalysis [Online]. 2016. Available from: <https://en.wikipedia.org/wiki/Catalysis>
- [33] Deutschmann, O., Knözinger, H., Kochloefl, K., and Turek, T. Heterogeneous Catalysis and Solid Catalysts. in Ullmann's Encyclopedia of Industrial Chemistry: Wiley-VCH Verlag GmbH & Co. KGaA, 2000.
- [34] [Online]. 2016. Available from: <https://en.wikipedia.org>
- [35] Karnaukhov, A.P. The texture of dispersed and porous materials [Online]. 1999. Available from: <http://eng.thesaurus.rusnano.com/wiki/article1179>
- [36] Matias, P. Transformation du methylcyclohexane et du n-heptane sur la zeolithe MCM-22. Ph.D. , Universidade Técnica de Lisboa, 2008.
- [37] Kumar, D., Schumacher, K., du Fresne von Hohenesche, C., Grün, M., and Unger, K.K. MCM-41, MCM-48 and related mesoporous adsorbents: their synthesis and characterisation. Colloids and Surfaces A: Physicochemical and Engineering Aspects 187–188 (2001): 109-116.
- [38] Čejka, J. and Mintova, S. Perspectives of Micro/Mesoporous Composites in Catalysis. Catalysis Reviews 49(4) (2007): 457-509.
- [39] Liu, Y., Zhang, W., and Pinnavaia, T.J. Steam-Stable Aluminosilicate Mesostructures Assembled from Zeolite Type Y Seeds. Journal of the American Chemical Society 122(36) (2000): 8791-8792.
- [40] Wang, W., Liu, P., Zhang, M., Hu, J., and Xing, F. The Pore Structure of Phosphoaluminate Cement Journal of Composite Materials 2 (2012): 104-112
- [41] Kamala, P. and Pandurangan, A. Mesoporous molecular sieves: alkylation of anisole using tert-butylalcohol. Catalysis Letters 110(1-2) (2006): 39-45.
- [42] Gore, P.H. Friedel-crafts and reaction. in Inter-science, p. 535. New York, 1967.

- [43] Sreevardhan Reddy, S., David Raju, B., Siva Kumar, V., Padmasri, A.H., Narayanan, S., and Rama Rao, K.S. Sulfonic acid functionalized mesoporous SBA-15 for selective synthesis of 4-phenyl-1,3-dioxane. Catalysis Communications 8(3) (2007): 261-266.
- [44] Tao, Y., Kanoh, H., and Kaneko, K. ZSM-5 Monolith of Uniform Mesoporous Channels. Journal of the American Chemical Society 125(20) (2003): 6044-6045.
- [45] Mbaraka, I.K., Radu, D.R., Lin, V.S.Y., and Shanks, B.H. Organosulfonic acid-functionalized mesoporous silicas for the esterification of fatty acid. Journal of Catalysis 219(2) (2003): 329-336.
- [46] Subramanion, L.J. Phytochemicals screening, DPPH free radical scavenging and xanthine oxidase inhibitory activities of Cassia fistula seeds extract. Journal of Medicinal Plants Research 5 (2011): 1941.
- [47] Wang, W., Liu, P., Zhang, M., Hu, J., and Xing, F. The Pore Structure of Phosphoaluminate Cement. Open Journal of Composite Materials 02(03) (2012): 104-112.
- [48] Ravikovitch, P.I. and Neimark, A.V. Density Functional Theory of Adsorption in Spherical Cavities and Pore Size Characterization of Templated Nanoporous Silicas with Cubic and Three-Dimensional Hexagonal Structures. Langmuir 18(5) (2002): 1550-1560.
- [49] Jacobs, P.A. and Von Ballmoos, R. Framework hydroxyl groups of H-ZSM-5 zeolites. The Journal of Physical Chemistry 86(15) (1982): 3050-3052.
- [50] Nuntang, S., Poompradub, S., Butnark, S., Yokoi, T., Tatsumi, T., and Ngamcharussrivichai, C. Organosulfonic acid-functionalized mesoporous composites based on natural rubber and hexagonal mesoporous silica. Materials Chemistry and Physics 147(3) (2014): 583-593.
- [51] Hegde, S.G., Kumar, R., Bhat, R.N., and Ratnasamy, P. Characterization of the acidity of zeolite Beta by FTi.r. spectroscopy and t.p.d. of NH₃. Zeolites 9(3) (1989): 231-237.
- [52] Matias, P. Transformation du methylcyclohexane et du n-heptane sur la zeolithe MCM-22. Ph.D, Universidade Técnica de Lisboa, 2008.

- [53] Siril, P.F., Davison, A.D., Randhawa, J.K., and Brown, D.R. Acid strengths and catalytic activities of sulfonic acid on polymeric and silica supports. Journal of Molecular Catalysis A: Chemical 267(1-2) (2007): 72-78.
- [54] Yadav, G.D. and Doshi, N.S. Alkylation of phenol with methyl-tert-butyl ether and tert-butanol over solid acids: efficacies of clay-based catalysts. Applied Catalysis A: General 236(1-2) (2002): 129-147.
- [55] Chaudhuri, B., Patwardhan, A.A., and Sharma, M.M. Alkylation of substituted phenols with olefins and separation of close-boiling phenolic substances via alkylation/dealkylation. Industrial & Engineering Chemistry Research 29(6) (1990): 1025-1031.





APPENDICES

จุฬาลงกรณ์มหาวิทยาลัย
CHULALONGKORN UNIVERSITY

1 Standard solution and calibration solution

1.1 Anisole standard solution

1.1.1 Stock standard solution 0.125 M

A 0.1417 g of anisole was accurately weighed in a 10 mL volumetric flask and made up to the mark with tetrahydrofuran (THF).

1.1.2 Working standard solution (0.075, 0.0375 and 0.01875 M)

The working standard solutions were prepared by dilution of the stock standard solution using a pipette and then made up to the mark with tetrahydrofuran (THF).

1.2 2-*tert*-butyl anisole standard solution

1.2.1 Stock standard solution 0.125 M

A 0.2075 g of 2-*tert*-butyl anisole was accurately weighed in a 10 mL volumetric flask and made up to the mark with tetrahydrofuran (THF).

1.2.2 Working standard solution (0.075, 0.0375 and 0.01875 M)

The working standard solutions were prepared by dilution of the stock standard solution using a pipette and then made up to the mark with tetrahydrofuran (THF).

1.3 4-*tert*-butyl anisole standard solution

1.3.1 Stock standard solution 0.125 M

A 0.2075 g of 4-*tert*-butyl anisole was accurately weighed in a 10 mL volumetric flask and made up to the mark with tetrahydrofuran (THF).

1.3.2 Working standard solution (0.05, 0.01, 0.005 and 0.001 M)

The working standard solutions were prepared by dilution of the stock standard solution using a pipette and then made up to the mark with tetrahydrofuran (THF).

1.4 Standard calibration solution

Three calibration solutions were prepared into a series of vials. The weight 0.50 g of stock and working anisole and butylated anisole solutions were transferred into the five vials and added 0.25 g of internal standard 0.1 M n- octane stock solution to the five standard solutions. Then, a 1 μL of each reaction mixture was analyzed by GC technique under the condition.



2. Calibration function

The calibration function was given by the following expression, obtained from the experimental data using the linear regression method.

$$\text{Linear regression equation: } Y = mX + b$$

2.1 Anisole calibration function

$$M_{A_n}/M_{I_S} = m(A_{A_n}/A_{I_S}) + b$$

$$M_{A_n} = \text{the mass of Anisole (g)}$$

$$M_{I_S} = \text{the mass of internal standard (n-octane, g)}$$

$$A_{A_n} = \text{the peak area of anisole}$$

$$A_{I_S} = \text{the peak area of n-octane}$$

In regression function X was represented by the term of A_{A_n}/A_{I_S} while Y was M_{A_n}/M_{I_S}

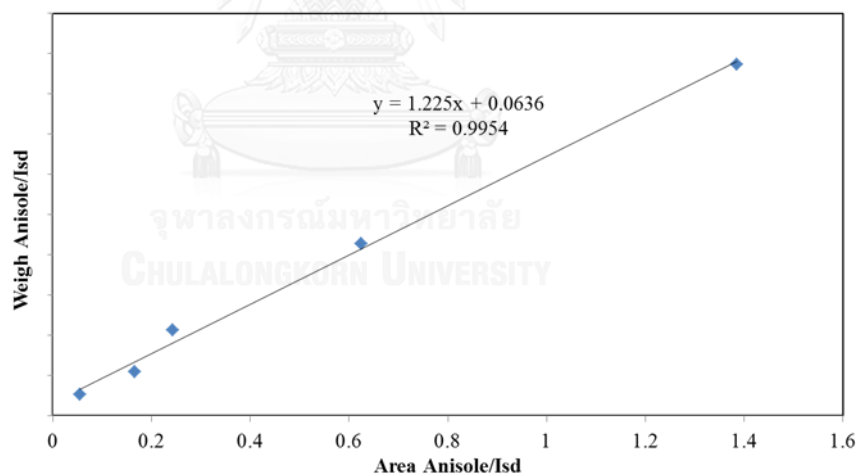


Figure A- 1Calibration curve of Anisole

2.2 2-*tert*-butyl anisole calibration functions

$$M_{2\text{TBA}}/M_{\text{IS}} = m(A_{2\text{TBA}}/A_{\text{IS}}) + b$$

$M_{2\text{TBA}}$ = the mass of 2-*tert*-butyl anisole (g)

M_{IS} = the mass of internal standard (n-octane, g)

$A_{2\text{TBA}}$ = the peak area of 2-*tert*-butyl anisole

A_{IS} = the peak area of n-octane

In regression function X was represented by the term of $A_{2\text{TBA}}/A_{\text{IS}}$ while Y was $M_{2\text{TBA}}/M_{\text{IS}}$

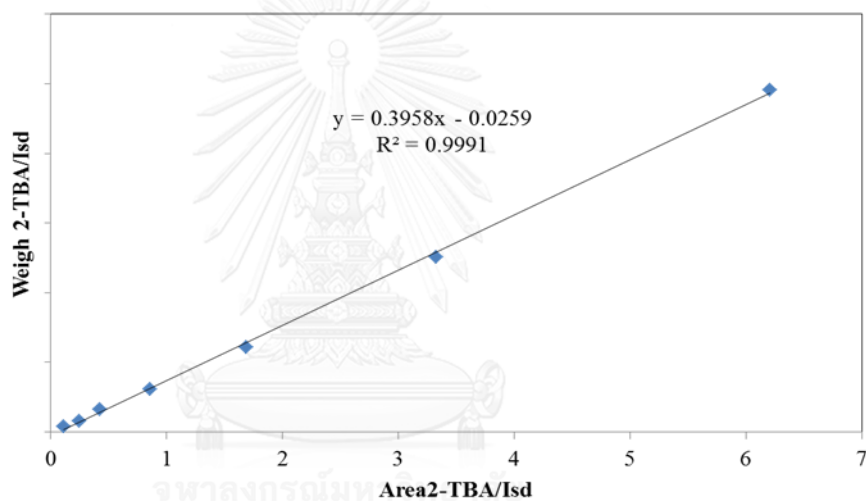


Figure A- 2 Calibration curve of 2-*tert*-butyl anisole

2.3 4-*tert*-butyl anisole calibration functions

$$M_{4\text{TBA}}/M_{\text{IS}} = m(A_{4\text{TBA}}/A_{\text{IS}}) + b$$

$M_{4\text{TBA}}$ = the mass of 4-*tert*-butyl anisole (g)

M_{IS} = the mass of internal standard (n-octane, g)

$A_{4\text{TBA}}$ = the peak area of 4-*tert*-butyl anisole

A_{IS} = the peak area of n-octane

In regression function X was represented by the term of $A_{4\text{TBA}}/A_{\text{IS}}$ while Y was $M_{4\text{TBA}}/M_{\text{IS}}$

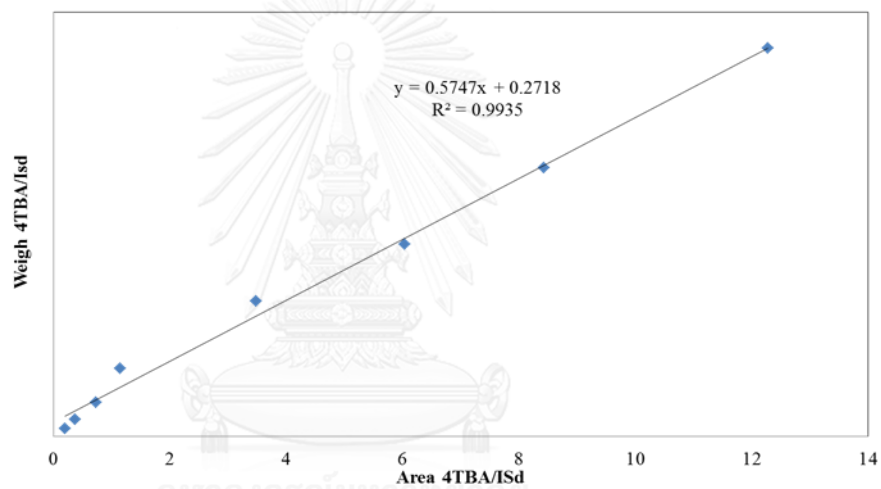


Figure A- 3 Calibration curve of 4-*tert*-butyl anisole

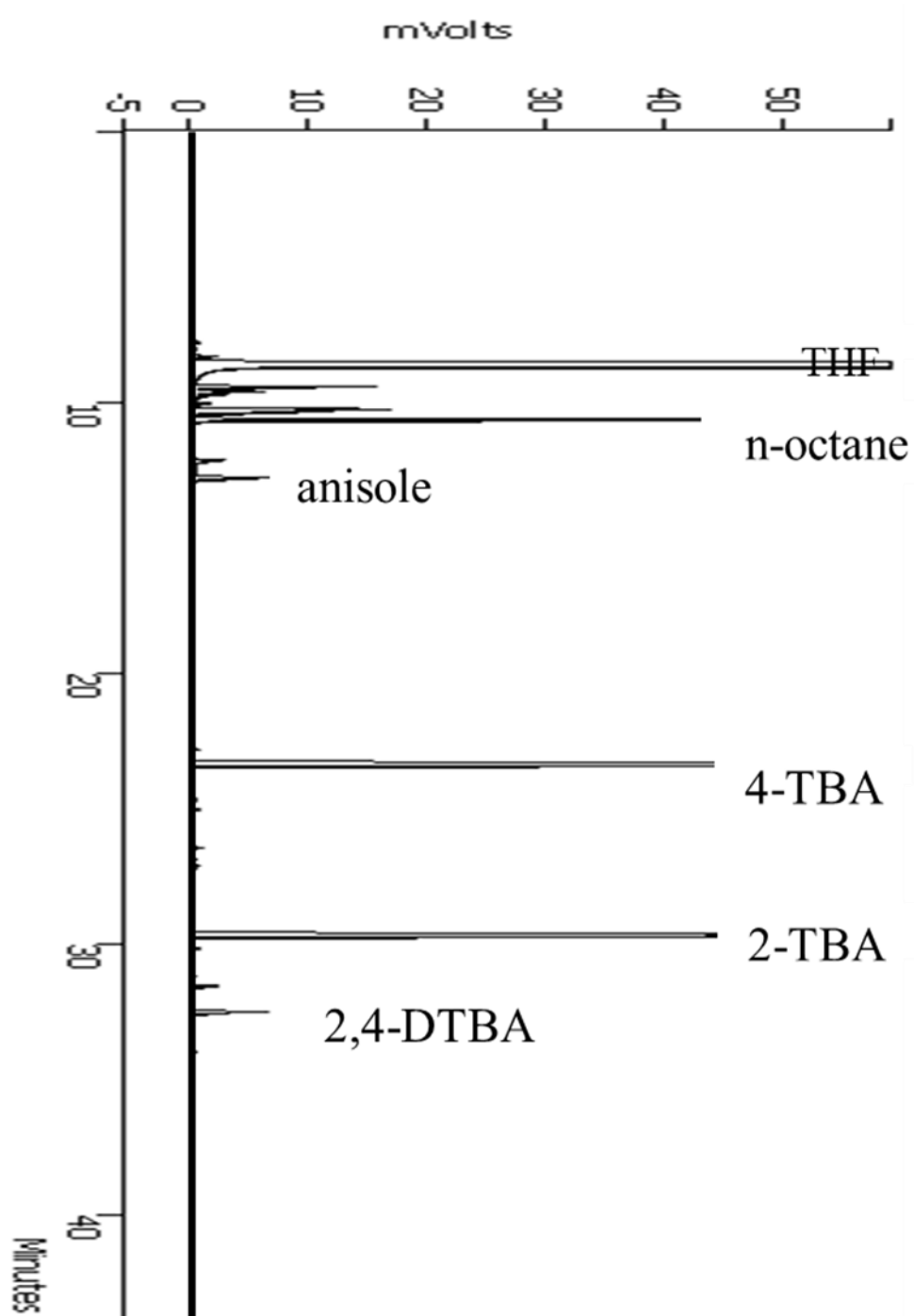


Figure A- 4 GC chromatogram of products from anisole alkylation over on MCA-Pr-SO₃H catalyst

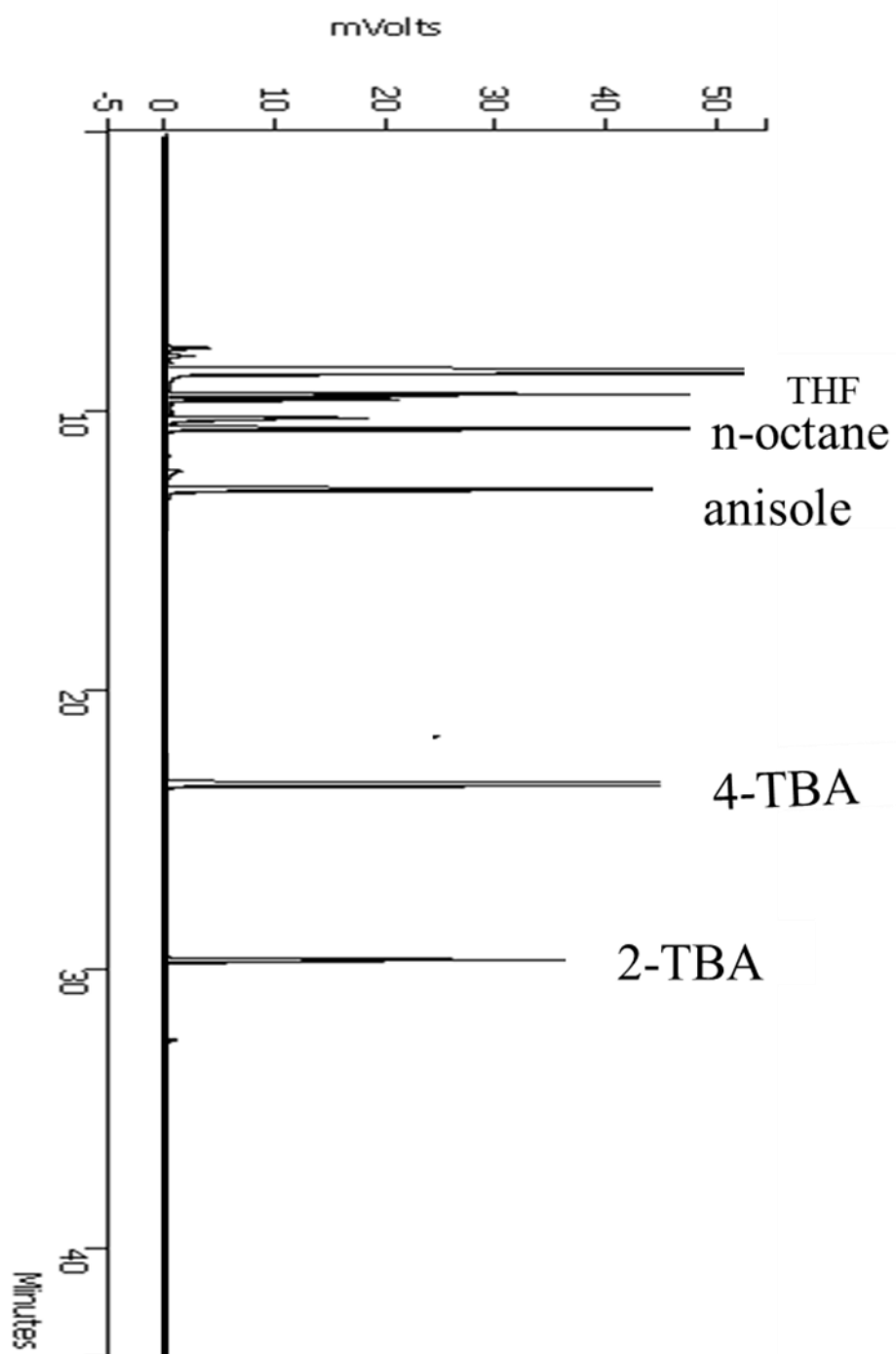


Figure A- 5 GC chromatogram of products from anisole alkylation over on ZM-30 catalyst

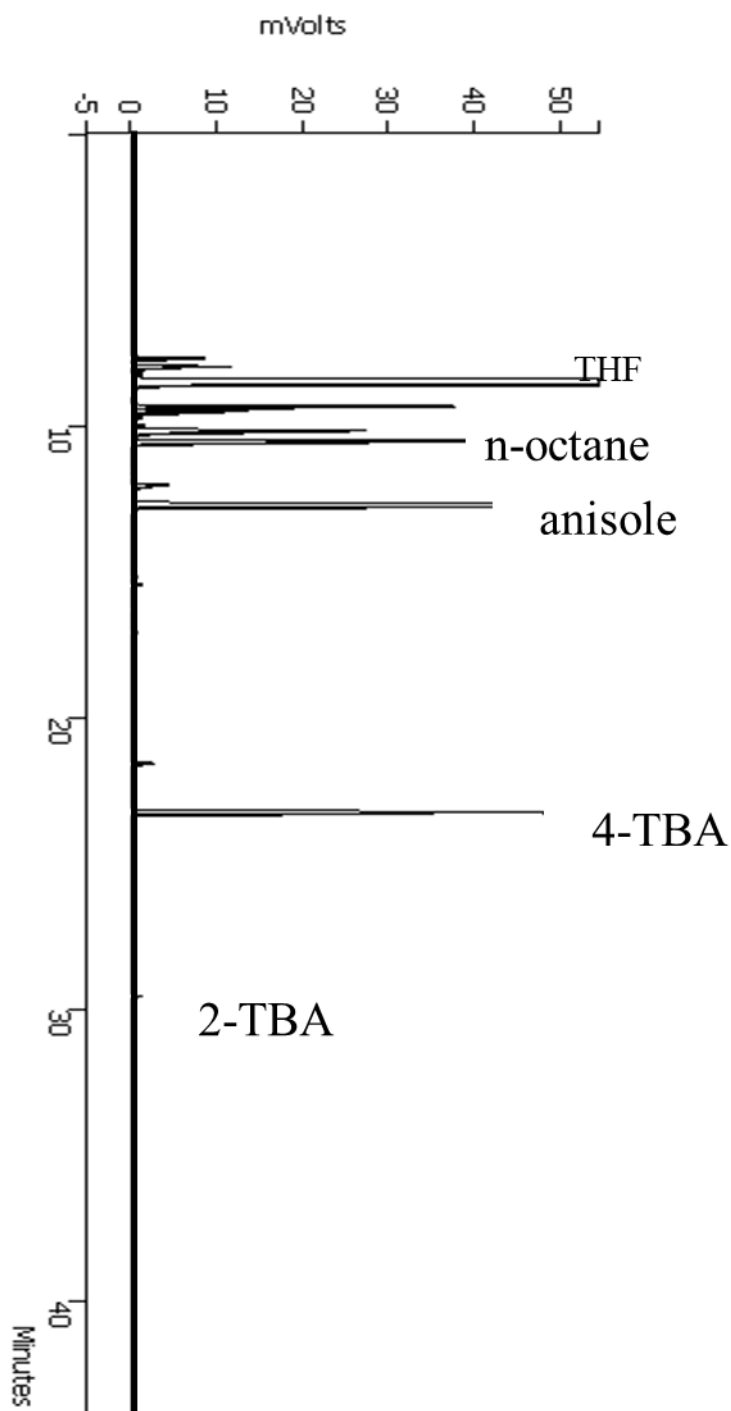


Figure A- 6 GC chromatogram of products from anisole alkylation over on ZSM-5 catalyst

VITA

Miss siripan Samutsri was born on February 3, 1990 in Roi et, Thailand. She graduated the Bachelor's Degree in Chemistry, Faculty of Science, Chulalongkorn University, in 2013. She continued her study in Organic Chemistry, Faculty of Science, Chulalongkorn University in 2013 and completed in 2016.

In 9-11 January 2016, she joins the Pure and Applied Chemistry International Conference (PACCON 2016) at Chulalongkorn University approval of proceeding and poster presentation in the title of "Preparation of Sulfonic acid functionalized cubic mesoporous Ia-3d (MCA)".

